

Electronic Thesis and Dissertation Repository

---

6-25-2018 2:45 PM

## Preparation and Characterization of Electrospun rGO-Poly(ester amide) Tissue Engineering Scaffolds

Hilary Stone  
*The University of Western Ontario*

Supervisor  
Mequanint, Kibret  
*The University of Western Ontario*

Graduate Program in Biomedical Engineering  
A thesis submitted in partial fulfillment of the requirements for the degree in Master of Engineering Science  
© Hilary Stone 2018

Follow this and additional works at: <https://ir.lib.uwo.ca/etd>



Part of the [Biomaterials Commons](#)

---

### Recommended Citation

Stone, Hilary, "Preparation and Characterization of Electrospun rGO-Poly(ester amide) Tissue Engineering Scaffolds" (2018). *Electronic Thesis and Dissertation Repository*. 5413.  
<https://ir.lib.uwo.ca/etd/5413>

This Dissertation/Thesis is brought to you for free and open access by Scholarship@Western. It has been accepted for inclusion in Electronic Thesis and Dissertation Repository by an authorized administrator of Scholarship@Western. For more information, please contact [wlsadmin@uwo.ca](mailto:wlsadmin@uwo.ca).

## **Abstract**

Tissue engineering scaffolds should support tissue maturation through exposure to biologically relevant stimuli and through successful cell infiltration. External electrical stimulation is particularly relevant for cardiac and neural applications, and requires conductive scaffolds to propagate electrical signals; cell infiltration is only possible with scaffolds that have sufficient porosity. The aim of this study was to impart conductivity and increased porosity of electrospun poly(ester amide) (PEA) scaffolds. Reduced graphene oxide (rGO) was incorporated into blend PEA and coaxial PEA-chitosan fibrous scaffolds, which increased scaffold conductivity and supported cardiac differentiation. The novel combination of ultrasonication and leaching of a sacrificial polymer was used to modify scaffold porosity, and resulted in an increase in pore area evaluated through image analysis. This approach aims to potentially promote tissue maturation with electrospun PEA scaffolds, by modifying both scaffold conductivity and porosity. This extends the relevance of electrospun PEA scaffolds to cardiac tissue engineering for the first time.

## **Keywords**

Tissue engineering, electrospinning, poly(ester amide)s, reduced graphene oxide, conductive scaffolds, cell infiltration, scaffold porosity

## **Acknowledgments**

I would like to first acknowledge my supervisor, Dr. Kibret Mequanint for his guidance and support throughout my time as an undergraduate and graduate student over the last four years. He motivated me to set high expectations and to work hard to meet them, providing invaluable guidance with research challenges. I appreciate the efforts he made to stay connected even when travelling, as well as his support and mentorship in my career planning.

I would like to thank the members of the Mequanint lab for their support. Specifically, I would like to thank Somiraa Said for her supervision and training when I was an undergraduate student. Although she has graduated and moved to a different lab, I am grateful for her ongoing friendship and mentorship. I would like to thank Kalin Penev for his expertise, guidance and mentorship with all aspects of the project, particularly regarding chemical synthesis. I would also like to thank Shigang Lin for his help with cell culture studies.

I would like to thank Andrew Cullen for his guidance and technical support with the electrical conductivity measurements. I would like to thank Aneta Borecki for her help with GPC, Yi-Kai (Ethan) Su for his help using the fluorescence plate reader, and Shengtai Zhou for his help with the two-probe unit. I would like to thank Karen Nygard and Dr. Richard Gardiner from the Biotron Experimental Climate Change Research Centre for their training and troubleshooting with SEM and TEM imaging.

I would like to acknowledge the Natural Sciences and Engineering Research Council (NSERC) and their Undergraduate Summer Research Award (USRA) program, as well as the Ontario Government and Ron Yamada Ontario Graduate Scholarships, for the financial support.

Finally, I would like to thank my family and friends for their ongoing support, especially my parents, siblings, partner, aunt and roommates.

# Table of Contents

Abstract.....	i
Acknowledgments.....	ii
Table of Contents.....	iii
List of Tables.....	vii
List of Figures.....	viii
List of Appendices.....	xii
List of Abbreviations.....	xiii
Chapter 1.....	1
1 Introduction.....	1
1.1 Scope.....	1
1.2 Thesis Outline.....	2
Chapter 2.....	4
2 Literature Review.....	4
2.1 Tissue Engineering.....	4
2.2 Scaffold Electrical Conductivity.....	5
2.2.1 Electrical Stimulation.....	5
2.2.2 Conductive Composite Scaffolds.....	6
2.3 Poly(ester amide)s.....	9
2.4 Graphene and rGO for Cardiac Tissue Engineering.....	10
2.4.1 Graphene and rGO.....	10
2.4.2 Cardiac Differentiation.....	11
2.5 Reduced Graphene Oxide Preparation.....	12
2.5.1 Graphene Oxide and Reduced Graphene Oxide.....	12
2.5.2 GO synthesis.....	14

2.5.3	rGO Synthesis .....	14
2.6	Electrical Conductivity Measurements .....	16
2.7	Electrospinning .....	17
2.7.1	Coaxial Electrospinning.....	20
2.7.2	Composite Electrospinning.....	22
2.8	Scaffold Porosity.....	25
2.8.1	Importance of Cell Infiltration .....	25
2.8.2	Increasing Scaffold Porosity.....	26
2.8.3	Image Analysis.....	27
2.9	Objectives .....	28
Chapter 3	.....	29
3	Materials and Methods.....	29
3.1	Materials .....	29
3.2	Monomer and Polymer Synthesis.....	29
3.2.1	Monomer Synthesis .....	30
3.2.2	Polymer Synthesis.....	30
3.3	GO and rGO Synthesis.....	31
3.3.1	GO Synthesis .....	31
3.3.2	rGO Synthesis.....	32
3.3.3	GO/rGO Characterization.....	33
3.4	rGO/PEA Composites.....	33
3.4.1	Composite Film Preparation .....	33
3.4.2	PEA Electrospinning.....	34
3.4.3	Coaxial Electrospinning.....	34
3.4.4	Blend Electrospinning.....	35
3.4.5	Composite Scaffold Characterization .....	36

3.5	Electrical Conductivity .....	36
3.6	Cell Proliferation and Differentiation .....	37
3.6.1	Cell Proliferation.....	37
3.6.2	Cell Differentiation .....	37
3.7	Combination of Ultrasonication and Sacrificial Polymer .....	38
3.7.1	Sacrificial Polymer Electrospinning .....	38
3.7.2	Scaffold Porosity Modification.....	39
3.8	Porosity Image Analysis .....	39
3.9	Statistical Analysis.....	40
Chapter 4	.....	42
4	Results and Discussion.....	42
4.1	GO and rGO Synthesis.....	42
4.2	rGO/PEA Composite Films and Fibrous Scaffolds .....	44
4.2.1	rGO/PEA Films.....	44
4.2.2	Coaxially-spun Fibrous Scaffolds.....	45
4.2.3	Blend Fibrous Scaffolds.....	49
4.3	Cell Proliferation and Differentiation .....	52
4.4	Scaffold Porosity Modifications .....	54
4.4.1	Porosity Modification Optimization .....	54
4.4.2	PVP/PEA System.....	55
4.4.3	PEO/PEA System .....	56
4.5	Discussion .....	57
Chapter 5	.....	67
5	Conclusions and Future Directions .....	67
5.1	Conclusions.....	67
5.2	Future Directions .....	68

References.....	70
Appendices.....	77
Curriculum Vitae .....	85

## List of Tables

Table 2-1: Conductive Composite Scaffolds .....	7
Table 2-2: Process, solution and ambient parameters that affect fiber morphology (Adapted from Ref <sup>2</sup> with permission from Mary Ann Liebert, Inc.).....	19
Table 2-3: Conductive Carbon-Polymer Composite Electrospinning .....	23



## List of Figures

Figure 2-1: Electrical stimulation set-up schematic, where the cell-scaffold construct is placed in a medium and connected to an electrical circuit through two electrodes. Reproduced from Ref <sup>18</sup> published by The Royal Society of Chemistry.....	6
Figure 2-2: 8-Phe-4 PEA structure, where the ‘8’ represents 8 methylene groups from the diacid, the ‘Phe’ represents the amino acid (L-phenylalanine) and the ‘4’ represents 4 methylene groups from the diol .....	9
Figure 2-3: Graphene-based material structures. A) Multi-layered graphene, B) Monolayer graphene, C) GO, D) rGO. Reproduced from Ref <sup>36</sup> published by BioMed Central Ltd. ....	13
Figure 2-4: Electrical Conductivity Measurement Set-ups.....	16
Figure 2-5: Basic electrospinning set-up. Reproduced from Ref <sup>53</sup> published by Taylor & Francis.....	18
Figure 2-6: Electrospinning needle modifications. A) blend B) multiple needle C) coaxial D) coaxial multiple needle E) triaxial. Reproduced from Ref <sup>2</sup> with permission from Mary Ann Liebert, Inc.....	20
Figure 2-7: Chitosan structure. Reproduced from Ref <sup>57</sup> with permission from Elsevier. ....	21
Figure 2-8: Effect of core-shell flow rate differential (core:shell, mL/h). Reproduced from Ref <sup>58</sup> with permission from Elsevier B.V.....	22
Figure 2-9: Effect of voltage on Taylor cone. Reproduced from Ref <sup>59</sup> with permission from The Royal Society of Chemistry.....	22
Figure 2-10: Schematic Illustration of Ultrasonication. Reproduced from Ref <sup>4</sup> with permission from Mary Ann Liebert, Inc.....	26
Figure 2-11: Different ratios of water-insoluble and water-soluble polymers. a-e: as spun composite scaffold with PLGA fibers (red) and PEG fibers (green) f-j: post leaching of PEG. Reproduced from Ref <sup>67</sup> and author retains copyright of this open access article.....	27

Figure 3-1: Coaxial electrospinning set-up, where two syringes are placed side by side and pushed by a single syringe pump. The lower syringe in the figure is connected directly into the core of the coaxial spinneret, while the upper syringe is connected through tubing and a luer connector to the shell of the coaxial spinneret. The coaxial spinneret is connected to the voltage supply. .... 35

Figure 3-2: Image Analysis. A) Top layer selection with binary mask. B) SPE layer accumulation. .... 40

Figure 4-1: rGO Reduction. A) GO and rGO FTIR where rGO was reduced by L-ascorbic acid and is representative of all rGO reductions. B) GO and rGO sheet resistance varied with reduction condition. rGO was reduced by either L-ascorbic acid (L-AA) or hydroiodic acid (HI). HI reduction was completed using GO concentrations of 4 mg/mL and 2 mg/mL (HI1 and HI2 respectively) and over 1 or 2 rounds of reduction (HI1-1 and HI1-2 for example respectively). C) rGO conductivity comparing experimental samples with purchased samples (Sigma-Aldrich) and literature values where Xu reported the L-AA sample<sup>30</sup> and Hu reported the HI sample.<sup>44</sup> Triplicate measurements on each sample were conducted for experimental measurements. .... 43

Figure 4-2: Composite rGO/PEA (A,C) and rGO/CS (B,D) films, showing the effect of rGO concentration on film resistance (A,B) and film uniformity (C,D). Purchased rGO was used. 3 replicates were measured on each sample, \* represents  $p < 0.05$ . .... 45

Figure 4-3: Coaxial electrospun scaffolds with PEA-CS as the core-shell respectively and then with rGO added in the core, shell or both core-shell. Core-shell PEA-(rGO/CS) has rGO in the shell. SEM images with 3  $\mu\text{m}$  scale bar are accompanied by the corresponding fiber diameter histograms. .... 46

Figure 4-4: (rGO/PEA)-CS coaxial electrospinning showing no clear core-shell structure. A) to C) Confocal microscopy where the shell auto-fluoresces blue (A) and the core is fluorescently labeled red (B) with the overlap in C. D) TEM image. .... 48

Figure 4-5: Coaxial scaffold conductivity. A) Conductivity of different coaxial scaffolds with 3 replicate measurements on each sample. B) Representative I-V curve of (rGO/PEA)-CS. 49

Figure 4-6: Effect of electrospinning parameters on blend rGO/PEA (B1) scaffolds A) 12.5 kV, 0.2 mL/h, 5 wt.% B) 12.5 kV, 0.2 mL/h, 7 wt.% C) 12.5 kV, 0.1 mL/h, 7 wt.% D) 6 kV, 0.1 mL/h 7 wt.%. Scale bar is 3  $\mu$ m. .... 50

Figure 4-7: Blend electrospun scaffolds where rGO was added either before electrospinning (B1) or during polymerization (P). SEM images with 3  $\mu$ m scale bar and fiber diameter histograms. B) Fiber diameters of different blend and coaxial scaffolds. At least 50 fibers were taken from 1 or 2 scaffolds. Different letters in B) indicate the significance at  $p < 0.05$ . .... 51

Figure 4-8: Blend scaffold conductivity. A) Conductivity of different blend scaffolds where rGO/PEA B1 has purchased rGO added before electrospinning, rGO/PEA B2 has synthesized rGO added before electrospinning, and rGO/PEA P has purchased rGO added during polymerization. 3 replicates were measured for each sample. B-C) Representative I-V curves of PEA and rGO/PEA P respectively. .... 52

Figure 4-9: Cell proliferation and differentiation on PEA, rGO/PEA P and (rGO/PEA)-CS scaffolds. A) 10T1/2 cell proliferation, each scaffold normalized to day 1,  $n = 3$ . B)-E) iPSC-derived MSC gene expression,  $n=1$  with 4 replicates where B) and D) demonstrate hGATA-4 gene expression and C) and E) demonstrate hNkx2.5 gene expression. B) and C) were treated with L-AA and D) and E) were treated with 5-aza. .... 53

Figure 4-10: PEA scaffold porosity using PVP as a sacrificial polymer A) SEM images of scaffolds with different modifications used for corresponding quantitative image analysis in B) and C). Two different ratios of PVP are used. Except for the PEA control scaffold, scaffolds are either only leached (left column) or are ultrasonicated prior to leaching (right column). Scale bar is 3  $\mu$ m. B) Pore area (medians graphed) of different scaffolds. C) Scaffold percolative efficiency (means graphed) of different scaffolds.  $N=3$ , \* represents  $p < 0.05$  compared to PEA control. .... 56

Figure 4-11: PEA scaffold porosity using PEO as a sacrificial polymer A) SEM images of scaffolds with different modifications used for corresponding quantitative image analysis in B) and C). Two different ratios of PEO were used. Except for the PEA control scaffold, scaffolds are either only leached (left column) or are ultrasonicated prior to leaching (right

column). Scale bar is 3  $\mu\text{m}$ . B) Pore area (medians graphed) of different scaffolds. C)  
Scaffold percolative efficiency (means graphed) of different scaffolds. N=3, \* represents  $p < 0.05$  compared to PEA control and # represents  $p < 0.05$  within group. .... 57

## List of Appendices

Appendix 1: Reaction schemes for PEA synthesis .....	77
Appendix 2: <sup>1</sup> H NMR results for monomer (top) and polymer (bottom) .....	78
Appendix 3: Electrical conductivity measurement set-ups. Four-probe with source measure unit (left) and two-probe (right).....	79
Appendix 4: The effect of rGO on CS electrospinning with CS (left) and rGO/CS (right). Scale bar is 3 μm .....	79
Appendix 5: Electrospinning optimization for sacrificial polymers PEO (left) and PVP (right). Scale bar is 3 μm .....	80
Appendix 6: Scaffold modification optimization. (Left): Different ultrasonication media result in different amounts of fiber swelling. 50 fibers were measured, * represents significance against the PEA as spun control, and # represents significance between groups where p <0.05. (Right): Effect of different ratios of sacrificial polymer where scale bar is 3 μm. ....	80
Appendix 7: Copyright Permissions .....	81

## List of Abbreviations

2D	Two-dimensional
3D	Three-dimensional
AcOH	Acetic acid
CNF	Carbon nanofibers
CNT	Carbon nanotubes
CS	Chitosan
DCM	Dichloromethane
DMF	N,N-dimethyl formamide
ECM	Extracellular matrix
ERK	Extracellular signal-related kinases
EtOH	Ethanol
FTIR	Fourier transform infrared spectroscopy
GIC	Graphite intercalation compound
GNW/NT	Gold nanowires/nanotubes
GO	Graphene oxide
GPC	Gel permeation chromatography
h	Hour
HI	Hydroiodic acid
iPSC	Induced pluripotent stem cell
I-V	Current-voltage (curve)
L-AA	L-ascorbic acid
MeOH	Methanol
min	Minute
MSC	Mesenchymal stem cell
NMR	Nuclear magnetic resonance
PEA	Poly(ester amide)
PEG	Poly(ethylene glycol)
PEO	Poly(ethylene oxide)
PVA	Poly(vinyl alcohol)
PVP	Poly(vinyl pyrrolidone)
rGO	Reduced graphene oxide
S	Siemens
SEM	Scanning electron microscopy
SPE	Scaffold percolative efficiency
TEM	Transmission electron microscopy

# Chapter 1

## 1 Introduction

This chapter provides an overall introduction to the thesis work.

### 1.1 Scope

Tissue engineering approaches repair, replace, and regenerate tissue for a range of drug discovery and clinical applications. Scaffolds are a key component of tissue engineering, as they support cells temporarily until they recreate their native extracellular matrix (ECM) at which point the scaffold should degrade.<sup>1</sup> Scaffolds are expected to mimic the ECM, encourage cell adhesion and interaction, and facilitate nutrient and waste diffusion.<sup>2</sup> There are a number of different scaffold fabrication methods, including particulate leaching, gas foaming, and electrospinning.<sup>3</sup>

Electrospinning is of particular interest as it creates fibrous scaffolds that mimic the native fibrous ECM and encourage cell adhesion through their high surface area-to-volume ratios. Electrospinning uses electrostatic forces to eject a charged polymer solution from a needle to form fibers on a grounded collector. However, a challenge with electrospinning is that the resulting nanofibers pack into dense meshes with low porosity, limiting cell infiltration and overall tissue maturation. Different methods attempt to increase scaffold porosity, including ultrasonication<sup>4</sup> and leaching of a sacrificial polymer.<sup>3</sup> One of the objectives of this study is to combine both of these methods and evaluate scaffold porosity.

Electrospinning setups can be modified to suit various applications; for example, the needle spinneret can be coaxial or triaxial to create multiple core-shell layers within the fibers. The versatility of electrospinning also extends to material selection: both natural and synthetic materials can be electrospun.<sup>2</sup> Poly(ester amide)s (PEA)s are a family of synthetic materials that can also contain natural components – amino acids. PEAs are beneficial for tissue engineering as they degrade into both acidic and basic degradation products, potentially limiting undesired pH drift. Other synthetic polymers are limited in

their tissue engineering applications as their degradation products are more acidic and can be toxic to some cells.<sup>5</sup>

Electrical stimulation is a biologically relevant stimulus necessary for cell-scaffold constructs to ensure tissue maturation, and is particularly relevant for cardiac, neural and skeletal muscle tissue.<sup>6</sup> Conductive scaffolds enhance the propagation of both external signals and cell-cell signaling.<sup>7</sup> However, PEA scaffolds are limited by their lack of conductivity. Graphene is a monolayer of carbon atoms known for its unique mechanical and electrical properties. Reduced graphene oxide (rGO) is somewhat similar to graphene and is easier to mass-produce compared to pure graphene. rGO is synthesized through the reduction of graphene oxide (GO), where the reduction restores the conductive properties.<sup>8</sup> Different reducing agents have different advantages and include L-ascorbic acid (L-AA) and hydroiodic acid (HI) among others.<sup>8</sup> Toxicity concerns are still being studied, but rGO is thought to be less toxic compared to GO, pure graphene<sup>9</sup> and carbon nanotubes (CNTs).<sup>10</sup> rGO has been used in composites to increase scaffold conductivity<sup>9-11</sup> and has been used to coat electrospun fibers<sup>12,13</sup> but there are limited examples of electrospinning rGO-containing materials,<sup>14,15</sup> particularly with the intent of improving conductivity.<sup>16</sup> The other objective of this study is to incorporate rGO into PEA electrospun scaffolds and evaluate the effect on scaffold conductivity.

Overall, this study aimed to improve electrospun PEA scaffolds for potentially supporting tissue maturation by encouraging cell infiltration and facilitating electrical stimulation; PEA scaffolds could then be extended to cardiac applications for the first time.

## **1.2 Thesis Outline**

The thesis is divided into five chapters, including this overall introduction. The literature review (Chapter 2) introduces current research challenges and progress within the field of tissue engineering scaffolds, as well as background theory to key concepts including electrospinning. The methodology (Chapter 3) details the materials and methods used in this study, including the synthesis of rGO, the fabrication of rGO/PEA composite films and fibrous scaffolds, and the evaluation of resulting conductivity and effect on cells. It also details the scaffold modification methods used to increase porosity and subsequent



evaluation through image analysis. The results (Chapter 4) highlights the findings from the various experiments and includes an overall discussion of the research relevance. Chapter 5 summarizes and concludes the work, providing direction for future work.

## Chapter 2

### 2 Literature Review

This chapter discusses the relevant background information and current research progress.

#### 2.1 Tissue Engineering

Tissue engineering is an emerging field that combines engineering and life sciences to improve the field of regenerative medicine. Tissue engineering has clinical applications as well applications within *in vitro* and *in vivo* disease models, drug and cosmetic testing, and cancer and other cell-based research.<sup>17</sup> Some common engineered tissues include bone, skin and blood vessels, and each requires different properties. Bone scaffolds require significant mechanical strength, while still allowing sufficient nutrient diffusion and vascularization by means of high porosity values. Skin also requires high permeability to facilitate nutrient diffusion, as well as the migration of epithelial cells; however, the focus is on elasticity. Blood vessels must be dynamic in nature, and have compliance to facilitate blood pumping and flow, and be resistant against rupture.<sup>2</sup> Other engineered tissues include cardiac or neural tissue, which require scaffolds to be conductive<sup>18</sup> (further discussed in Chapter 2.2).

Cardiac tissue engineering is of particular interest as cardiomyocytes have limited regeneration potential<sup>10</sup> and therefore cardiac damage is permanent. Cardiac damage results from myocardial infarctions, coronary artery disease and congenital heart defects,<sup>19</sup> which leads to scar tissue formation along with cardiomyocyte death. Scar tissue formation alters cardiac contractile and electrophysiological properties,<sup>7</sup> ultimately resulting in heart failure.<sup>19</sup> Tissue regeneration could provide a resolution to cardiac damage.

Scaffolds, often a key component in tissue engineering, provide a structure to which cells can attach, allowing the cells to then migrate and proliferate. Scaffolds can be made of natural or synthetic materials (further discussed in Chapter 2.3), and facilitate mass transfer of nutrients and waste products provided there is sufficient scaffold porosity

(further discussed in Chapter 2.8). These scaffolds also influence cell behavior both mechanically and biologically, thus assisting in the development of three-dimensional (3D) tissue structures.<sup>1</sup> The scaffolds mimic the cells' native ECM,<sup>2</sup> providing support until the cells have proliferated and produced their own ECM; the scaffold template can then degrade. There are different fabrication methods including particulate leaching, gas foaming and electrospinning (further discussed in Section 2.7),<sup>20</sup> depending on the specific scaffold requirements.

## **2.2 Scaffold Electrical Conductivity**

For some tissues (e.g. neural and cardiac), scaffolds may be beneficial if they are electrically conductive in order to facilitate external stimulation, a useful tool in tissue engineering.

### **2.2.1 Electrical Stimulation**

Chemical, mechanical and electrical stimuli are important cues during development, and these natural stimuli can be used to improve the quality of tissue-engineered constructs.<sup>6</sup> While internal electrical fields play a large role in the nervous and cardiac systems through action potentials, they also control general cellular functions including cell migration, gene expression and long-range intercellular signaling. Cells generate electricity through their resting membrane potential.<sup>6</sup>

Electrical stimuli are transduced through the calcium/calmodulin pathway by increasing intracellular calcium, and follow a similar pathway in the body as mechanotransduction or chemotaxis.<sup>6</sup> Electrical stimulation can be used to control cell proliferation and differentiation and organize tissue structure; it can also influence cell migration, enhance wound healing and bone remodeling, and improve regeneration of nervous or cardiac tissue.<sup>6</sup> For example, electrical stimulation can directly influence neural cells and guide their growth and adhesion, and influence the ECM remodeling.<sup>18</sup> Electrical stimulation functionality could be added to bioreactors, and complex stimulation patterns could be programmed appropriately. Conductive scaffolds could also be used to evenly distribute electrical stimuli throughout the scaffold material to regulate cell attachment and proliferation.<sup>6</sup> An example of an electrical stimulation set-up is shown in Figure 2-1.

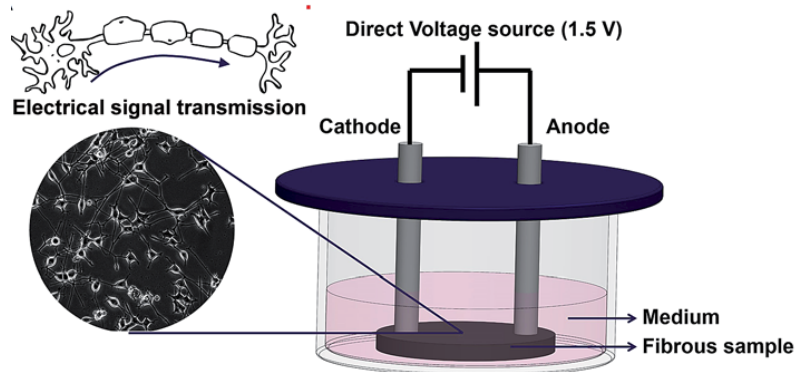


**Figure 2-1:** Electrical stimulation set-up schematic, where the cell-scaffold construct is placed in a medium and connected to an electrical circuit through two electrodes. Reproduced from Ref<sup>18</sup> published by The Royal Society of Chemistry.

In cardiac tissue engineering, electrical stimulation is particularly useful to guide cell alignment and differentiation, as well as cell coupling to influence the tissue's contractile properties.<sup>6</sup> In the native myocardium, cardiomyocytes are the contractile cells of the heart and form a functional syncytium. This syncytium is formed through gap junctions between the cells and allows electrical signals to propagate throughout the cardiac tissue and to produce contractile motion to efficiently pump blood out of the heart. There needs to be electromechanical coupling and electrical synchronization within the engineered construct and between the engineered and the host tissue. External electrical field stimulation promotes this electrical synchronization, to encourage functional gap junctions and to increase cell alignment and cardiac gene expression.<sup>19</sup> For instance, conductive gold-coated collagen fibers showed that electrical stimulation can enhance cardiac gene expression in MSCs in cardiomyogenic media.<sup>21</sup>

### 2.2.2 Conductive Composite Scaffolds

Conductive scaffolds are useful for electrical stimulation, as they encourage electrical signal propagation.<sup>10</sup> Composite materials are often used to increase the electrical conductivity of the scaffolds and are designed for tissue engineering applications that benefit from electrical stimulation and conductive scaffolds, primarily cardiac and neural tissues. As presented in Table 2-1, many of the conductive composite materials are carbon based, including rGO, graphene and CNT, but some groups have used gold

nanowires/nanotubes (GNW/NT). Some groups used electrospinning to form fibrous scaffolds while other groups used various methods to form other porous scaffolds.

**Table 2-1: Conductive Composite Scaffolds**

<b>Conductive Material</b>	<b>Scaffold Type</b>	<b>Other Materials</b>	<b>Application</b>	<b>Year &amp; Reference</b>
rGO	Hydrogel	GelMA	Cardiac	2016 <sup>10</sup>
CNF	Porous	Chitosan	Cardiac	2014 <sup>11</sup>
Gold	Nanofiber film	Collagen	Cardiac/Neural	2011 <sup>21</sup>
CNT	Hydrogel	GelMA	Cardiac	2013 <sup>22</sup>
GNW	Porous	Alginate	Cardiac	2012 <sup>23</sup>
GNT/NW	Porous	Polyurethane	Cardiac	2016 <sup>24</sup>
Graphene	Fibrous	Blend Poly(vinyl alcohol)/Alginate	Neural	2017 <sup>16</sup>
rGO	Coated/core-shell fibrous	Blend PLGA/Polyvinyl chloride (PVC)	General tissue engineering/ conductive cell culture	2016 <sup>13</sup>

Gold nanowires/nanotubes (GNT/NW) were incorporated into poly(urethane) (PU).<sup>24</sup> PU-GNT/NW composites facilitated electrical stimulation to promote cardiomyocyte spreading and alignment; the PU control under electrical stimulation did not enhance cell spreading or alignment. While the incorporation of gold into the composite may have improved cell adhesion compared to the control, electrical stimulation was also needed to improve cell proliferation.<sup>24</sup> Dvir *et al.* formed GNW-alginate composites that showed higher cardiac gene expression of cardiomyocytes, higher calcium transients and synchronous contraction behavior compared to the control. The GNW may have provided a conductive bridging effect throughout the alginate scaffold, decreasing the scaffold's resistance and increasing the level of Cx43 (gap junction protein) even before electrical stimulation.<sup>23</sup> These two studies show how GNW can be used to increase the conductivity of the scaffold, support cardiac cell phenotype and facilitate electrical stimulation.

Carbon materials like carbon nanofibers (CNF) have shown useful and Vunjak-Novakovic and coworkers<sup>11</sup> incorporated CNF into chitosan (CS) to form scaffolds through the precipitation method. The composite scaffolds had similar conductivity as ventricular muscle (0.3-0.6 S/m). The CNF improved the structural integrity and conductivity of the CS scaffolds and resulted in significantly higher metabolic activity of

neonatal cardiomyocytes. Even without external electrical stimulation, the composite scaffolds enhanced the scaffold's ability to propagate electrical signals as well as the cardiac phenotype and gene expression of the cardiomyocytes.<sup>11</sup>

Shin *et al.* investigated both carbon nanotubes (CNT)<sup>22</sup> and reduced graphene oxide (rGO),<sup>10</sup> as fillers in GelMA hydrogels. rGO is similar to graphene and is described in more detail in Chapters 2.4 and 2.5. Both CNT-GelMA and rGO-GelMA were electrically more conductive than the GelMA control, providing signal propagation. When cardiomyocytes were cultured on CNT-GelMA and rGO-GelMA, they demonstrated higher spontaneous beating behavior and higher cardiac gene expression on both scaffolds compared to the control. With the CNT-GelMA scaffolds, cell adhesion and phenotype were also investigated and cardiomyocytes showed greater adhesion, alignment and sarcomeric structures on the composite scaffold compared to the control.<sup>22</sup> The rGO-GelMA scaffolds responded to an externally applied electric field while the non-conductive control did not.<sup>10</sup>

Coating methods have also been used as an alternative to incorporating the conductive material as filler into a host polymer. Biris and coworkers<sup>21</sup> used gold to form gold-coated collagen nanofiber films for mesenchymal stem cell (MSC) differentiation into either cardiac or neural lineages, with the appropriate differentiation factors. Cell attachment on gold-coated collagen was greater compared to collagen. As well, when exposed to electrical stimulation, the conductive and fibrous gold-coated collagen scaffolds accelerated differentiation into either cardiac or neural lineages.<sup>21</sup> PLGA/poly(vinyl chloride) was electrospun into a graphene oxide (GO) solution, dried, and then reduced with hydroiodic acid (HI) to form an rGO coating. Human bone marrow MSCs (bmMSCs) showed improved cell spreading and proliferation compared to a rGO film as a result of the fibrous topography.<sup>13</sup>

Conductive material-polymer composites offer great potential for introducing conductivity to scaffolds and facilitating external electrical stimulation; this is particularly relevant to ensuring cardiomyocyte maturation within the construct.

### 2.3 Poly(ester amide)s

Tissue engineered scaffolds can be fabricated from a range of natural and synthetic materials. Poly(ester amide)s (PEAs) are a class of synthetic biomaterials that have promising properties for a range of biomedical applications. Not only can PEAs be used for tissue engineered scaffolds, but also for drug delivery, and as hydrogels, non-viral gene carriers, smart (sensing) materials and medical adhesives.<sup>25</sup> PEAs have both synthetic and natural components<sup>26</sup> including amino acids, diols and dicarboxylic acids (Figure 2-2), and are able to form films and fibers.<sup>27</sup> This composition is useful particularly in terms of the degradation products, which are both acidic and basic and therefore have the potential to produce a buffering effect and a less acidic environment. As well, some of PEAs degradation products are amino acids, which are already present in the body.<sup>5</sup>

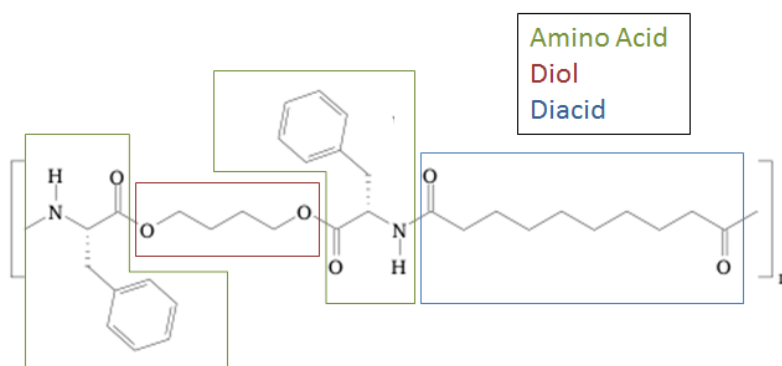


**Figure 2-2:** 8-Phe-4 PEA structure, where the ‘8’ represents 8 methylene groups from the diacid, the ‘Phe’ represents the amino acid (L-phenylalanine) and the ‘4’ represents 4 methylene groups from the diol

PEAs are an improvement from both polyesters and polyamides, gaining beneficial characteristics from both groups of polymers. The ester linkages make PEAs easily degradable through both enzymatic and hydrolytic degradation, while the amide groups provide mechanical and thermal properties through strong hydrogen bonds.<sup>25</sup> Another advantage of PEAs is the possibility of functionalization through the amino acid side chains. PEAs are often functionalized with L-lysine, L-glutamic acid and L-aspartic acid. Functionalization is valuable as it allows the development of biomimetic materials

through the immobilization of growth factors and other signaling molecules that enable the scaffold to interact with the cells and encourage certain cell behaviour.<sup>26</sup>

However, a limitation to PEAs is their lack of conductivity and thus their inability to facilitate electrical stimulation. A conductive composite should be considered to improve PEA scaffold conductivity.

## **2.4 Graphene and rGO for Cardiac Tissue Engineering**

As discussed in Chapter 2.2, graphene and rGO have been used in composite materials to increase electrical conductivity and facilitate electrical stimulation. This is because of their unique set of properties, including their high conductivity and surface area; even without electrical stimulation, they have also been shown to induce cardiac differentiation of stem cells through their nanotopography. As PEA is a non-conductive scaffold material and does not facilitate electrical stimulation, it is proposed that rGO could be incorporated to increase scaffold conductivity and support cardiac tissue engineering scaffolds. Preparation of graphene and rGO is discussed in Chapter 2.5.

### **2.4.1 Graphene and rGO**

Graphene is a two-dimensional monolayer sheet of carbon where the carbon atoms are all  $sp^2$  hybridized<sup>28</sup> so they have  $\sigma$  bonds that create a lattice structure and conjugated  $\pi$  orbitals that create a delocalized electron network.<sup>29</sup> As a result, graphene has a number of unique properties including excellent mechanical, thermal, and conductive properties along with a large surface area.<sup>7</sup> rGO is similar to pristine graphene but has a lower conductivity<sup>8</sup> as a result of any remaining oxygen-containing functional groups as well as defects throughout the lattice due to the oxidation and reduction processes.<sup>30</sup>

Graphene and rGO are seen as potential candidates for cardiac tissue engineering composite scaffolds as they have high mechanical strength and electrical conductivity, which natural biomaterials lack. In terms of cytotoxicity, 2D graphene is less cytotoxic compared to carbon nanotubes (CNT) as shape and composition affects cytotoxicity,<sup>10</sup> and while further studies are needed, rGO is considered to be less cytotoxic compared to GO or pure graphene.<sup>9</sup> There is no significant cytotoxicity risk from rGO.<sup>10</sup>



### 2.4.2 Cardiac Differentiation

As cardiomyocytes have limited regeneration potential, stem cells are promising alternatives for myocardial regeneration since they have superior proliferation and can be differentiated into cardiomyocytes.<sup>31</sup> To confirm cardiomyogenic differentiation, cardiac marker gene and protein expressions are evaluated. These cardiac genes and proteins include early transcription factors cardiac homeobox protein (Nkx2.5) and GATA binding factor 4 (GATA-4), contractile proteins  $\alpha$ -myosin heavy chain ( $\alpha$ -MHC),  $\beta$ -MHC and cardiac troponin T (cTnT), and gap junction protein Cx43.<sup>32</sup> L-ascorbic acid (L-AA) has been used to induce cardiomyogenic differentiation of induced pluripotent stem cells (iPSCs),<sup>33</sup> and 5-azacytidine (5-aza) has been used to induce cardiomyogenic differentiation of MSCs. It has been reported that Nkx2.5 expression, along with other cardiac genes, were only up-regulated in MSCs in the presence of 5-aza.<sup>31</sup> This differentiation is partly due to extracellular signal related kinases (ERK) activation because an ERK inhibitor blocked 5-aza-induced ERK phosphorylation. ERK activation occurs naturally during embryonic development in mesodermal differentiation. As well as up-regulating cardiac gene and protein expression, 5-aza down-regulated expression of stem cell-associated proteins Sox2 and Nanog and did not result in any osteogenic differentiation.<sup>31</sup>

There are only a few studies on the effect of graphene on cardiomyogenic differentiation of stem cells. Vitronectin-coated graphene film on glass showed enhanced cardiomyogenic differentiation of human embryonic stem cells (hESCs) with increased gene expression of cardiomyogenic transcriptional factors, contractile proteins and gap junction proteins.<sup>32</sup> The nano-roughness of graphene is thought to contribute to cardiomyogenic differentiation as it promotes vitronectin adsorption and cell adhesion and proliferation; it also upregulates ERK signaling.<sup>32</sup>

A comparative study on MSC differentiation on graphene culture and coverslip, without the use of exogenous cardiomyogenic inducers in the culture media, demonstrated that graphene enhanced cardiomyogenic differentiation, with enhanced expression of an early cardiomyogenic transcriptional factor, a gap junction protein and cardiomyogenic contractile proteins.<sup>34</sup> This is attributed to graphene's upregulation of ECM proteins

including collagen, fibronectin and laminin, where laminin is known to promote cardiomyocytes' ability to propagate electrical signals. Graphene also upregulated cell signaling molecules; this includes focal adhesion components paxillin and vinculin as well as ERK that are activated during cardiomyogenic differentiation. This highlights how graphene-ECM interactions induced cardiomyogenic differentiation.<sup>34</sup> The strong affinity between ECM proteins and carbon-based nanomaterials may be due to protein adsorption.<sup>10</sup> rGO sheets adsorb proteins via hydrophobic interactions as well as electrostatic interactions with any remaining oxygen in rGO; the  $sp^2$  configuration of rGO also allows  $\pi$  bonds to be formed between its delocalized electrons and the proteins.<sup>10</sup>

Overall, graphene has potential to promote cardiomyogenic differentiation<sup>7</sup> and interacts well with ECM proteins. Based on its potential to support electrical stimulation and cardiomyogenic differentiation, graphene and rGO are well suited for cardiac tissue engineering.

## **2.5 Reduced Graphene Oxide Preparation**

There are multiple ways to produce graphene, including chemical vapour deposition, graphite exfoliation and chemical oxidation-reduction.<sup>35</sup> The product of oxidation-reduction is more accurately described as reduced graphene oxide (rGO).

### **2.5.1 Graphene Oxide and Reduced Graphene Oxide**

The oxidation-reduction method of producing graphene from graphite is useful for scale-up production.<sup>35</sup> Graphite (bulk graphene) is first oxidized and exfoliated to graphene oxide (GO) and then reduced to form the final product of rGO. The different structures can be seen in Figure 2-3. rGO is similar to pristine graphene but may have residual oxygen-containing functional groups as well as defects throughout the lattice.<sup>8</sup> The extent of GO reduction can be tuned to achieve the desired surface oxygen content.<sup>10</sup>

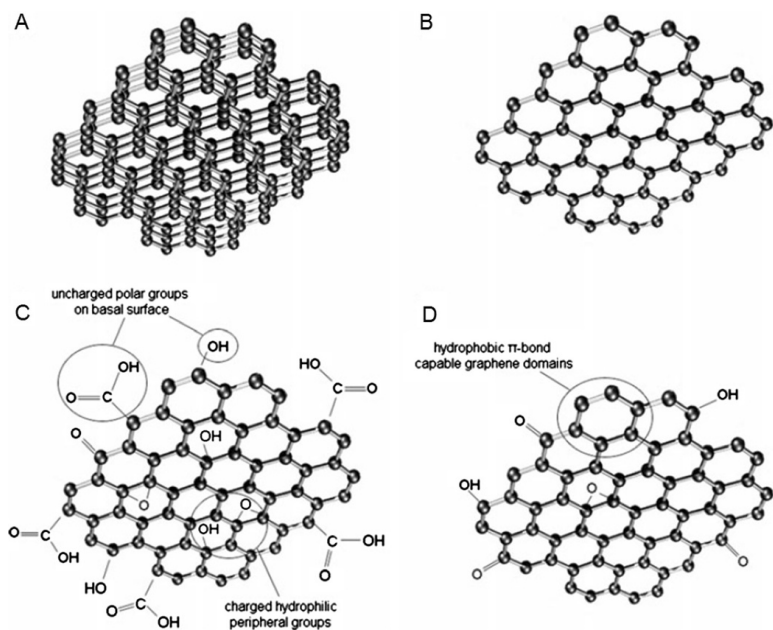


**Figure 2-3:** Graphene-based material structures. A) Multi-layered graphene, B) Monolayer graphene, C) GO, D) rGO. Reproduced from Ref<sup>36</sup> published by BioMed Central Ltd.

GO has many oxygen-containing functional groups, including hydroxyl and epoxide groups on the basal plane, as well as carboxyl and carbonyl groups on the sheet edge. As a result, GO is significantly more hydrophilic compared to graphene or rGO.<sup>10</sup> These oxygen-containing functional groups are bound to sp<sup>3</sup> carbons, so GO has both sp<sup>2</sup> and sp<sup>3</sup> hybridization, which differs from the sole sp<sup>2</sup> hybridization in graphene.<sup>37</sup> The change in hybridization disrupts the long-range conjugated structure by blocking conductive connecting pathways between the sp<sup>2</sup> domains,<sup>8</sup> greatly reducing the electrical conductivity of GO. The electrical conductivity of GO and pristine graphene is 0.1 and 10<sup>4</sup> S/cm respectively,<sup>9</sup> while rGO has an electrical conductivity between that of GO and pristine graphene.<sup>8</sup> The purpose of reducing GO to rGO is to increase the material's electrical conductivity by restoring the sp<sup>2</sup> hybridization and π orbitals, but this compromises its potential for functionalization and dispersion in water.<sup>9</sup> The difference in electrical conductivity can be used to confirm the oxidation and reduction processes and can be measured with the two-probe or four-probe method as discussed in Chapter 2.6.

There are other characterization methods as well. FTIR is commonly used as GO has characteristic peaks representing the range of oxygen-containing functional groups, while

those peaks are greatly reduced or non-existent with rGO. Visual observations can also confirm the processes; GO is a brown solution while rGO is black.<sup>10</sup>

### 2.5.2 GO synthesis

The synthesis of graphene oxide is well established and three main oxidation processes have been used throughout history.<sup>38</sup> First Brodie used potassium chlorate ( $\text{KClO}_3$ ) and fuming nitric acid ( $\text{HNO}_3$ ) in the 1800s. Staudenmaier improved upon Brodie's method slightly by adding  $\text{KClO}_3$  over time and adding concentrated sulfuric acid ( $\text{H}_2\text{SO}_4$ ). In the 1950s Hummers and Offeman changed the oxidizing agents to potassium permanganate ( $\text{KMnO}_4$ ) and  $\text{H}_2\text{SO}_4$ .<sup>38</sup>  $\text{KMnO}_4$  is an advantageous replacement for  $\text{KClO}_3$ , as it is not explosive.<sup>39</sup> Hummers and Offeman<sup>39</sup> also included  $\text{NaNO}_3$  in the reaction; this is preferred over fuming  $\text{HNO}_3$  as it eliminates acid mist formation.<sup>40</sup> As a result, the Hummers method is commonly used with modifications. The original Hummers method still releases toxic gases including  $\text{NO}_2$ ,  $\text{N}_2\text{O}_4$  and it is hard to remove  $\text{Na}^+$  and  $\text{NO}_3^-$  ions, so Marcano *et al.*<sup>41</sup> removed  $\text{NaNO}_3$  and used  $\text{H}_3\text{PO}_4$  instead. A study by Chen *et al.*<sup>40</sup> removed  $\text{NaNO}_3$  and found that  $\text{KMnO}_4$  alone is sufficient for oxidation. Another modification is the addition of a pre-oxidation step with potassium persulfate ( $\text{K}_2\text{S}_2\text{O}_8$ ) to ensure complete oxidation.<sup>42</sup> After the different oxidations by  $\text{K}_2\text{S}_2\text{O}_8$  and  $\text{KMnO}_4$ , the solution is washed with hydrochloric acid ( $\text{HCl}$ ) to remove the metal ions and the resulting stable suspension is graphite oxide. This graphite oxide suspension is exfoliated via ultrasonication to form a homogenous yellow-brown stable GO solution.<sup>42</sup>

Mechanistically, during oxidation graphite is first intercalated by  $\text{H}_2\text{SO}_4$  to form  $\text{H}_2\text{SO}_4$ -graphite intercalation compound (GIC).<sup>43</sup> The oxidizing agent then diffuses in between the layers of  $\text{H}_2\text{SO}_4$ -GIC and replaces the GIC to form pristine graphite oxide. This significantly slower step is rate-determining and diffusion-controlled. Water then exfoliates the graphite oxide, separating the layers to form GO; water allows the oxidant to be removed and reacts with the oxygen-containing functional groups.<sup>43</sup>

### 2.5.3 rGO Synthesis

The reduction of GO to form rGO can be performed in a number of different processes, including thermal annealing, electrochemical reduction, chemical reduction, and others.

The aim of reduction is to improve electrical conductivity; so this is a key criterion in comparing reduction methods,<sup>8</sup> along with ease, non-toxicity and yield.

Thermal annealing has a dual effect: it both removes the oxygen-containing functional groups and exfoliates GO to ensure single layer rGO.<sup>8</sup> GO is rapidly heated so that CO<sub>2</sub> gas is produced and the resulting pressure exfoliates GO. However, with the removal of CO<sub>2</sub>, the rGO sheet is broken up which negatively impacts conductivity. Furthermore, the high temperature process is energy intensive. Electrochemical reduction uses a regular electrochemical cell and the electron exchange between the electrodes and GO results in GO reduction. There are no hazardous reducing agents and byproducts,<sup>8</sup> but this method has not yet been scaled up.<sup>38</sup>

Chemical reduction is very appealing because scale-up is economical, easier and the process can be done in solution<sup>30</sup> at room or moderate temperatures. In addition, chemical reduction maintains the planar carbon structure, which is beneficial to maintain conductivity. Within the chemical reduction method, reducing agents include hydrazine, sodium borohydride (NaBH<sub>4</sub>), hydroiodic acid (HI) and L-ascorbic acid (L-AA) among others.<sup>8</sup>

Hydrazine has been commonly used and has resulted in a rGO conductivity close to 100 S/cm, but surfactants are often needed to minimize agglomeration.<sup>8</sup> As well, hydrazine is both toxic and explosive,<sup>8</sup> and can leave behind bound nitrogen that causes heteroatomic impurities.<sup>38</sup> NaBH<sub>4</sub> in a two-step procedure can achieve a rGO conductivity of around 16 S/cm; however, it is at least slightly reactive to water (the main solvent) which is problematic.<sup>8</sup> HI can produce a rGO conductivity of around 45 S/cm. Hu *et al.* also used HI in combination with hydrazine hydrate so that the hydrazine removed the hydroxyl groups while HI removed the epoxy groups; this gave a conductivity of around 80 S/cm.<sup>44</sup>

L-AA is an environmentally friendly alternative that has resulted in rGO conductivities just under 10 S/cm.<sup>30,45</sup> L-AA reduction also resulted in fewer defects, showed no significant weight loss in GO compared to hydrazine reduction,<sup>46</sup> and the oxidized products of L-AA may stabilize the rGO suspension.<sup>45</sup> Ammonia can be used to minimize

rGO agglomeration through electrostatic repulsion, as the alkaline conditions favor negatively charged carboxylate groups on GO.<sup>30</sup> Sonication can be used to accelerate GO reduction.<sup>47</sup>

## 2.6 Electrical Conductivity Measurements

The four-probe as well as the two-probe method are commonly used to measure electrical conductivity of different materials including films and composite materials. Electrical conductivity ( $\sigma$  in S/cm) is the reciprocal of bulk resistivity ( $\rho$  in  $\Omega$ -cm) as seen in Equation 2-1.<sup>48</sup>

$$\sigma = \frac{1}{\rho} \quad (2-1)$$

The four-probe set-up is commonly used to measure thin films. There are four probes on the surface of the material as seen in Figure 2-4.<sup>48</sup>

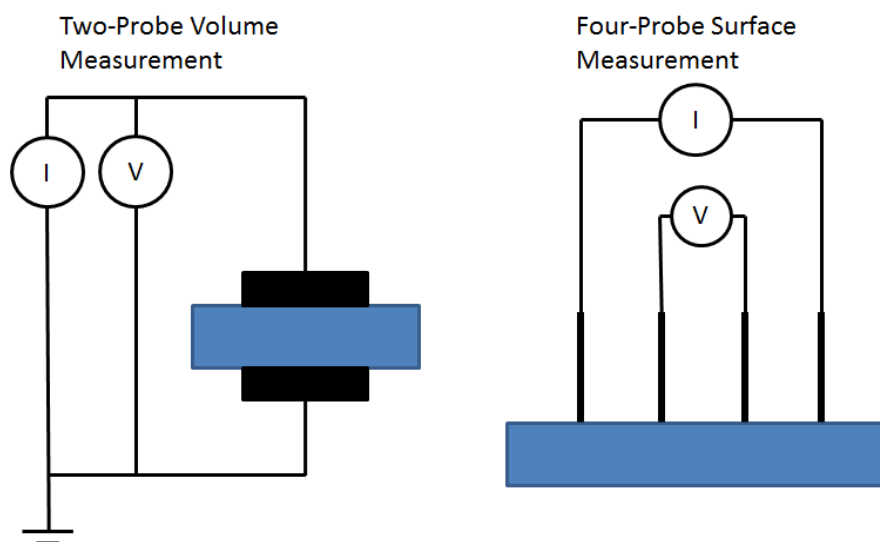


**Figure 2-4:** Electrical Conductivity Measurement Set-ups

Current is sourced through the outer probes and the potential difference is measured through the inside probes. Bulk resistivity is related to the sheet resistance ( $R_s$  in  $\Omega$ /square) and thickness ( $t$  in cm) through Equation 2-2.<sup>48</sup>

$$\rho = R_s * t \quad (2-2)$$

When  $t \ll s$ , or  $t/s < 1/5$ , where  $t$  is thickness and  $s$  is the probe spacing, the material is considered a thin film and thickness can be disregarded and sheet resistance can be calculated as in Equation 2-3, where  $V$  is potential difference (in Volts) and  $I$  is current (in Amperes). Sheet resistance is technically measured in  $\Omega$ , but often labeled as  $\Omega/\text{square}$  to distinguish sheet resistance from bulk resistance. The term  $\Omega/\text{square}$  is used because the sheet resistance of a square is independent of the size of the square.<sup>49</sup>

$$R_s = \frac{\pi}{\ln 2} * \frac{V}{I} \approx 4.532 * \frac{V}{I} \quad (2-3)$$

There are different two-probe set-ups, where one directly measures bulk or volume resistivity with electrodes on either side of the material as seen in Figure 2-4. Bulk resistivity is normalized by a geometrical factor, as shown in Equation 2-4, where  $A$  is surface area ( $\text{cm}^2$ ) and  $t$  is thickness (cm). Conductivity is again calculated using Equation 2-1.<sup>50</sup>

$$\rho = \frac{V}{I} * \frac{A}{t} \quad (2-4)$$

## 2.7 Electrospinning

As mentioned in Chapter 2.1, there are many different scaffold fabrication methods. Electrospinning is a particularly useful method, as it produces fibrous scaffolds. Fibrous scaffolds have high surface area to volume ratios, which improve cell adhesion. Electrospinning forms nanofibers that have dimensions similar to those of collagen in the ECM. These fibers can be used to incorporate functional materials including drugs, growth factors, enzymes, magnetic and semiconductor nanoparticles, and chromophores.<sup>51</sup> Compared to self-assembly and phase separation, other modes of producing fibrous scaffolds, electrospinning is more cost-effective and produces long continuous fibers. Fiber orientation and diameter can also be controlled.<sup>52</sup> Electrospinning is a versatile method and can easily be scaled for greater production. The method has been used for a variety of natural and synthetic materials including PEA, poly(glycolic acid), poly(L-lactic acid), and poly ( $\epsilon$ -caprolactone), as well as collagen,

chitosan and gelatin. Composite combinations are also possible. Endothelial cells, smooth muscle cells, mesenchymal stem cells, fibroblasts and neural stem cells among others have been seeded onto electrospun scaffolds.<sup>51</sup>

Electrospinning uses electrostatic forces to eject a charged polymer-solvent solution from a syringe to a grounded collector; the solvent evaporates and polymer fibers form a mesh scaffold on the collector. The grounded collector can either be flat and static, or cylindrical and rotating.<sup>2</sup> This can be visualized through Figure 2-5.

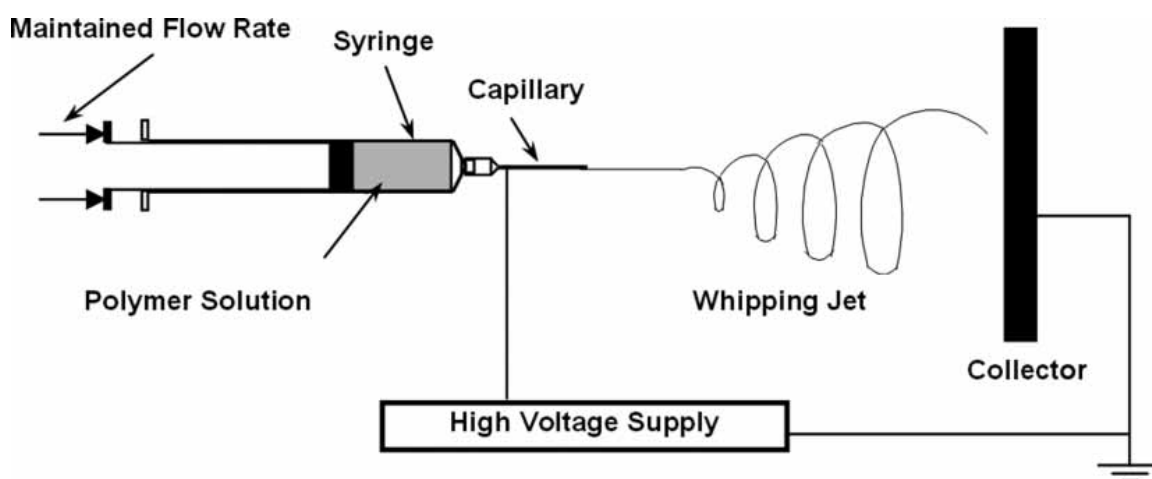


**Figure 2-5:** Basic electrospinning set-up. Reproduced from Ref<sup>53</sup> published by Taylor & Francis.

As the polymer is pushed out of the syringe, surface tension forces create a spherical drop of material.<sup>54</sup> In the presence of an electrical field (based on the set voltage and working distance between needle and collector), the polymer becomes charged and the charges accumulate on the surface. The accumulated charges experience Coulomb repulsion, which favors the formation of a jet instead of a spherical drop. Once there is sufficient electrical field and therefore sufficient repulsive electrostatic charge, the electrostatic force overcomes the surface tension force and the drop becomes conical; material is then ejected from the Taylor cone. This material jet undergoes bending instability and whipping motion as a result of the charge repulsion, the solvent evaporates, and fibers are deposited on the grounded collector.<sup>54</sup>



Solution viscosity is affected by molecular weight and solution concentration.<sup>53</sup> There is a critical minimum viscosity, as sufficient polymer chain entanglements are needed to ensure fiber formation and prevent the electrospaying of droplets. Electrospaying occurs when there is a Rayleigh instability, where there is insufficient viscosity or resistance to the electrostatic force so the jet is broken up. Beaded fibers result when there are moderate but insufficient chain entanglements.<sup>53</sup> If the viscosity is too high, the resistance to the electrical field is too large and the polymer jet will not form.<sup>2</sup> Adjustment is required to balance the opposing forces to create uniform, bead-free fibers.<sup>54</sup>

Along with solution viscosity (molecular weight and solution concentration), there are many other parameters that need to be adjusted to produce bead-free fibers. Some of these parameters are summarized in Table 2-2.

**Table 2-2: Process, solution and ambient parameters that affect fiber morphology (Adapted from Ref<sup>2</sup> with permission from Mary Ann Liebert, Inc.)**

<b>Parameters</b>	<b>Effect on fiber morphology</b>
Polymer molecular weight	Increasing molecular weight reduces bead formation
	Higher molecular weight results in irregular shape and larger pores
Polymer solution concentration	Low solution concentrations/viscosities result in defects (beads, junctions)
	High solution concentration reduces bead formation and increases fiber diameter
Voltage	Increasing voltage decreases fiber diameter
	High voltage results in bead formation
Solution conductivity	Higher conductivity creates uniform charge density bead-free fibers with decreased fiber diameter
Solution flow rate	Higher flow rate results in larger fiber diameter and bead formation
Working distance	A minimum distance is required to obtain dried and uniform fibers
	Observable beading if distance is too close or too far
Grounded target	Metal collectors yield smoother fibers
	Porous collectors result in porous fiber and geometry structure
	Rotating drum collects aligned fibers
Temperature	Higher temperature and decreased solution viscosity results in smaller fiber diameter
Humidity	Increasing humidity resulted in the appearance of circular pores on the fibers
Air velocity	Increasing air velocity results in larger fiber diameter

Electrospinning is a very versatile method with a number of different possible modifications. For example, the needle spinneret can be modified to create multi-component fibers in different forms as seen in Figure 2-6.

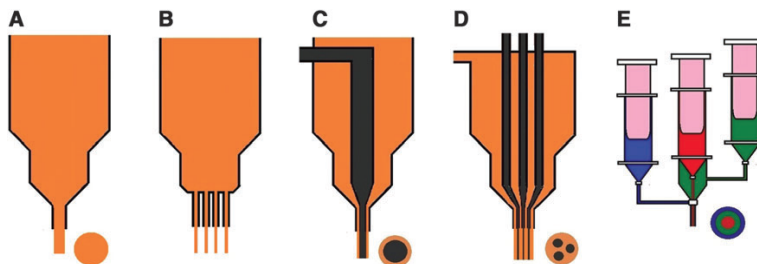


**Figure 2-6:** Electrospinning needle modifications. A) blend B) multiple needle C) coaxial D) coaxial multiple needle E) triaxial. Reproduced from Ref<sup>2</sup> with permission from Mary Ann Liebert, Inc.

### 2.7.1 Coaxial Electrospinning

The needle tip can be modified to a coaxial or triaxial spinneret to form various core-shell fibers. Core-shell fibers can also be used to encapsulate drugs, proteins, genes or other factors, and is significantly useful to lengthen the time of the component's release profile or to protect the material from a reactive environment.<sup>53</sup> Hollow fibers are possible through removal of the core post-electrospinning. Core-shell morphology is also useful to create multifunctional fibers; for example, the core can reinforce the mechanical strength of the fibers while the shell can ensure positive cell-material interactions. This is beneficial for tissue engineering scaffolds.<sup>53</sup> This is also relevant to PEA, which has tunable mechanical properties and is well suited for the core. PEA could be combined with a very biocompatible polymer such chitosan (CS). CS is biocompatible, structurally resembles native glycosaminoglycans in the ECM as seen in Figure 2-7 and is widely used in tissue engineering.<sup>55</sup> CS has also been shown to support cardiomyogenic differentiation.<sup>56</sup>

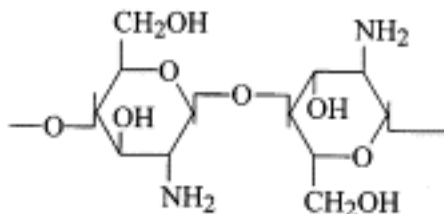


**Figure 2-7:** Chitosan structure. Reproduced from Ref<sup>57</sup> with permission from Elsevier.

In coaxial electrospinning, the shell solution accumulates charges due to the electric field, and once electrostatic forces overcome surface tension forces, the shell extends out as a jet. The core gets dragged through contact friction along with the shell. If the solvents are miscible, mixing of the core and shell is possible.<sup>53</sup> In order to achieve proper core-shell morphology, a number of criteria must be met. One polymer should not precipitate in the other solvent, and there should be low interfacial tension between the core and shell solutions. As well, low vapor pressure solvents should be used to prevent rapid evaporation; this can trap solvent and can cause the core structure to collapse into a ribbon-like structure once the solvent eventually evaporates. The shell should be electrospinnable and have a higher viscosity, conductivity and flow rate compared to the core. The higher shell conductivity means the shell will be pulled at a faster rate and drag the core along as intended.<sup>53</sup> A flow rate differential between the shell and the core is particularly important. There needs to be a minimum core to shell flow rate ratio of 1:3 to ensure there is enough shell material to cover the core material as is visualized in Figure 2-8.<sup>58</sup>

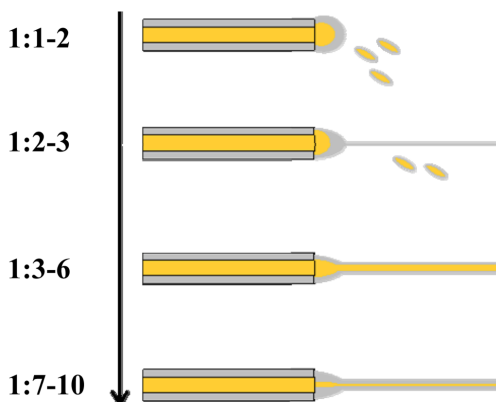


**Figure 2-8:** Effect of core-shell flow rate differential (core:shell, mL/h). Reproduced from Ref<sup>58</sup> with permission from Elsevier B.V.

Just as with conventional electrospinning, the voltage needs to be optimized to ensure a stable Taylor cone. Figure 2-9 shows the effects of voltage on the Taylor cone. If the voltage is too low, the gravitational force can dominate, increasing the size of the Taylor cone and the likelihood of core-shell mixing if the solvents are miscible. If the voltage is too high, the Taylor cone can recede within the spinneret and result in the separation of core and shell solutions.<sup>53</sup>

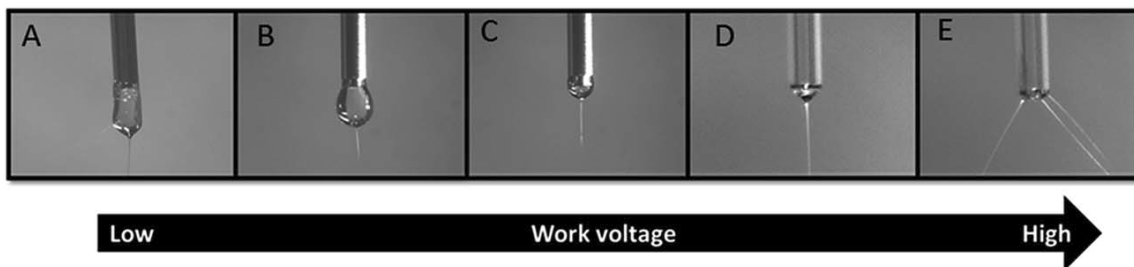


**Figure 2-9:** Effect of voltage on Taylor cone. Reproduced from Ref<sup>59</sup> with permission from The Royal Society of Chemistry.

### 2.7.2 Composite Electrospinning

Instead of using a coaxial spinneret to use different materials in a core-shell structure, electrospinning blend composites are also a possibility. This is relevant with the incorporation of rGO into the PEA fibrous scaffolds in order to increase scaffold conductivity. In order for composites to be electrospun properly and to improve

conductivity, there needs to be sufficient interaction between the filler and the polymer matrix.<sup>35</sup> This means that the filler, in this case a graphene-based material, needs to be well dispersed within the matrix in order to maximize the graphene surface area. With composite preparation in general, there are three mixing processes: solvent mixing, melt processing and *in situ* polymerization. These methods take advantage of van der Waals force and potential  $\pi$ - $\pi$  stacking interactions, which are possible with graphene-based materials. Hydrogen bonding is more relevant to GO, which has plenty of oxygen-containing functional groups. Graphene can be covalently modified to improve dispersion within the matrix, but this disrupts graphene's conjugation and therefore compromises the composite's conductivity. There is also the option of coating the electrospun fibers with another material instead of electrospinning a composite solution. These different methods impact the filler-matrix interaction, and *in situ* polymerization usually results in stronger interactions and greater conductivity. Conductivity is increased as the filler concentration is increased up until the percolation concentration; this is the minimum concentration of conductive filler needed to form conductive paths throughout the insulating polymer.<sup>35</sup> This percolation concentration or threshold should be minimized, which can be accomplished through *in situ* polymerization.<sup>60</sup>

A number of groups have electrospun carbon-polymer composites (Table 2-3).

**Table 2-3: Conductive Carbon-Polymer Composite Electrospinning**

<b>Carbon Material</b>	<b>Scaffold Fabrication</b>	<b>Other Materials</b>	<b>Application</b>	<b>Year &amp; Reference</b>
GO/rGO	Electrospinning	Blend PCL	General Tissue Engineering	2015 <sup>15</sup> , 2016 <sup>61</sup>
rGO	Electrospinning	Blend PVP/MnCo <sub>2</sub> O <sub>4</sub>	Biosensor	2015 <sup>14</sup>
Graphene	Electrospinning	Blend SF	Bone Tissue Engineering	2017 <sup>62</sup>
Graphene	Electrospinning	Blend PVA/alginate	Neural Tissue Engineering	2017 <sup>16</sup>
CB	Electrospinning	PU	General Conductivity	2007 <sup>60</sup>
rGO	Electrospinning	SF	General Tissue Engineering	2018 <sup>63</sup>
GO/rGO	Electrospinning	PVA	N/A	2012 <sup>64</sup>

Many groups used the solvent mixing process in creating the composite: the carbon material was ultrasonicated in the solvent, followed by the addition of the polymer.<sup>14-16,61-63</sup> Surfactants have also been used.<sup>16</sup> However, if there are issues with dispersion, *in situ* polymerization may be a good option.

The interaction between the filler and matrix is very important, so concentration of rGO should be optimized. Nalvuran *et al.* used rGO in SF at 0.1, 1 and 2 w/v% rGO,<sup>63</sup> while Ramazani and Karimi used rGO in PCL at 0.1, 0.5 and 1 wt.% rGO and found 0.1 wt.% to be the critical loading concentration. Above this concentration the sheets stack together instead of dispersing well within the PCL matrix; they have stronger interactions within themselves compared to with PCL. The authors proposed that the -CH<sub>2</sub> groups of PCL interact with the  $\pi$ -orbitals as well as through van der Waals interactions. These bonds are stronger than the hydrogen bonds between PCL and GO (because more equilibrium stress was found in rGO/PCL fibers compared to GO/PCL fibers).<sup>15</sup> High concentrations of graphene and thus incomplete dispersion of graphene can disrupt jet flow and clog the needle.<sup>62</sup>

The conductive nature of the carbon filler affects the electrospinning process. The conductive particles with their sp<sup>2</sup> hybridization domains, conjugated  $\pi$  bonds and free electron transport, result in higher electric charge storage in the polymer solution.<sup>61</sup> Usually with higher conductivity, it takes longer for the charges to dissipate so the fiber diameter is decreased (also noted in Table 2-2). Both conductivity ( $\sigma$ ) and permittivity ( $\epsilon$ ) affect electrospinning and are related through the charge relaxation time ( $\tau_c$ ) as seen in Equation 2-5.<sup>61</sup>

$$\tau_c = \frac{\epsilon}{4\pi\sigma} \quad (2-5)$$

The carbon filler also affects viscosity, where attraction and increased bonding increases viscosity, while repulsion and decreased bonding decreases viscosity.<sup>64</sup> For example, Tan *et al.* electrospun GO and rGO with poly(vinyl alcohol) (PVA) and found that GO increased the overall amount of hydrogen bonding and viscosity. On the other hand, rGO did not form hydrogen bonds with PVA and disrupted the PVA inter-chain hydrogen bonding; this overall decrease in hydrogen bonding decreased the viscosity.<sup>64</sup> As

mentioned earlier, viscosity is an important parameter in electrospinning and affects chain entanglement; this then affects how much electrostatic force is needed to form non-beaded, uniform fibers.<sup>53</sup> Viscosity, related to solution concentration as noted in Table 2-2, also affects fiber diameter.

## **2.8 Scaffold Porosity**

A challenge with scaffold fabrication by electrospinning is the small pore size and overall porosity values of electrospun scaffolds. This is a result of the small fiber diameters that encourage cell adhesion but pack together densely in scaffold form, therefore reducing pore area and interconnectivity and overall porosity.<sup>2</sup> Larger, more interconnected pores and high overall porosity values are required for greater cell migration and nutrient diffusion (as introduced in Chapter 2.1). Larger pores allow the cells to infiltrate into the scaffold instead of being restricted to surface growth. A normal cell diameter is about 10-15  $\mu\text{m}$ , while nanofiber scaffolds typically have pore diameters of only 1-10  $\mu\text{m}$  indicating a current problem in electrospun scaffolds. Cell infiltration is extremely important in tissue engineering, as it is associated with vascularization and overall tissue maturation.<sup>3</sup>

### **2.8.1 Importance of Cell Infiltration**

Cell infiltration allows the cell to experience a more realistic 3D environment; 3D scaffolds better recapitulate the ECM as compared to a 2D cell culture and this positively affects the cell behavior.<sup>65</sup> Cell adhesion, mechanotransduction and diffusible factors all impact cell behavior and these parameters differ in 2D environments as compared to 3D environments. For example, cell geometry changes based on whether adhesions to the scaffold or ECM are formed on one surface of the cell or surrounding the cell. As well, mechanotransduction, electrical stimulation and different forces in the body affect cell behavior, and the cell experiences these forces differently for both 2D and 3D environments. Diffusible factors also regulate certain cell processes by forming gradients in the ECM. The gradients quickly reach equilibrium in a 2D environment, while the gradients are sustained for a longer time period in a 3D environment, which is beneficial

for the cell. Clearly a 3D environment benefits the cells, and cell infiltration is necessary for cells to take advantage of the electrospun scaffold 3D environment.<sup>65</sup>

### 2.8.2 Increasing Scaffold Porosity

There are a number of approaches to increase porosity and cell infiltration in electrospun scaffolds. Methods include ultrasonication,<sup>4</sup> salt leaching, cryogenic electrospinning, inclusion of a sacrificial polymer, laser irradiation, wet electrospinning using a bath collector, and a production of a combination of nanofibers and microfibers. Most of these methods have only emerged in the last few years<sup>3</sup> and have had their own successes and challenges in improving cell infiltration.

Ultrasonication is a post-electrospinning method in which the scaffold is subjected to ultrasonic vibrations to increase the porosity and pore sizes of the scaffold.<sup>4</sup> The scaffold is placed in a medium such as deionized water and the ultrasonic vibrations travel through the medium and mechanically separate the scaffold fibers shown in Figure 2-10 decreasing the spatial density of the fibers. Both ultrasonication time and energy can be adjusted to affect the porosity and pore sizes, and ultrasonication resulted in increased cell infiltration.<sup>4</sup>

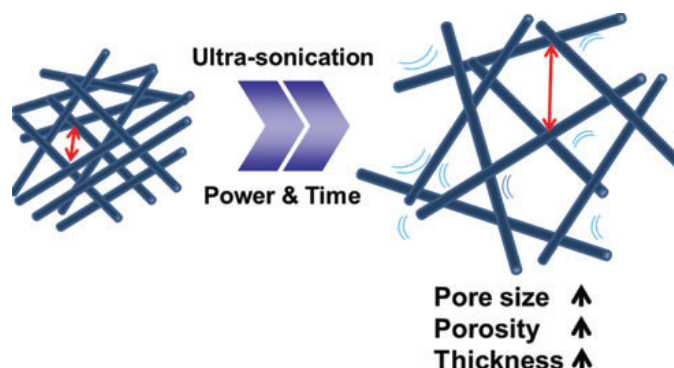


**Figure 2-10:** Schematic Illustration of Ultrasonication. Reproduced from Ref<sup>4</sup> with permission from Mary Ann Liebert, Inc.

Inclusion of a sacrificial polymer is a method in which two polymers (one of which is water soluble) are electrospun together.<sup>66</sup> Once the composite scaffold is formed, the scaffold is immersed in water in order to leach out the water-soluble, sacrificial polymer,



leaving behind voids in the scaffold to improve cellular infiltration. Larger pores and less dense scaffolds were observed and cellular infiltration improved with increasing percentages of sacrificial polymer electrospun.<sup>66</sup> Figure 2-11 shows poly(ethylene glycol) (PEG) as a sacrificial fiber as spun, and dissolved after the leaching stage. This figure also shows that the ratios of the two polymers are often altered to achieve desirable levels of both mechanical integrity and porosity for cell infiltration.

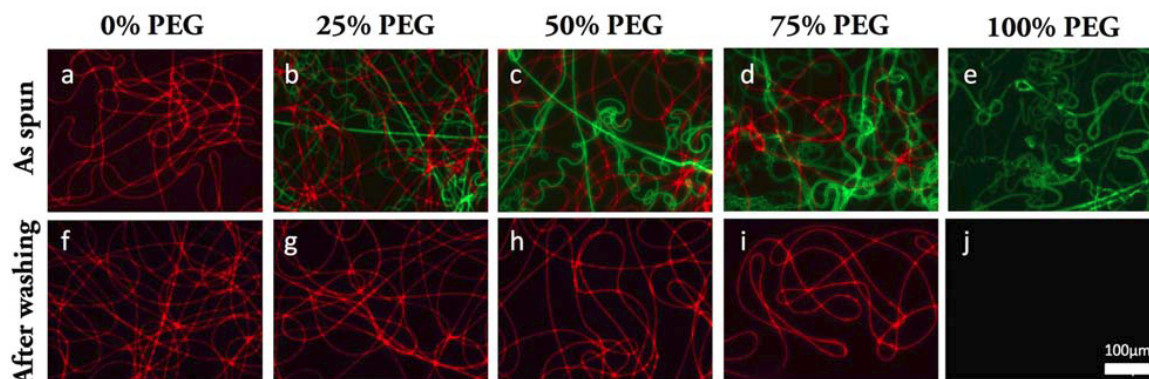


**Figure 2-11:** Different ratios of water-insoluble and water-soluble polymers. a-e: as spun composite scaffold with PLGA fibers (red) and PEG fibers (green) f-j: post leaching of PEG. Reproduced from Ref<sup>67</sup> and author retains copyright of this open access article.

Poly(ethylene oxide) (PEO) has commonly been used as a sacrificial polymer for its water solubility.<sup>66</sup> Poly(vinyl pyrrolidone) (PVP) has also been used in composite scaffolds and leached out using water,<sup>68</sup> but not for the specific application of a sacrificial polymer.

### 2.8.3 Image Analysis

Image analysis can be used to evaluate scaffold porosity of a 2D SEM image, by measuring individual pore areas as well as overall scaffold porosity or % porosity (total pore area compared to total scaffold area). Scaffold percolative efficiency (SPE) as introduced by Tehrani *et al.*<sup>69</sup> can also be measured, and reflects pore interconnectivity and how well cells can migrate through the scaffold. SPE (unitless) considers % porosity as well as a factor of interconnectivity (b) where SPE follows Equation 2-6.

$$SPE = \frac{\% \text{ porosity}}{|b|} \quad (2-6)$$

The interconnectivity factor is determined through a simulation; 6 sections of a 2D scaffold image are overlapped one layer at a time and the % porosity of each accumulated layer is calculated and graphed. The graph is fit to an exponential curve  $F(x)$  (Equation 2-7), and the interconnectivity factor is the exponential coefficient ( $b$ ).

$$F(x) = ae^{bx} \quad (2-7)$$

The interconnectivity factor represents the blocking rate of interconnected pores: the less interconnected the pores, the faster the pore channel is blocked. Thus the exponential curve is steeper with a larger absolute value of  $b$  and a smaller SPE value. SPE has been shown to correlated with in vitro cell infiltration results.<sup>69</sup>

## 2.9 Objectives

The overall objective of this study is to address challenges of electrospun PEA scaffolds, which limit the potential for proper tissue maturation. PEA, being a non-conductive material, does not facilitate electrical stimulation, which is critical for applications such as cardiac and neural tissue engineering. Furthermore, the electrospun fibers pack too densely and limit cell infiltration. Specifically this study aims to:

- (i) modify the conductivity of PEA scaffolds by incorporating rGO into films and fibrous scaffolds. rGO was synthesized and incorporated into PEA films. rGO was incorporated into blend PEA and coaxial PEA-chitosan scaffolds, and electrospinning parameters were optimized. Scaffold conductivity and cell behavior on the scaffold were evaluated.
- (ii) modify the porosity of the electrospun PEA scaffolds. Ultrasonication and inclusion of a sacrificial polymer were combined and the effects on scaffold porosity were evaluated

## Chapter 3

### 3 Materials and Methods

This chapter details the methodologies used to modify the conductivity and porosity of electrospun PEA scaffolds.

#### 3.1 Materials

L-phenylalanine, anhydrous sodium carbonate ( $\text{Na}_2\text{CO}_3$ ) and chitosan (CS, 85% de-acetylated) were purchased from Alfa Aesar. 1-4 Butanediol was purchased from J.T. Baker. Potassium permanganate ( $\text{KMnO}_4$ ) was purchased from EMD Millipore. Sebacoyl chloride, *p*-toluene sulfonic acid monohydrate, graphite (flakes, -100 mesh), phosphorous pentoxide ( $\text{P}_2\text{O}_5$ ), potassium persulfate ( $\text{K}_2\text{S}_2\text{O}_8$ ), L-ascorbic acid (L-AA), hydroiodic acid (HI, 57%), reduced graphene oxide (rGO, >6 S/cm), poly (ethylene oxide) (PEO), poly(vinyl pyrrolidone) (PVP), and 5-azacytidine (5-aza) were purchased from Sigma-Aldrich. Vibrant DiI cell-labeling solution and CyQuant Cell Proliferation Assay kit were purchased from Invitrogen. Sulfuric acid ( $\text{H}_2\text{SO}_4$ , 98%), hydrogen peroxide ( $\text{H}_2\text{O}_2$ , 30%), hydrochloric acid (HCl, 37%), ammonium hydroxide ( $\text{NH}_4\text{OH}$ , 28%), dichloromethane (DCM), ethyl acetate, N,N-dimethylformamide (DMF), glacial acetic acid (AcOH, 99%), and methanol (MeOH) were purchased from Caledon. Toluene was purchased from Fischer, ethanol (EtOH, 95%) was purchased from Commercial Alcohols and chloroform ( $\text{CHCl}_3$ ) was purchased from VWR. Trizol reagent was purchased from ThermoFisher Scientific. Dulbecco's Modified Eagle Media (DMEM) and Hanks' Balanced Salt Solution (HBSS) was purchased from Gibco, and Mesenchymal Stem Cell Expansion Media was purchased from Cellular Engineering Technologies. 10T1/2 cells (from mouse embryos) were purchased from ATCC, and induced pluripotent stem cell-derived mesenchymal stem cells (iPSC-derived MSCs) were a gift from Dr. Laird's Lab at the University of Western Ontario.

#### 3.2 Monomer and Polymer Synthesis

Both the 8-Phe-4 PEA polymer and its precursor monomer PB-*p*-toluene sulfonate salt monomer were synthesized and characterized as follows.

### 3.2.1 Monomer Synthesis

PB-*p*-toluene sulfonate salt was the monomer synthesized using lab protocol and using a molar ratio of 2:1:2 of L-phenylalanine, 1, 4-butanediol, and *p*-toluene sulfonic acid monohydrate respectively in an acid-catalyzed condensation. The reaction scheme is shown in Appendix 1.

10.0 g of L-phenylalanine, 2.44 mL of 1,4-butanediol and 12.5 g of *p*-Toluene sulfonic acid monohydrate were added to a round-bottom flask attached to a Dean-stark apparatus, and refluxed in toluene at 140 °C for 48 h. The monomer was then purified: it underwent vacuum filtration while being washing with toluene, followed by a first recrystallization in deionized water (deionized H<sub>2</sub>O) that included hot filtration followed by overnight precipitation in a refrigerator. Another recrystallization in deionized H<sub>2</sub>O was carried out before a final vacuum filtration. There was some batch-to-batch variation, and yields ranged between 40 and 55%. Monomer purity was confirmed using <sup>1</sup>H NMR shown in Appendix 2.

### 3.2.2 Polymer Synthesis

The PEA synthesized by interfacial polymerization as per in-house established procedure<sup>70</sup> was a PBSe, an abbreviation for L-phenylalanine – 1,4-butanediol – sebacoyl chloride. More specifically the PEA was labeled 8-Phe-4, indicating that the polymer has 8 methylene groups from the sebacoyl chloride and 4 methylene groups from the 1,4-butanediol. PEA was synthesized using a molar ratio of 1:1:2 of the PB-*p*-toluene sulfonate salt monomer, sebacoyl chloride and Na<sub>2</sub>CO<sub>3</sub> respectively. The reaction scheme is presented in Appendix 1.

PB salt monomer (3.3 g) and 0.96 g of Na<sub>2</sub>CO<sub>3</sub> were dissolved in 15 mL of deionized H<sub>2</sub>O in a round bottom flask, and then connected to an addition funnel closed off except to a nitrogen balloon. 7.5 mL of DCM was added into the addition funnel, followed by 0.78 mL of sebacoyl chloride and another 7.5 mL of DCM. The contents of the additional funnel were slowly added to the PB monomer and left to react for 12 h. The DCM solvent was removed in vacuo using a RotoVap, and excess water was also removed. The polymer was then purified using a Soxhlet extractor with ethyl acetate at 110 °C for 48 h, and then cut into small pieces and dried in vacuo. There was some batch-to-batch variation with yields between 50 and 80%, molecular weights (M<sub>n</sub>) between 40 and 80 kDa, and a polydispersity index (M<sub>w</sub>/M<sub>n</sub>) between

1.7 and 2.2. Gel permeation chromatography gave the molecular weight and polydispersity index.  $^1\text{H}$  NMR confirmed the purity of the polymer shown in Appendix 2.

### 3.3 GO and rGO Synthesis

Both rGO and its precursor GO were synthesized in the lab. Two different reducing agents were used to prepare rGO: L-AA and HI. Different characterizations confirmed successful preparation.

#### 3.3.1 GO Synthesis

Graphene oxide (GO) was synthesized using the modified Hummer's method with a pre-oxidation step as adapted by Kovtyukhova,<sup>42</sup> and reported in literature.<sup>71</sup> 1 g of flake graphite was combined with 12 mL  $\text{H}_2\text{SO}_4$ , 2.5 g of  $\text{K}_2\text{S}_2\text{O}_8$  and 2.5 g of  $\text{P}_2\text{O}_5$  and reacted for 6 h at 80 °C. The solution was quantitatively transferred into 500 mL of chilled deionized  $\text{H}_2\text{O}$  and stirred overnight. Pre-oxidized graphite was filtered (0.45  $\mu\text{m}$  membrane filter), washed with deionized  $\text{H}_2\text{O}$  and left overnight at ambient conditions to be dried. Pre-oxidized graphite was stirred with 17 mL  $\text{H}_2\text{SO}_4$  for 10 min. 15 g  $\text{KMnO}_4$  and 5 mL  $\text{H}_2\text{SO}_4$  were slowly added over 30 min to the solution in an ice bath to ensure temperature remained below 15 °C. The combination of  $\text{KMnO}_4$  and  $\text{H}_2\text{SO}_4$  resulted in the active oxidizing species diamanganese heptoxide ( $\text{Mn}_2\text{O}_7$ ). The solution was removed from ice bath and stirred for 3 h, while the temperature was maintained to 35°C. Subsequently, it was transferred into 250 mL of chilled deionized  $\text{H}_2\text{O}$  in an ice bath - to ensure temperature remained below 50 °C – and stirred for 4 h. Finally, it was transferred into 700 mL of deionized  $\text{H}_2\text{O}$  and 20 mL of 30%  $\text{H}_2\text{O}_2$  was added to quench the reaction and react with any remaining  $\text{Mn}_2\text{O}_7$  before the solution was centrifuged (Beckman-Coulter Allegra X-22R) for 5 min at 4500 RPM (3900g) and the supernatant was discarded. The solid graphite oxide was washed through centrifugation, where the supernatant was discarded after each wash. There were 3 cycles of washing with 10% HCl through centrifugation for 5 min each at 4500 RPM (3900g) to remove metal ions. There were then 5 cycles of washing with deionized  $\text{H}_2\text{O}$  through centrifugation (Sorvall RC6 Plus) for 10 min each at 10,000 RPM (15,000g). The supernatant was removed at each stage and the resultant solid was dried under vacuum at 50 °C for 24 h.<sup>72</sup> The product was graphite oxide, which is bulk or multi-layered graphene oxide, and has the same chemical structure as

GO; ultrasonication was required to separate the multiple layers of graphite oxide and produce GO.

### 3.3.2 rGO Synthesis

Two separate reducing agents were used to reduce GO to form reduced graphene oxide (rGO): L-ascorbic acid (L-AA) and hydroiodic acid (HI).

With the L-AA reduction, a protocol from Xu *et al.* was followed until the filtration step.<sup>30</sup> 0.1 mg/mL graphite oxide was used. 30 mg of solid graphite oxide from the previous step was dispersed in 300 mL of deionized H<sub>2</sub>O through 90 min of ultrasonication (Branson 3210 Ultrasonic Bath). The solution was centrifuged (Beckman-Coulter Allegra X-22R) for 30 min at 4500 RPM (3900g) and the GO-containing supernatant was used in the reduction. 300 mg of L-AA was added to the supernatant along with approximately 400  $\mu$ L of NH<sub>4</sub>OH until the pH was approximately 9. The solution was ultrasonicated for 30 min (Branson 3210 Ultrasonic Bath) and then stirred for 2 h at approximately 95 °C. The solution turned from brown to black as expected with the reduction. Some of the solution was filtered (0.2  $\mu$ m membrane filter) to form a film that was characterized through FTIR and electrical conductivity measurements. The rest of the solution was poured into 20 cm of dialysis tubing (Spectra/Por, MWCO 12-14 kDa) and left in a 2 L dialysate of deionized H<sub>2</sub>O for 48 h with the dialysate changed regularly. Dialyzed solution was freeze-dried overnight (Labconco Freeze Dry System) to produce a powder, labeled 'rGO L-AA'.

With the HI reduction, a protocol was adapted from Dr. Xing's lab at the University of Manitoba.<sup>73</sup> Different concentrations of graphite oxide were used: 4 mg/mL ('HI1') and 2 mg/mL ('HI2') in 20 mL of deionized H<sub>2</sub>O. Probe sonication (Qsonica Misonix XL-2000) was used to disperse graphite oxide for 30 min. 2 mL of HI was added and the solution was stirred at room temperature for 16 h. Approximately 1.5 mL of NH<sub>4</sub>OH was added until the pH was neutral to quench the reaction. Some of the solution was filtered (0.2  $\mu$ m membrane filter) to form a film for FTIR characterization and electrical conductivity measurements, labeled either 'rGO HI1-1' and 'rGOH2-1'. The rest of the solution was poured into dialysis tubing and left in a dialysate of deionized H<sub>2</sub>O for 48 h with the dialysate changed regularly. The solution then went through a second round of reduction; once again 2 mL of HI was

added to the GO solution in a beaker and stirred for 16 h at room temperature. The neutralization, filtration and dialysis procedures were repeated once and finally the dialysis products were freeze-dried overnight to produce a powder, labeled either 'rGO HI1-2' or 'rGOH1-2'.

### **3.3.3 GO/rGO Characterization**

Solid graphite oxide was analyzed using FTIR (Attenuated Total Reflection FTIR, Bruker Vector 22) to confirm the addition of oxygen functional groups and thus the successful oxidation of graphite. rGO was also analyzed with FTIR to confirm the removal of the oxygen functional groups and the reduction of GO. Electrical conductivity measurements were taken on the solid graphite oxide and the rGO films, using the four-probe set-up as described in Section 3.5. Conductivity measurements were taken in triplicate, at different locations on the films.

## **3.4 rGO/PEA Composites**

rGO was incorporated with PEA and CS in both film and fibrous forms. Different rGO samples were used, including a purchased rGO and rGO HI2-2 synthesized in the lab. By using purchased rGO, it was possible to optimize rGO synthesis while optimizing electrospinning scaffold preparation simultaneously. As well, it was possible to confirm the similar effects between the purchased and experimentally prepared rGO.

### **3.4.1 Composite Film Preparation**

Blend rGO/PEA films were formed with varying concentrations of rGO: 0, 0.1, 0.5 and 1 wt.%. Purchased rGO was used. For the PEA control film (0 wt.% rGO), 2 wt.% PEA was dissolved in 1.58 mL DMF and was poured into a Teflon mold and left in a vacuum oven at 60 °C for 2.5 h. The same protocol was followed for the blend films, with an additional initial step: rGO at each respective concentration was dispersed in 1.58 mL DMF via ultrasonication (Branson 3210 Ultrasonic Bath) for 60 min prior to the addition of PEA. Blend rGO/CS films were also formed using the same protocol, using 2 w/v% CS in 1.5 mL 90% AcOH.

### 3.4.2 PEA Electrospinning

The electrospinning setup included a syringe pump (KD Scientific 200), a HV Power Supply (Gamma High Voltage Research) and a custom rotating mandrel collector. Becton-Dickinson 0.5 mL glass syringes were used with 22 gauge stainless steel needle spinnerets. PEA was electrospun at 5 wt.% (for a molecular weight ( $M_n$ ) of 60 kDa and adjusted appropriately for different molecular weights) in a 9:1 wt. ratio of  $\text{CHCl}_3$ :DMF.

### 3.4.3 Coaxial Electrospinning

The coaxial electrospinning setup used a prebuilt coaxial needle spinneret (Ramé-hart, 22 inner gauge and 18 outer gauge) with a luer coupling and tubing for the second syringe shown in Figure 3-1. The same syringe pump was used for both syringes. PEA was loaded into the core at the standard concentration and solvent. CS was loaded into the shell in 90% AcOH at 3.5 w/v%, which is lower than desirable, as the shell spinneret diameter limited more viscous solutions. A PEA-CS control was electrospun. 0.1 wt.% purchased rGO was included in either the PEA core solution, the CS shell solution or both solutions; the various combinations were labeled (rGO/PEA)-CS, PEA-(rGO/CS) and (rGO/PEA)-(rGO/CS) respectively. rGO was added to the polymer through the solvent mixing method; rGO was ultrasonicated in the appropriate solvent for 60-90 min prior to addition of the polymer and subsequent mixing. Working distance remained constant at 12 cm, while voltage and flow rate were optimized.



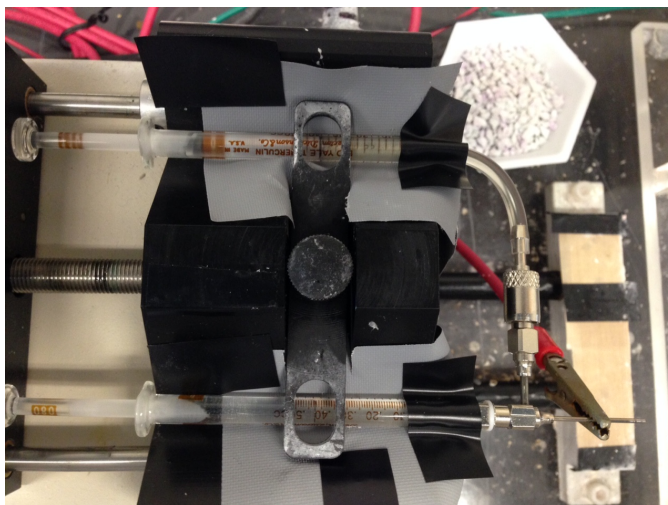


**Figure 3-1:** Coaxial electrospinning set-up, where two syringes are placed side by side and pushed by a single syringe pump. The lower syringe in the figure is connected directly into the core of the coaxial spinneret, while the upper syringe is connected through tubing and a luer connector to the shell of the coaxial spinneret. The coaxial spinneret is connected to the voltage supply.

#### 3.4.4 Blend Electrospinning

0.1 wt.% rGO was included into PEA for blend rGO/PEA fibrous scaffolds. In order to ensure sufficient rGO/PEA composite interaction, solvent mixing and *in situ* polymerization techniques were used. For the solvent mixing technique, as was used in coaxial electrospinning, rGO was ultrasonicated in 9:1 wt.%  $\text{CHCl}_3$ :DMF for 60-90 min prior to the addition of PEA and subsequent vortexing. Either purchased rGO or synthesized rGO (HI2-2) was used in blend fibrous scaffolds rGO/PEA B1 and B2 respectively. For *in situ* polymerization, 3 mg purchased rGO (~0.1 wt.% of expected product) was incorporated into the reaction through the addition of deionized  $\text{H}_2\text{O}$ . Prior to polymerization, rGO was ultrasonicated in 15 mL of deionized  $\text{H}_2\text{O}$  with the stir bar; this solution was then added to the PB monomer and  $\text{Na}_2\text{CO}_3$  during the reaction. All other PEA synthesis steps proceeded as normal. This fibrous scaffold was labeled rGO/PEA P. When electrospun with rGO, the PEA concentration was increased to 7 wt.% for the same molecular weight. Working distance remained constant at 12 cm, while voltage and flow rate were optimized.

### 3.4.5 Composite Scaffold Characterization

Scaffold morphology was imaged with scanning electron microscopy (SEM Hitachi S3400N). Samples were first sputter coated (Anatech Ltd. Hummer VI Sputtering System) with gold/palladium for 4 min and imaged with SEM at 10kV and 5000x magnification. Fiber diameters were measured using ImageJ. At least 50 fibers were measured in total, from 1 or 2 samples for each scaffold.

Core-shell fiber morphology was evaluated using transmission electron microscopy (TEM Phillips CM10) and confocal microscopy (Zeiss LSM800). For TEM, fibers were electrospun directly on uncoated copper grids for approximately 60 seconds before being imaged at 80kV. For confocal, 1  $\mu$ L of DiI was added to the core PEA solution prior to electrospinning, following a similar protocol.<sup>74</sup> Fibers were electrospun directly onto a microscope slide and then covered with mounting media and cover glass. Fibers were imaged at 63x magnification.

Electrical conductivity measurements were taken on the rGO/PEA composite films and fibrous scaffolds, using the four-probe or two-probe set-up as described in Section 3.5. Conductivity measurements were taken in triplicate, on different locations on the films or fibrous scaffolds.

### 3.5 Electrical Conductivity

Electrical conductivity measurements were done using either a four-probe or a two-probe set-up. The four-probe method was used for GO, rGO and composite films, while the two-probe method was used for the fibrous scaffolds. Some background introduction to these methodologies is discussed in Chapter 2.6. With the four-probe method, four pin probes 2 mm apart were placed on the surface of the scaffold. Using a Keithley 2611 SourceMeter (a source measure unit), current was sourced through the outer probes and voltage was measured through the inner probes. The set-up can be seen in Appendix 3. Measured resistance was converted to surface resistance, and thickness used to calculate conductivity. Thickness was measured using an analog micrometer (Mitutoyo 111-166).

With the two-probe method, the fibrous scaffold was clamped between two 3.3 cm diameter copper electrode plates connected to the source measure unit as seen in Appendix 3.

Measured resistance, contact surface area and thickness were used to calculate bulk resistivity and then conductivity. The source current was varied and the associated voltage was measured and recorded in order to generate current-voltage (IV) curves.

### **3.6 Cell Proliferation and Differentiation**

Three scaffolds were chosen for cell experiments, including the PEA control, the rGO/PEA P blend scaffold (*in situ* polymerization), and the (rGO/PEA)-CS coaxial scaffold. Fibers were electrospun onto aluminum foil. Cell proliferation of each scaffold was evaluated using 10T1/2 cells, while potential to facilitate cardiac differentiation was evaluated using human mesenchymal stem cells (MSCs).

#### **3.6.1 Cell Proliferation**

10T/2 cells were used to ensure that the scaffolds were not cytotoxic. A 2D control (tissue culture plastic) was used along with the three fibrous scaffold samples; the experiment was done in triplicate. Samples were cut to fit into 12-well plate, secured in plate with grease and sterilized with 70% EtOH. 100,000 cells were seeded per well and cultured in DMEM media with 5% FBS, penicillin/streptomycin (P/S(+)) for 1, 3 or 7 days. Media was changed at day 3 for day 7 samples. CyQuant Cell Proliferation Assay kit was used. For the 2D control, media was removed and 200  $\mu$ L lysis buffer was added to well. Cells were scrubbed off the bottom of the well plate, and the lysis buffer (with cells) was returned to an Eppendorf tube and left in -80  $^{\circ}$ C until all the samples were collected. The fibrous scaffold samples were removed from well-plate and put in the lysis buffer in an Eppendorf tube left in -80  $^{\circ}$ C until all the samples were collected. Once all the samples were collected, the samples were thawed, vortexed and refrozen. 180  $\mu$ L of lysis buffer containing cell material from each sample tube was transferred to a black 96 well plate with a clear bottom. Right before the fluorescent reading, 20  $\mu$ L of Cyquant GR dye working solution was added to the well plate and incubated for 5 min while shaking in the Tecan Infinite M1000 Pro fluorescence plate reader.

#### **3.6.2 Cell Differentiation**

Mesenchymal stem cells (MSCs) derived from induced pluripotent stem cells (iPSCs) were used. Scaffolds were cut to fit into 12-well plate, secured in plate with grease and sterilized with 70% EtOH. Scaffolds were coated with 0.1% gelatin for 1 h at 37  $^{\circ}$ C before cell seeding.

The cells were seeded at a density of 20,000 cells/cm<sup>2</sup> and cultured with stem cell complete medium (MSC Expansion Media) until confluent. For the first experiment, 50 µg/mL of L-ascorbic acid (L-AA) was added once and cells were cultured for 3 and 7 days. One well was used for each scaffold and time point. For the second experiment, 10 µM of 5-azacytidine (5-aza) was added for 24 h following a HBSS wash and media change and cells were cultured for 7 days; this was repeated on day 7 for the cells cultured for 14 days. The HBSS wash and media change was required to minimize any cell death from lengthy exposure to 5-aza.<sup>31</sup> Two wells were used for each scaffold and time point. At each time point, total RNA was extracted using Trizol reagent: manufacturer's instructions were followed. Complementary DNA was synthesized using 1 µg total RNA primed with random primers; the Pomegra Random Hexamers (ThermoFisher Scientific) protocol was followed. qRT-PCR was carried out in 10 µL reaction volumes, using a CFX96 Real-Time System (C1000 Touch Thermal Cycler, Bio-Rad), and determined with iQ SyBR Green Supermix (Bio-Rad); manufacturer's instructions were followed. Human GATA binding protein 4 (GATA-4) was the first gene of interest, and had the forward and reverse sequence of GCTCCTTCACTTCCAACATCT and GGGAGAGACATGTACAAGCTG. Human Nkx2.5 was the second gene of interest, and had the forward and reverse sequence of GCACCCACCCGTATTTATGTT and GGGTCAACGCACTCTCTTTAA.

### **3.7 Combination of Ultrasonication and Sacrificial Polymer**

In order to improve porosity of PEA electrospun scaffolds and allow for cell infiltration, ultrasonication and sacrificial polymer methods were combined. First, sacrificial polymer (PEO and PVP) electrospinning parameters were optimized. Next, scaffold modification parameters were optimized, including ultrasonication time and medium, and sacrificial polymer ratio and leaching time. Image analysis was used to evaluate changes in scaffold porosity.

#### **3.7.1 Sacrificial Polymer Electrospinning**

PEO was electrospun starting with parameters found in literature<sup>66</sup> and further adjusted. 25% (w/v) PEO in 3:2 deionized H<sub>2</sub>O:EtOH was electrospun at 20 kV and 0.2 mL/h through a 22 gauge needle at a working distance of 12 cm from the rotating mandrel collector. PVP was

also electrospun starting with parameters found in literature<sup>68</sup> and further adjusted. 8% (w/v) PVP in 4:1 CHCl<sub>3</sub>:MeOH was electrospun at 20 kV and 0.4 mL/h through an 18 gauge needle at a working distance of 9 cm from the rotating mandrel collector. Images of both sacrificial polymer fibers can be seen in Appendix 5. PEA was electrospun with a sacrificial polymer, either PVP or PEO. Electrospinning was sequential, with alternate layers of PEA and the sacrificial polymer, resulting in multi-layered composite scaffolds. Three different ratios of sacrificial polymer to PEA were used, including 25/75, 50/50 and 75/25 sacrificial polymer/PEA.

### **3.7.2 Scaffold Porosity Modification**

For ultrasonication, time and medium were optimized. Scaffolds were immersed in a medium in an ultrasonicator bath, for either 1, 10 or 30 min. A number of media were used, including water, ethyl acetate and aqueous EtOH solutions. After ultrasonication, the scaffolds were vacuum-dried for 48 h. SEM images were used to select time and medium; fiber diameters before and after ultrasonication for each medium were measured using ImageJ.

For leaching of a sacrificial polymer, leaching time and ratio of sacrificial polymer were optimized. The multi-layered composite scaffolds were immersed in 90% EtOH solutions for up to 72 h in order to leach out the sacrificial polymer. Three different ratios of sacrificial polymer to PEA were used in order to find the optimal balance between increased scaffold porosity and maintained scaffold mechanical integrity.<sup>67</sup> SEM images were used to select leaching time and ratio of sacrificial polymer. After leaching, the scaffolds were vacuum-dried for 48 h. The multi-layered composite scaffolds were additionally modified by combining both ultrasonication and leaching of the sacrificial polymer. The scaffolds were ultrasonicated for 30 min in 90% aqueous EtOH and left immersed for 72 h to leach out the sacrificial polymer.

### **3.8 Porosity Image Analysis**

Samples were prepared for SEM (Hitachi 2400N) by sputter-coating (Anatech Ltd. Hummer VI Sputtering System) with gold for 3 min. In the SEM, a voltage of 10kV was used. Images were taken at 1000x, 2500x and 5000x magnification.

ImageJ was the software used for image analysis. A protocol was created and implemented to measure the average pore area, overall % porosity and SPE of each image. Pore area and SPE were considered to be useful parameters; a certain pore area is required to allow the cell to fit through the pore and a certain level of interconnectivity is needed to allow the cell to travel throughout the scaffold.

Once the scale was calibrated in ImageJ, the top 1 or 2 fibrous layers were selected manually and labeled with a binary mask shown in Figure 3-2A. This step is necessary as the SEM images show the multiple layers that make up the scaffold, while the quantification parameters refer to a single scaffold layer. ImageJ measured the pore areas, and average pore area and overall % porosity was calculated.

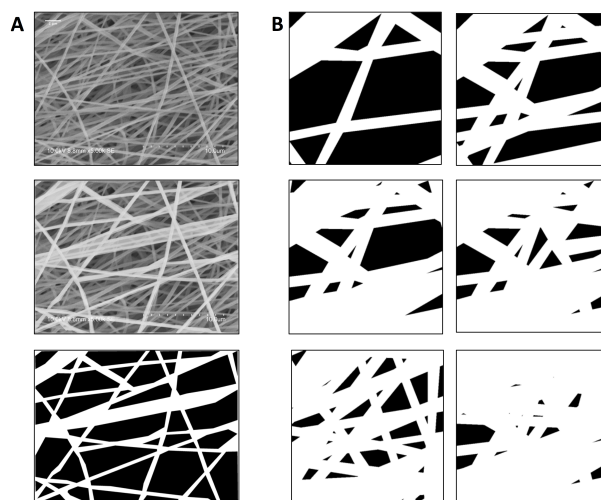


**Figure 3-2:** Image Analysis. A) Top layer selection with binary mask. B) SPE layer accumulation.

SPE was calculated by overlapping six sections of the binary mask one layer at a time as shown in Figure 3-2B. The % porosity was measured at each accumulation of layers, graphed and fit by an exponential curve. The absolute value of the exponential coefficient was used as the interconnectivity factor and SPE was calculated using Equation 2-6.

### 3.9 Statistical Analysis

GraphPad Prism 4 was used for statistical analysis. For conductivity data, triplicate measurements were performed on each sample. A standard t-test was used to compare

different samples against the control sample. For fiber diameter data, at least 50 fibers total were measured from one or two scaffolds, and a one-way ANOVA was used for analysis. For the cell differentiation study, a two-way ANOVA was used to analyze the qPCR data. For porosity data, triplicate experiments were performed. A standard t-test was used to compare means of Gaussian distribution data against the control, while a non-parametric t-test was used to compare medians against the control for the data that did not follow a Gaussian distribution.  $P < 0.05$  was considered as statistically significant.

## Chapter 4

### 4 Results and Discussion

This chapter presents and discusses the results of the different experiments.

#### 4.1 GO and rGO Synthesis

The preparation of rGO occurred through the oxidation-reduction method: the oxidation of graphite to form GO and the reduction of GO to form rGO. During GO synthesis in the pre-oxidation step, the solution was a dark-blue. During oxidation, the addition of  $\text{KMnO}_4$  in  $\text{H}_2\text{SO}_4$  resulted in initial dark green color of the solution and then dark black-purple. With the addition of  $\text{H}_2\text{O}_2$  the solution changed to a bright yellow, changed to a yellow-brown throughout the washing stages, and dried as a brown solid. During rGO synthesis, the brown solution turned to black and resulted in some precipitation of black agglomerates.

FTIR was used to confirm the addition and then the removal of oxygen functional groups through the oxidation and reduction processes respectively. Figure 4-1A shows the presence of hydroxyl groups around  $3400\text{ cm}^{-1}$ , carboxyl groups around  $1600\text{ cm}^{-1}$ , C-OH stretching around  $1200\text{ cm}^{-1}$  and epoxide groups around  $1000\text{ cm}^{-1}$  in the GO sample. There are also small peaks representing the carbonyl groups around  $1750\text{ cm}^{-1}$  and hydroxyl deformation around  $1400\text{ cm}^{-1}$ . Figure 4-1A also shows the absence of these groups with rGO. One representative sample of rGO is shown, as differences in reducing agent (either L-AA or HI) did not significantly change the FTIR results. Both methods removed the majority of the oxygen functional groups.



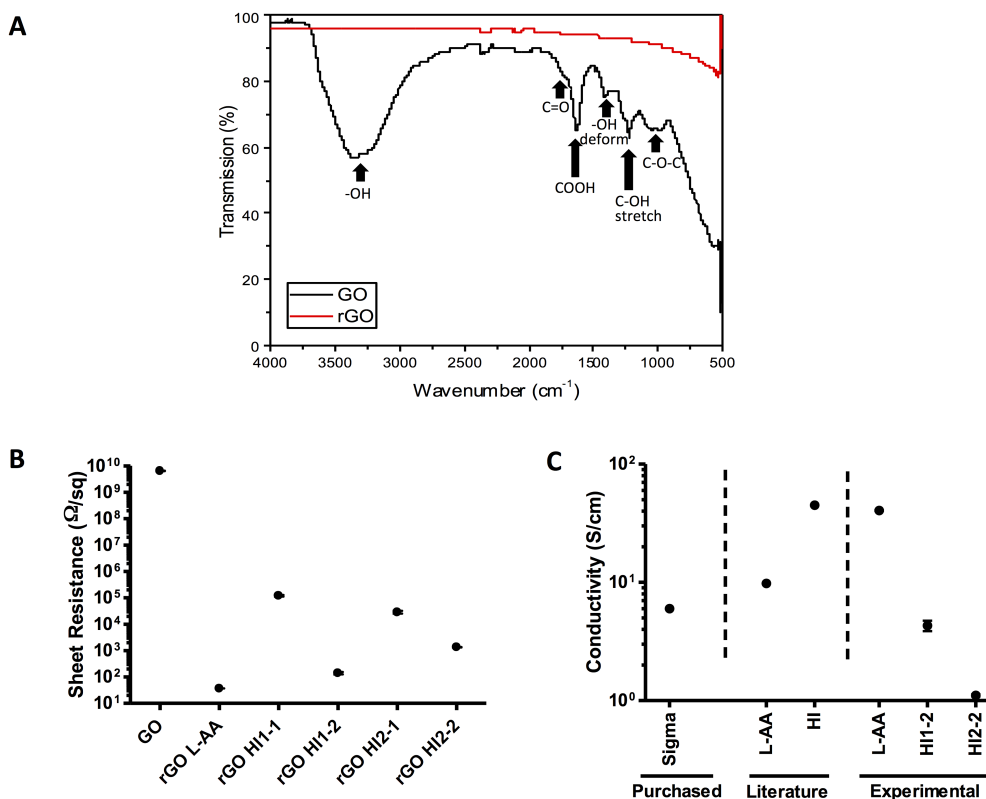


**Figure 4-1: rGO Reduction.** A) GO and rGO FTIR where rGO was reduced by L-ascorbic acid and is representative of all rGO reductions. B) GO and rGO sheet resistance varied with reduction condition. rGO was reduced by either L-ascorbic acid (L-AA) or hydroiodic acid (HI). HI reduction was completed using GO concentrations of 4 mg/mL and 2 mg/mL (HI1 and HI2 respectively) and over 1 or 2 rounds of reduction (HI1-1 and HI1-2 for example respectively). C) rGO conductivity comparing experimental samples with purchased samples (Sigma-Aldrich) and literature values where Xu reported the L-AA sample<sup>30</sup> and Hu reported the HI sample.<sup>44</sup> Triplicate measurements on each sample were conducted for experimental measurements.

Electrical conductivity of the different rGO films was measured to determine the degree of reduction compared to the GO control. This provides useful additional information compared to FTIR, as it allows a comparison between the different reduction methods. The sheet resistance of GO and the various rGO samples was compared, as the samples could be considered thin films and thickness was not required for the calculation. The lower the sheet resistance, the higher the conductivity as described in Equation 2-1 and 2-2, and rGO L-AA had the lowest sheet resistance as seen in Figure 4-1B. rGO HI had two different starting GO concentrations (4 mg/mL and 2 mg/mL for rGO HI1 and HI2 respectively), and required a

second round of reduction (HI1-2 and HI2-2) to achieve a lower sheet resistance that is comparable with rGO L-AA. After the second reduction, a lower sheet resistance was achieved with HI1-2 at 4 mg/mL starting GO concentration, compared to HI2-2. While rGO L-AA had a lower sheet resistance compared to the rGO HI samples, the L-AA reduction method had limited potential for scale up with the lowest starting GO concentration (0.1 mg/mL).

Sheet resistance comparisons were suitable to compare the different experimental reaction conditions; however, in order to compare results to literature values and the purchased product, conductivity was considered. The conductivity comparison is seen in Figure 4-1C, and all values were between 1 and 100 S/cm. Overall, different GO reduction methods and conditions were explored and rGO was synthesized with an electrical conductivity comparable to the purchased product.

## **4.2 rGO/PEA Composite Films and Fibrous Scaffolds**

rGO (either purchased or synthesized) was incorporated into PEA and CS to form composite films and electrospun fibrous scaffolds. Electrospinning parameters were optimized.

### **4.2.1 rGO/PEA Films**

PEA films were fabricated with varying concentrations of purchased rGO (0, 0.1, 0.5 and 1 wt.%) and the film resistance was measured with the 4-probe set-up. The different films and their respective resistances are shown in Figure 4-2A and C. At concentrations of 0.5 wt.% rGO and above, the films primarily contained rGO and were non-uniform and contained void spaces; these films reduced the film resistance by at least  $10^4$ . At 0.1 wt.%, this composite film was more uniform, contained no void spaces and still resulted in a significantly lower film resistance compared to the PEA control.

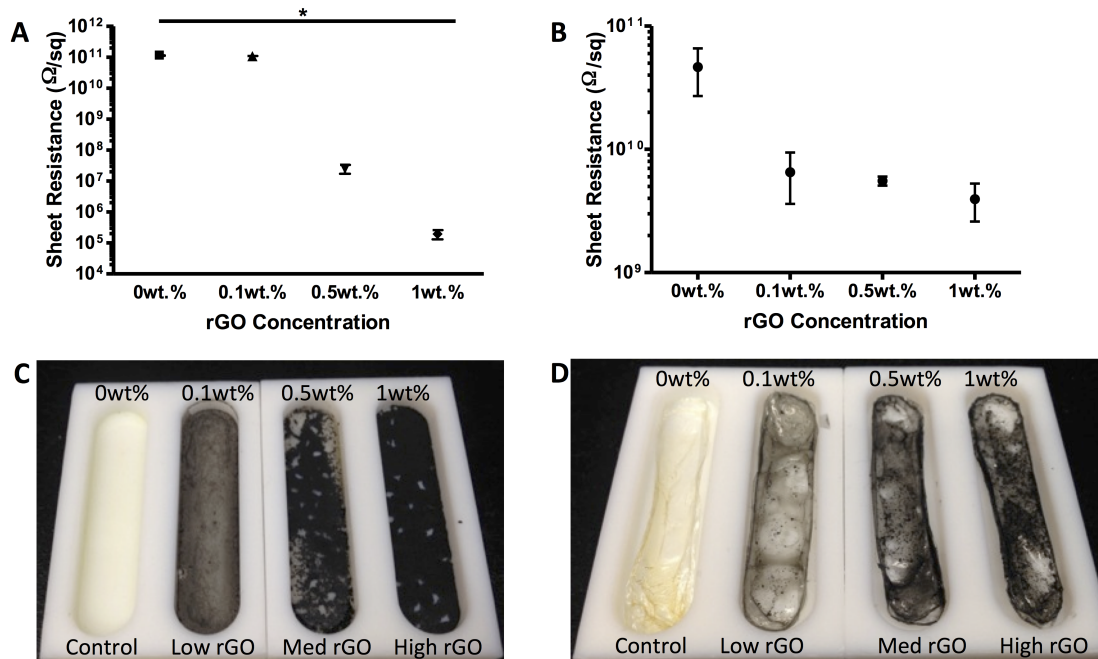


**Figure 4-2:** Composite rGO/PEA (A,C) and rGO/CS (B,D) films, showing the effect of rGO concentration on film resistance (A,B) and film uniformity (C,D). Purchased rGO was used. 3 replicates were measured on each sample, \* represents  $p < 0.05$ .

CS films with the same varying concentrations of rGO (0, 0.1, 0.5 and 1 wt.%) were also fabricated as CS was used with PEA during coaxial electrospinning. Figure 4-2B and D show the films and their respective resistances. rGO did not disperse as well and all three films with rGO were non-uniform and did not significantly reduce the film resistance; this was noted for future electrospinning studies. Based on this data, 0.1 wt.% rGO was used for subsequent studies.

#### 4.2.2 Coaxially-spun Fibrous Scaffolds

With coaxial electrospinning, PEA was loaded into the core compartment while CS was loaded into the shell compartment, forming the PEA-CS control. This combination was used so that PEA could reinforce the fiber mechanical properties while CS could favorably interact with cells. In Figure 4-3, PEA-CS showed separate PEA fibers and electrospayed CS droplets. The addition of rGO resulted in the removal of electrospayed droplets. rGO was added either to the PEA solution, to the CS solution or to both solutions before being loaded into the syringe. When rGO was added to the CS shell, labeled PEA-(rGO/CS), the resultant

fibers had a relatively narrow diameter distribution but were non-uniform with beads present. This changed when rGO was added to the PEA core, labeled (rGO/PEA)-CS, where the resultant fibers had a wider diameter distribution but had non-beaded fibers. The fiber diameter distribution increased again when rGO was included in both the core and the shell, labeled (rGO/PEA)-(rGO/CS), with non-beaded fibers once again. (rGO/PEA)-CS was considered to have the best fiber morphology, with its Gaussian distribution and uniform, non-beaded fibers. As a result, (rGO/PEA)-CS was used for further experiments.

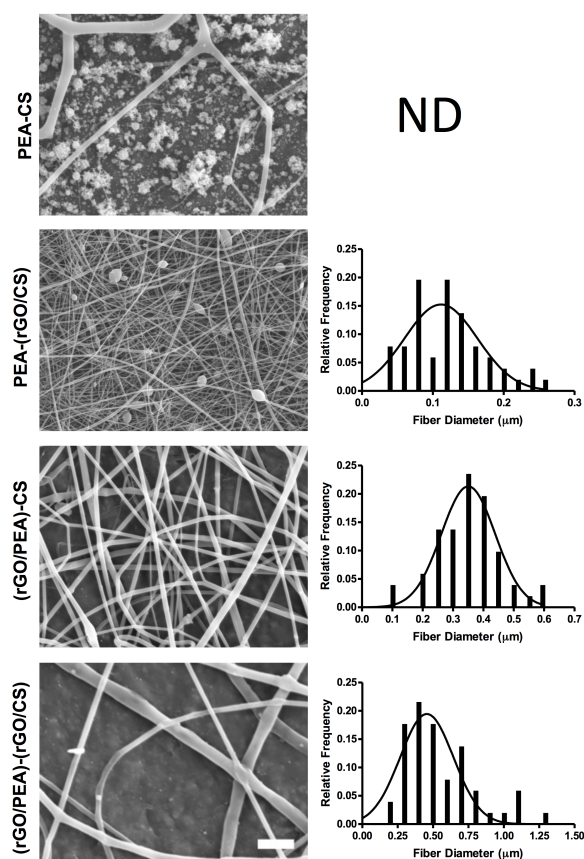


**Figure 4-3:** Coaxial electrospun scaffolds with PEA-CS as the core-shell respectively and then with rGO added in the core, shell or both core-shell. Core-shell PEA-(rGO/CS) has rGO in the shell. SEM images with 3 μm scale bar are accompanied by the corresponding fiber diameter histograms.

Different electrospinning parameters were used for the fibrous scaffolds shown in Figure 4-3, particularly flow rate and voltage. For the PEA-CS control, 0.1 mL/h and 18 kV was used. The flow rate was increased from 0.1 to 0.2 mL/h for all scaffolds incorporating rGO, and the

voltages used were 12, 11 and 14 kV for PEA-(rGO/CS), (rGO/PEA)-CS and (rGO/PEA)-(rGO/CS) respectively. The increased flow rate ensured that there was a continuous flow of shell material, and the voltage was adjusted to optimize the Taylor cone.

While SEM images could describe fiber diameter and uniformity, as well as the presence or absence of beading, confocal microscopy and TEM were used to evaluate the core-shell morphology of the coaxial scaffolds. Figure 4-4A-C shows confocal images of a representative coaxial scaffold, (rGO/PEA)-CS, where Figure 4-4C is the overlap of Figure 4-4A and B. Fluorescent red DiI was added to PEA and CS auto-fluoresces blue; the red fluorescent core aligned with the blue fluorescent shell well. This demonstrates the lack of any clear core-shell structure, and instead the PEA core was mixed with the CS shell. This is further shown with TEM in Figure 4-4D, where there is non-uniform mixing of material through the fibers but the material is not separated into a core and a shell. The results were similar in the other coaxial electrospun scaffolds.

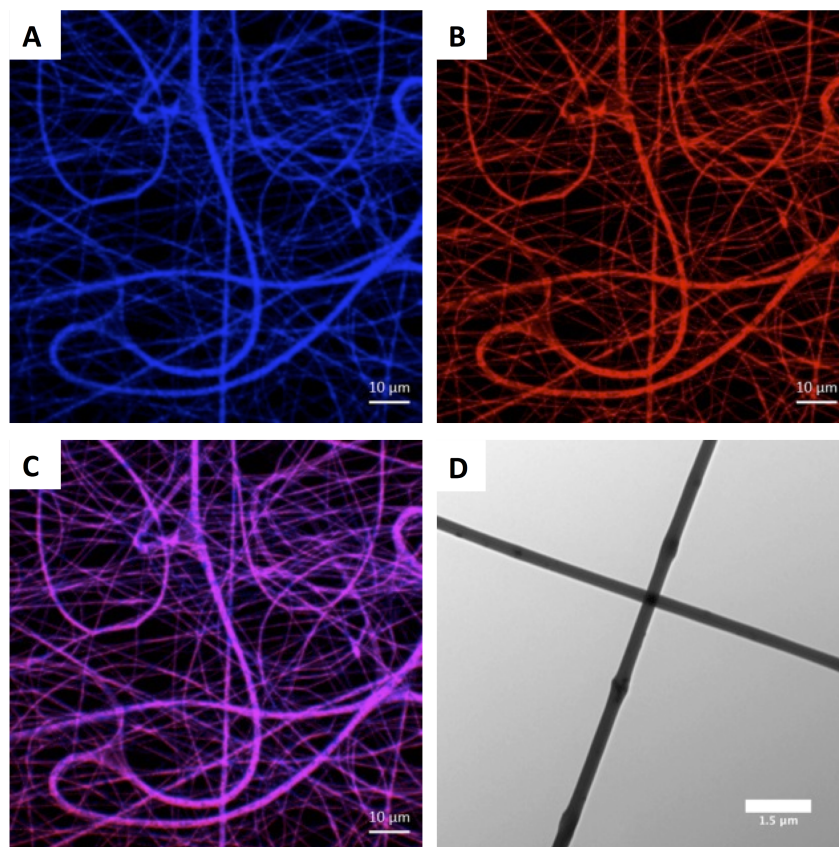


**Figure 4-4:** (rGO/PEA)-CS coaxial electrospinning showing no clear core-shell structure. A) to C) Confocal microscopy where the shell auto-fluoresces blue (A) and the core is fluorescently labeled red (B) with the overlap in C. D) TEM image.

The scaffolds were evaluated for electrical conductivity using the two-probe method. The two-probe method was used instead of the four-probe method, as the scaffolds were still very resistive (low conductivity) which made it more difficult to measure. The two-probe method allows for a shorter path of resistance through the thickness of the scaffold (less than 0.5 mm) as opposed to between the four-probe pins (2 mm apart). The (rGO/PEA)-CS scaffold showed a slight increase ( $\sim 10^2$  times) in conductivity in comparison to the PEA-CS scaffold as seen in Figure 4-5A, but the conductivity was still relatively low and in the order of  $10^{-11}$  S/cm. The current-voltage (I-V) curve of (rGO/PEA)-CS in Figure 4-5B was linear over the selected low current range. Low current was required to produce voltages that were measurable by the source measure unit. Overall, the coaxial scaffolds did not show true core-shell structure and only moderately improved the scaffold conductivity.

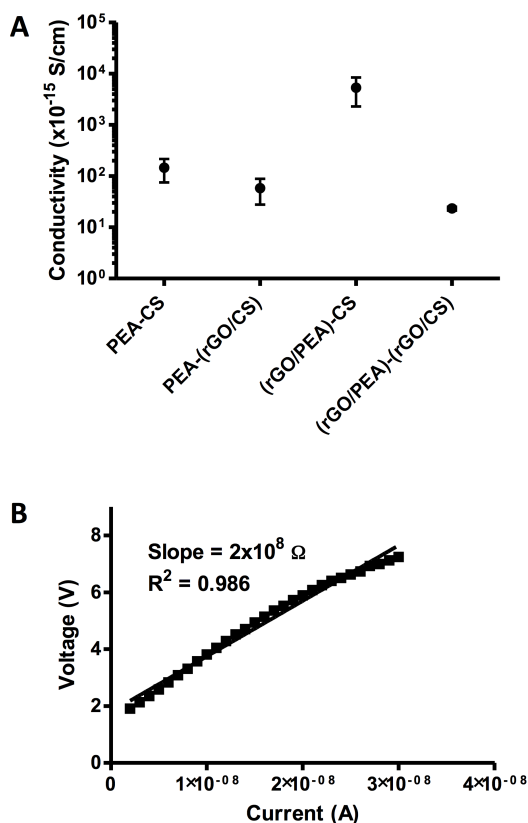


**Figure 4-5:** Coaxial scaffold conductivity. A) Conductivity of different coaxial scaffolds with 3 replicate measurements on each sample. B) Representative I-V curve of (rGO/PEA)-CS

#### 4.2.3 Blend Fibrous Scaffolds

As in the core-shell formulation, 0.1 wt.% rGO was incorporated into PEA for blend rGO/PEA fibrous scaffolds. In order to ensure sufficient rGO/PEA composite interaction, the solvent mixing as well as *in situ* polymerization techniques were used. rGO/PEA B1 and B2 denote the scaffolds prepared using solvent mixing to incorporate purchased rGO and synthesized rGO respectively. rGO/PEA P denotes the scaffold prepared through *in situ* polymerization, which produced a polymer composite with slightly darker coloring compared to PEA demonstrating the inclusion of rGO. NMR and GPC confirmed the PEA structure, which was not affected by the incorporation of rGO during the interfacial polymerization.

PEA has been electrospun previously to form bead-free fibers.<sup>26</sup> However, when rGO was added to PEA and electrospun, the electrospinning parameters required adjustment to remove the beads from the fibers. Initial addition of rGO resulted in bead formation as seen in Figure 4-6A; this figure shows rGO/PEA B1, but rGO/PEA B2 and P required similar adjustments. By increasing PEA concentration (Figure 4-6B), decreasing flow rate (Figure 4-6C) and decreasing voltage (Figure 4-6D) beads were removed from the fibers.

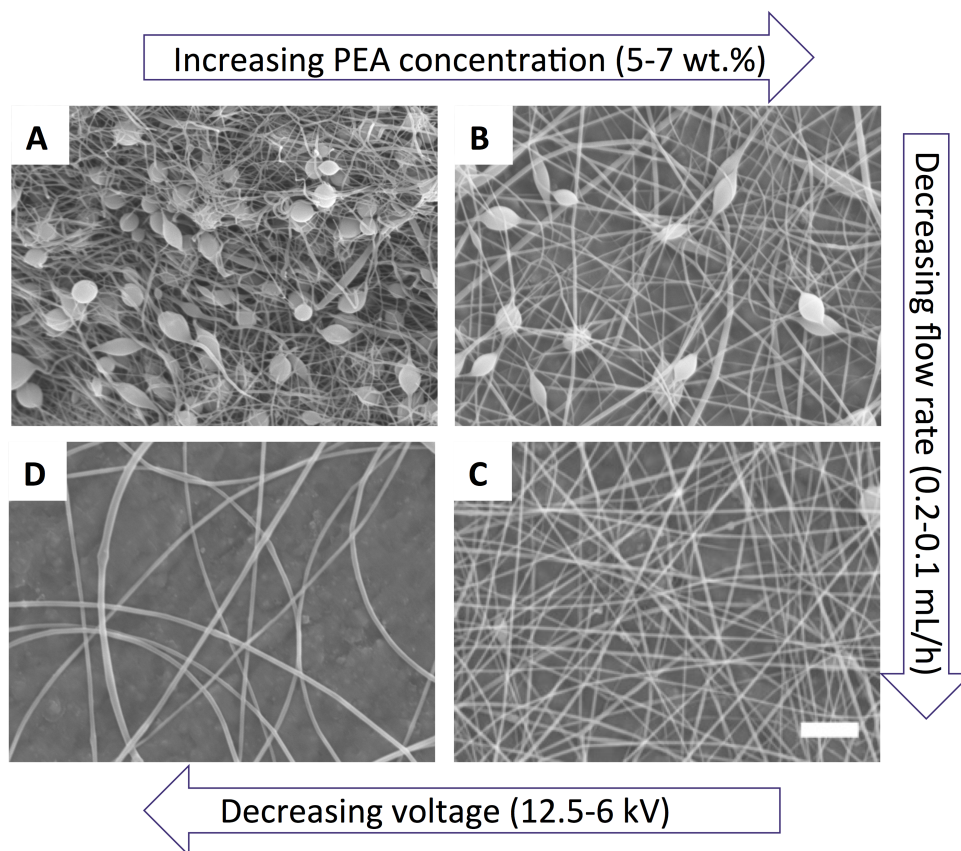


**Figure 4-6:** Effect of electrospinning parameters on blend rGO/PEA (B1) scaffolds A) 12.5 kV, 0.2 mL/h, 5 wt.% B) 12.5 kV, 0.2 mL/h, 7 wt.% C) 12.5 kV, 0.1 mL/h, 7 wt.% D) 6 kV, 0.1 mL/h 7 wt.%. Scale bar is 3  $\mu$ m.

The method of rGO addition did not affect fiber morphology, shown in Figure 4-7A, which compares rGO/PEA B1 and rGO/PEA P. The rGO/PEA fibers were relatively uniform in diameter and followed a Gaussian distribution. PEA fiber diameters differed significantly with the addition of rGO in both the blend and coaxial scaffold samples, shown in Figure 4-7B. The rGO/PEA B1 sample had a smaller fiber diameter compared to PEA as spun, while



rGO/PEA P had a larger fiber diameter. The PEA-(rGO/CS) coaxial sample had an even smaller fiber diameter compared to PEA, while (rGO/PEA)-(rGO/CS) had an even larger fiber diameter and (rGO/PEA)-CS had a similar diameter.

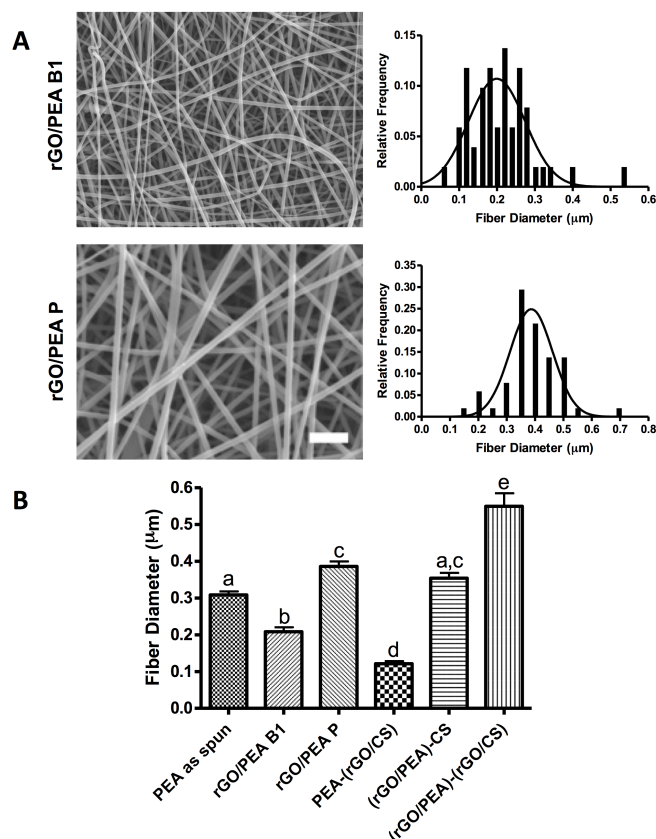


**Figure 4-7:** Blend electrospun scaffolds where rGO was added either before electrospinning (B1) or during polymerization (P). SEM images with 3 μm scale bar and fiber diameter histograms. B) Fiber diameters of different blend and coaxial scaffolds. At least 50 fibers were taken from 1 or 2 scaffolds. Different letters in B) indicate the significance at  $p < 0.05$ .

The difference in rGO addition method affected scaffold conductivity in the different samples as seen in Figure 4-8A. Solvent mixing resulted in little to no improvement in conductivity, while *in situ* polymerization resulted in a sample with  $\sim 10^3$ x improvement in conductivity. The I-V curves shown in Figure 4-8B and C showed linear Ohmic behavior within a certain current range, thus the slope of the curve represented the resistance in that range. The rGO/PEA P scaffold had a lower resistance compared to PEA confirming the improvement in conductivity.

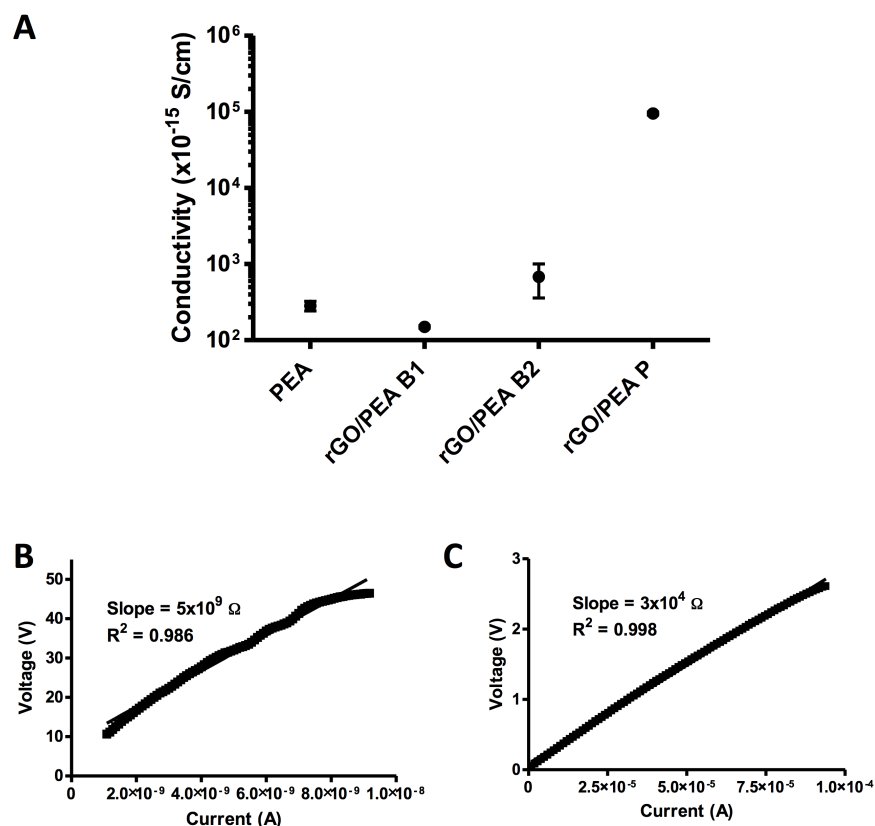


**Figure 4-8:** Blend scaffold conductivity. A) Conductivity of different blend scaffolds where rGO/PEA B1 has purchased rGO added before electrospinning, rGO/PEA B2 has synthesized rGO added before electrospinning, and rGO/PEA P has purchased rGO added during polymerization. 3 replicates were measured for each sample. B-C) Representative I-V curves of PEA and rGO/PEA P respectively

Overall, the rGO/PEA P scaffold had uniform, non-beaded fibers and the greatest increase in scaffold conductivity.

### 4.3 Cell Proliferation and Differentiation

Three fibrous scaffolds were chosen for cell culture experiments, including the PEA control, (rGO/PEA)-CS and rGO/PEA P. The latter two scaffolds were chosen for their acceptable fiber morphology and improvements in scaffold conductivity. Cell viability and cardiac differentiation potential were evaluated.

For cell proliferation, 10T1/2 cells were cultured for 7 days on the three different scaffolds as well as tissue culture plastic as the 2D control. DNA quantification was measured using the

CyQuant Cell Proliferation assay and a fluorescence plate reader. While Figure 4-9A does not show significant cell proliferation in any of the four samples, there was a slight fold-increase in fluorescence from day 1 to day 7 demonstrating some cell growth. (rGO/PEA)-CS and rGO/PEA P scaffolds supported 10T1/2 cell growth over 7 days at a level comparable to the PEA and 2D control.

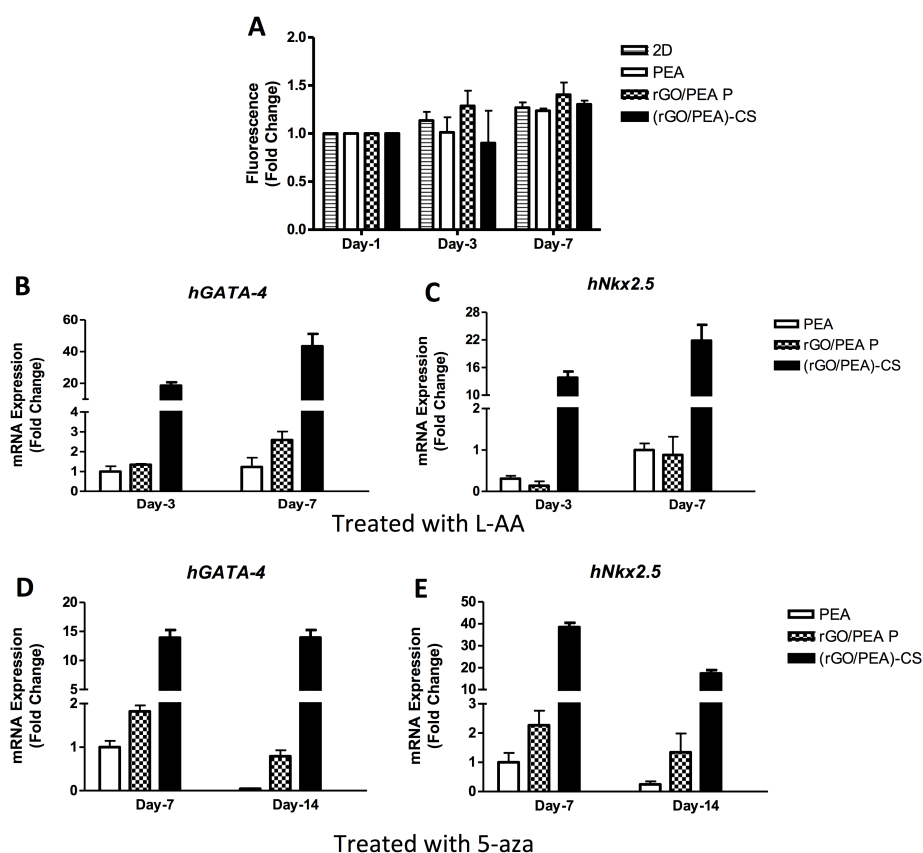


**Figure 4-9:** Cell proliferation and differentiation on PEA, rGO/PEA P and (rGO/PEA)-CS scaffolds. A) 10T1/2 cell proliferation, each scaffold normalized to day 1, n=3. B)-E) iPSC-derived MSC gene expression, n=1 with 4 replicates where B) and D) demonstrate *hGATA-4* gene expression and C) and E) demonstrate *hNkx2.5* gene expression. B) and C) were treated with L-AA and D) and E) were treated with 5-aza.

For cell differentiation, iPSC-derived MSCs were cultured with either L-AA or 5-aza to promote cardiac differentiation. The cells were cultured for 7 days on the 3 different scaffolds with an initial 50  $\mu\text{g/mL}$  dose of L-AA or the cells were cultured for 14 days with an initial and midpoint dose of 5-aza. The rGO-containing scaffolds upregulated *GATA-4* and *Nkx2.5* expression with both differentiation factors as seen in Figure 4-9B-E. Compared to the PEA

control on day 7, the rGO/PEA P sample showed approximately two-fold increase in Nkx2.5 expression with 5-aza treatment and two-fold increase in GATA-4 expression with L-AA and 5-aza treatments. The (rGO/PEA)-CS sample showed at least 10x fold expression of both genes compared to the PEA control at all time points and with both differentiation factors. On day 14, expression of both genes was generally lower compared to day 7. Two-way ANOVA determined that both scaffold type and culture time significantly affected Nkx2.5 expression in these samples with both differentiation factors. With GATA-4 expression in these samples, two-way ANOVA determined that both scaffold type and culture time had a significant effect with L-AA but only the scaffold type had a significant effect with 5-aza.

#### **4.4 Scaffold Porosity Modifications**

While the rGO-containing electrospun scaffolds were not cytotoxic, it is known that electrospun scaffolds limit cell infiltration and therefore overall tissue maturation. In an effort to increase electrospun PEA scaffold porosity and improve cell infiltration, ultrasonication was combined with the leaching of different sacrificial polymers.

##### **4.4.1 Porosity Modification Optimization**

Ultrasonication time and medium were optimized. Based on qualitative SEM images, it was determined that 30 min had the greatest effect on the scaffolds; further experiments used 30 min as the time point. All three media resulted in significantly larger fibers; however, ethyl acetate resulted in the greatest fiber swelling, significantly different from the fiber swelling in water and 90% EtOH as seen in Appendix 6. SEM images showed less fiber fusion after exposure to 90% EtOH compared to water. Subsequent experiments used 90% EtOH as the medium.

Leaching time and ratio of the sacrificial polymer were also optimized. Based on qualitative SEM images, it was determined that 72 h had the greatest effect on the scaffolds so 72 h was used as the leaching time. After leaching it was clear that higher ratios of sacrificial polymer lacked mechanical integrity. SEM images in Appendix 6 showed that the 75/25 sacrificial polymer samples were more compact with lower pore areas as compared with the 25/75 sacrificial polymer samples, this was consistent with preliminary quantitative pore area

analysis. Only scaffolds with 25/75 and 50/50 ratios of sacrificial polymer were used in subsequent experiments.

#### **4.4.2 PVP/PEA System**

In evaluating the effectiveness of PVP as a sacrificial polymer, SEM images provided qualitative comparison as seen in Figure 4-10A. Quantitative information on pore area and scaffold percolative efficiency (SPE) was extracted from the SEM data using image analysis and is shown in Figure 4-10B&C respectively.

The pore area data was analyzed using non-parametric t-tests, comparing the different scaffold modifications against the PEA as spun control. Non-parametric t-tests were used because the pore area data failed a normality test and did not follow a Gaussian distribution. As a result, medians were compared and graphed as seen in Figure 4-10B. While ultrasonication resulted in a significant increase in pore area, the leaching of PVP (with or without ultrasonication) did not significantly change the pore area.

The SPE data did follow a Gaussian distribution and so the means were compared and graphed as seen in Figure 4-10C. Neither ultrasonication nor the leaching of PVP appeared to have an effect on scaffold SPE.

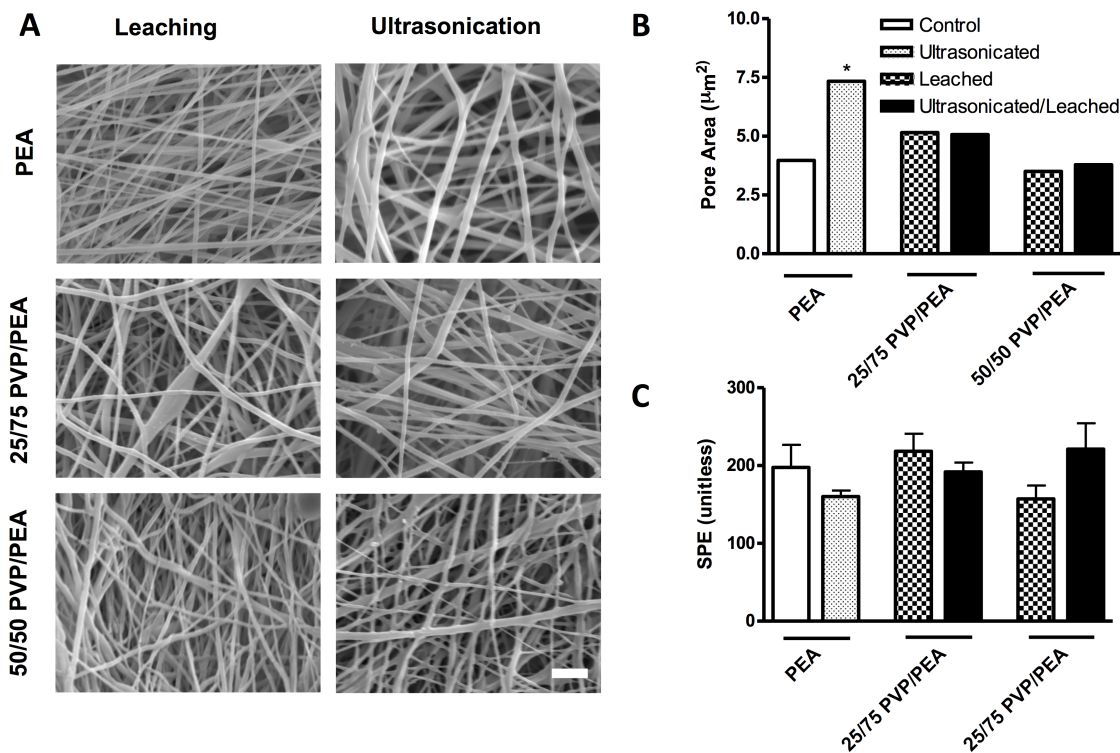


**Figure 4-10:** PEA scaffold porosity using PVP as a sacrificial polymer A) SEM images of scaffolds with different modifications used for corresponding quantitative image analysis in B) and C). Two different ratios of PVP are used. Except for the PEA control scaffold, scaffolds are either only leached (left column) or are ultrasonicated prior to leaching (right column). Scale bar is 3  $\mu\text{m}$ . B) Pore area (medians graphed) of different scaffolds. C) Scaffold percolative efficiency (means graphed) of different scaffolds. N=3, \* represents  $p < 0.05$  compared to PEA control.

#### 4.4.3 PEO/PEA System

Similar to the PVP/PEA samples, SEM images of the different scaffold modifications were analyzed to evaluate pore area and SPE (shown in Figure 4-11A). The medians were graphed for pore area and the means were graphed for SPE as seen in Figure 4-11B&C. Despite a lack of statistical significance, SPE showed a general trend of improvement with the sacrificial PEO fibers, increasing pore area with an increasing percentage of PEO. Pore area also showed an improvement with the sacrificial PEO fibers; there was a significant increase in pore areas with most modified scaffolds. Leaching of PEO showed a significant improvement compared to the PEA control at the 25/75 ratio but not at the 50/50 ratio. Scaffolds treated with both ultrasonication/leaching showed significant improvement at both ratios compared to

the PEA control, and the combination of methods even showed significant increase compared to leaching alone at the 50/50 ratio.

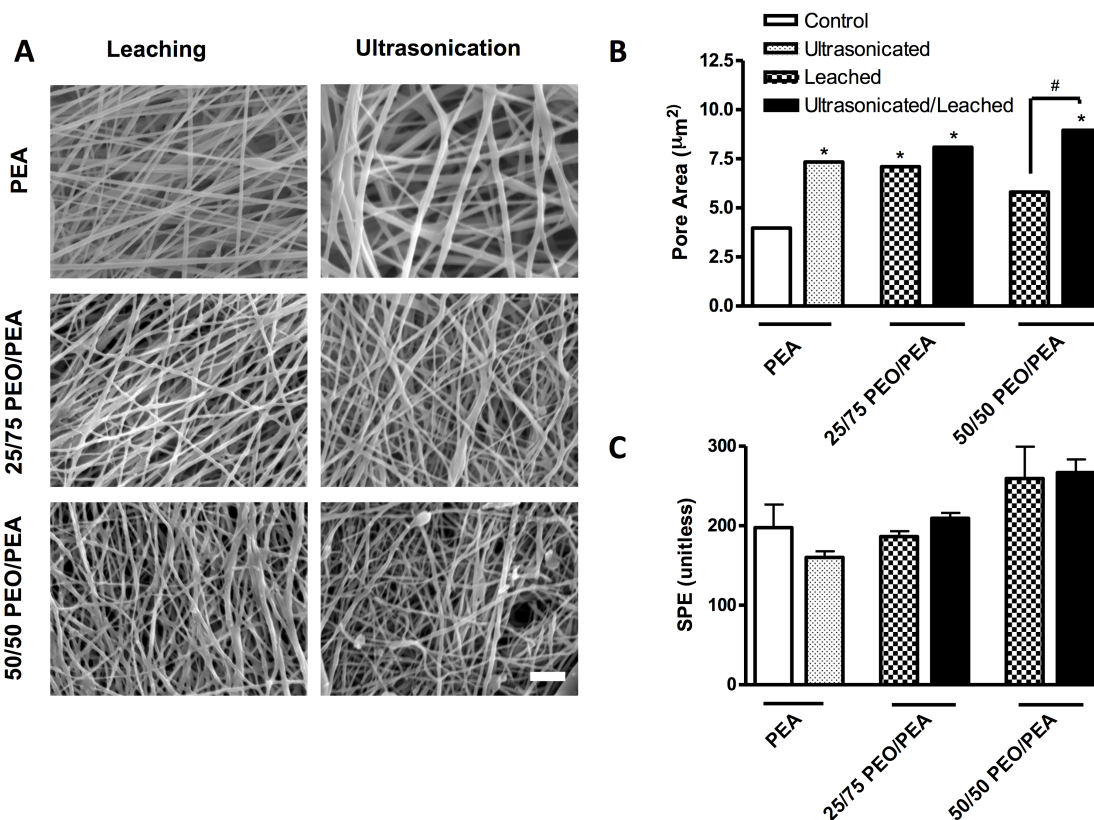


**Figure 4-11:** PEA scaffold porosity using PEO as a sacrificial polymer A) SEM images of scaffolds with different modifications used for corresponding quantitative image analysis in B) and C). Two different ratios of PEO were used. Except for the PEA control scaffold, scaffolds are either only leached (left column) or are ultrasonicated prior to leaching (right column). Scale bar is 3  $\mu\text{m}$ . B) Pore area (medians graphed) of different scaffolds. C) Scaffold percolative efficiency (means graphed) of different scaffolds. N=3, \* represents  $p < 0.05$  compared to PEA control and # represents  $p < 0.05$  within group.

#### 4.5 Discussion

In this thesis, rGO was synthesized and incorporated into PEA films and fibrous scaffolds. The precursor GO synthesis proceeded with expected color changes throughout the reactions. The dark blue pre-oxidation solution color, the bright yellow solution color following the addition of  $\text{H}_2\text{O}_2$ , and the yellow-brown final graphite oxide solution observed during the reaction are consistent with literature reports.<sup>42</sup> FTIR was used to further confirm the

preparation of GO. Unlike rGO, GO contains multiple oxygen functional groups including hydroxyl, carbonyl, carboxyl and epoxide groups. The FTIR results shown in Figure 4-1A were in agreement with reported peaks<sup>37</sup> and confirmed successful oxidation. The addition of the oxygen-containing functional groups is known to disrupt the conjugation and therefore greatly increasing the material resistance compared to graphene or rGO<sup>8</sup> (Figure 4-1B).

L-AA and HI reducing agents were used to prepare rGO. Synthesis proceeded as expected with L-AA: the brown solution turned black with minimal agglomeration of rGO. However, two rounds of reduction with HI were required; after the first reduction the solution was dark brown instead of black. FTIR showed the removal of the oxygen-containing functional groups with both methods. However, electrical conductivity measurements were needed for further comparison of the different reduction methods, because restoration of conductivity is a primary goal of reduction.<sup>8</sup> Conductivity is increased due to a restoration in the long-range  $sp^2$  hybridization in rGO allowing the delocalized flow of electrons.<sup>8</sup> Even with the removal of the oxygen-containing functional groups, defects can negatively impact conjugation and therefore negatively impact conductivity.<sup>30</sup> As a result, conductivity measurements were useful in addition to the FTIR confirmation.

Reduction with L-AA resulted in sufficient conductivity – reduction was actually greater than that reported in literature (Figure 4-1C) – but is limited in its potential for scale-up. This method starts with only 0.1 mg/mL GO in a 300 mL solution, so it would take multiple batches (and multiple days) in order to freeze dry the entire volume into rGO powder. When the working volume was split in half (doubling the starting GO concentration), the majority of the material precipitated out of solution into large agglomerates preventing the possibility of forming proper single-layer rGO. Scale-up of this process still needs improvement.

Reduction with HI, as mentioned above, required two rounds of reduction. When the reaction temperature was increased from room temperature to 95°C, following a protocol in literature (Figure 4-1C), undesirable large agglomerates precipitated. Two different starting concentrations of GO were used (4 mg/mL and 2 mg/mL) and after both rounds of reduction, HI1-2 (4 mg/mL GO) had a higher conductivity than HI2-2. This could be beneficial because higher starting GO concentrations are promising for larger-scale production of rGO. While the



rGO reduced with HI had a lower conductivity than experimental L-AA, all experimental rGO were within an order of magnitude of the purchased sample. The HI reduction method also had a lower 20 mL working volume, meaning that only one batch was required for freeze-drying; this makes it easier to produce larger quantities of rGO.

PEA films incorporating rGO were fabricated prior to electrospinning in order to optimize the concentration of rGO (Figure 4-2A&C). Four different concentrations were used based on literature,<sup>15</sup> and 0.1 wt.% rGO was chosen based on these films. The composite sample resulted in a significant reduction in PEA film resistance while maintaining a relatively uniform film compared to the higher concentrations of rGO. 0.1 wt.% rGO is also reported to be the critical loading concentration in poly( $\epsilon$ -caprolactone) to ensure proper dispersion and stronger interactions between rGO and the polymer chains through van der Waals forces.<sup>15</sup> CS films did not show the same decrease in resistance with the addition of rGO presumably due to poor dispersion of rGO, which is visually seen in Figure 4-2D. GO/CS are known to have strong interactions, due to the covalent bonding between the carboxyl groups in GO and the amino groups in CS.<sup>9</sup> rGO/CS also has potential for strong interactions with some remaining oxygen-containing functional groups, but required rGO stabilization with a triblock copolymer (with two blocks poly(ethylene oxide), one block poly(propylene oxide)).<sup>75</sup> The film thickness also did not appear uniform, and appeared to have a wrinkled texture. This non-uniformity made it more difficult to measure the sheet resistance. This lack of resistance reduction in CS films may extend and pose a similar issue in coaxial scaffolds.

Film preparation was useful in determining the optimum rGO loading concentration, but incorporating rGO into electrospun fibrous scaffolds is important so that the scaffolds better mimic the native ECM. Electrospinning involves the balance of electrostatic force with viscoelastic and surface tension forces.<sup>54</sup> The incorporation of rGO affected this balance by decreasing the required voltage, and therefore electrospinning parameters were adjusted in order to create uniform, bead-free fibers with core-shell structure if desired.

When 0.1 wt.% rGO was incorporated into PEA by blending, electrospun scaffolds were beaded and process parameters required adjustment to remove beads. Beads are considered as defects and a negative aspect to electrospinning.<sup>76</sup> Beading may be reduced by increasing

solution concentration, decreasing voltage, and decreasing flow rate<sup>2</sup> (Table 2-2, Figure 4-6). The voltage was reduced to 6 kV for bead-free fibers, which is much lower than the 18 – 20 kV needed for pure PEA fibers, demonstrating the influence that rGO had on the electrospinning solution conditions. This is interesting, because this voltage reduction has not been directly discussed, based on the literature review. With the addition of rGO, a lower voltage was required to overcome the viscoelastic and surface tension forces to form fibers. Therefore, rGO could have decreased the viscoelastic forces by disrupting inter-chain bonding<sup>64</sup> or increased the solution conductivity due to enhanced dielectric constants that result in solutions that store greater charge.<sup>61</sup> Since higher dielectric constants lower the voltage required to create the minimum electrostatic charge,<sup>77</sup> rGO could have increased the solution conductivity so the polymer was more easily charged and less voltage was required to achieve the same electrostatic force. There is also the possibility that rGO both decreased viscosity and increased solution conductivity to some extent. Not surprisingly, rGO also decreased the voltage required in coaxial electrospinning, as would be expected given its effect in blend electrospinning. For all three coaxial scaffolds, with rGO incorporated in the shell, core, or both, the voltage was optimized (ranging between 11 and 14 kV) in order to achieve a single fiber jet ejecting from the Taylor cone at the needle tip. Higher voltages are known to result in multiple ejecting fiber jets while lower voltages are unable to sufficiently pull the solution from the needle tip (refer to Figure 2-9).<sup>59</sup> The flow rate for all three of these coaxial scaffolds remained at 0.2 mL/h as 0.1 mL/h was not sufficient for the shell material to be fully pushed through the spinneret.

Without rGO, the PEA-CS control formed electrospayed droplets along with fibers as seen in Figure 4-3. The CS shell was electrospayed, possibly because the 0.1 mL/h flow rate was insufficient for CS to be pushed out of the shell continuously. However it was also likely that CS was electrospayed because the CS concentration was below the critical minimum polymer concentration, which is required to ensure entanglements between the polymer chains and therefore fiber formation.<sup>78</sup> The small cross-sectional area of the coaxial spinneret shell also limited the solution concentration that could be pushed through the orifice, presenting a possible barrier to fiber formation. For successful coaxial electrospinning, the shell should be electrospinnable on its own,<sup>53</sup> but this is difficult with CS. CS requires a high concentration to form sufficient entanglements and subsequent fibers, which then requires a high voltage. rGO

lowered that required voltage, making CS easier to electrospin with a higher concentration (see Appendix 4), but when added in the shell in the PEA-(rGO/CS) scaffold, it is not known whether rGO also increased the viscosity and number of entanglements. As mentioned earlier, rGO could decrease the viscosity by disrupting inter-chain bonding,<sup>64</sup> but it might be possible that rGO interacted with CS and increased bonding and therefore increased chain entanglements to produce fibers instead of droplets. However, beading was still present as seen in Figure 4-3. While the PEA-(rGO/CS) scaffold was beaded, when rGO was added in the core or in both the core and the shell, bead-free fibers were obtained. PEA-(rGO/CS) had a narrow, Gaussian fiber diameter distribution when considering the sections of fibers without beads, though the fit was moderate. (rGO/PEA)-CS also had a Gaussian fiber diameter distribution, while (rGO/PEA)-(rGO/CS) had a wide distribution that was skewed to the left. It was not clear why the different locations of rGO addition affected fiber morphology. Usually in coaxial electrospinning, the shell should be electrospinnable and have a higher conductivity so that the shell pulls the core.<sup>53</sup> Contrary to this, when rGO was added to the PEA core (making the core both more conductive and electrospinnable), the core may have pulled the shell and resulted in uniform, bead-free fibers. As well, based on the film preparation studies, rGO was better dispersed in PEA than in CS, which may have had an effect. The incorporation of rGO in different locations may have also affected the interfacial tension, which is an important parameter in coaxial electrospinning.<sup>53</sup>

Average fiber diameters of the different scaffolds, both blend and coaxial, differed significantly between samples, as seen in Figure 4-7B. Compared to PEA, rGO/PEA B1 decreased in fiber diameter, which is consistent with literature<sup>15</sup> and can be explained by the fact that increased charge density enhances the elongational forces creating smaller fiber diameters.<sup>62</sup> rGO/PEA P increased in fiber diameter, which was not expected, but may be explained by the *in situ* polymerization process. The resulting composite polymer had a lower molecular weight and therefore required a slightly larger concentration for electrospinning resulting in slightly larger fibers and further optimization may be beneficial. PEA-(rGO/CS) greatly decreased the fiber diameter, but this diameter only considers the fibrous sections in between beads and so may not be an accurate representation. (rGO/PEA)-(rGO/CS) showed an increase in fiber diameter, which may be a result of increased core conductivity which can increase core diameter.<sup>79</sup> It also may represent some collapsed, ribbon-like fibers that are seen

in Figure 4-3. (rGO/PEA)-CS also had an increased core conductivity, so it is interesting that there was no significant increase from PEA.

All the coaxial electrospun scaffolds, including (rGO/PEA)-CS, showed no clear core-shell morphology in confocal or TEM, as seen in Figure 4-4, showing that the PEA and CS solutions were mixed. This is possible because the solvents are miscible.<sup>53</sup> Core-shell mixing can also occur when the Taylor cone is unstable and there are multiple jets ejecting from the Taylor cone.<sup>59</sup> A minimum shell:core flow rate ratio is 3:1 was proposed to ensure that there is sufficient shell material to surround the core material.<sup>58</sup> However the single syringe pump in this electrospinning setup limited the shell:core flow rate ratio to 1:1. This is likely the cause of the absence of clear core-shell morphology. While proper core-shell structures were not achieved, coaxial electrospinning remains a useful tool in creating fibers containing both CS and PEA as blend CS/PEA fibers were not possible. Combining the CS solution with the PEA solution (with their own respective solvents) resulted in precipitation/gelation. Therefore, in order for PEA and CS to be electrospun together, the two solutions needed separation through the coaxial spinneret until ejection from the needle tip. This unconventional approach is novel as PEA and CS have not been combined into a single fiber before, and the coaxial spinneret allows the combination of two materials with different solvent systems (organic and aqueous acid). With different equipment and further optimization, this work could be improved to prepare proper core-shell PEA-CS fibers. While core-shell morphology was not achieved, coaxial electrospinning was successfully optimized to produce multi-component, bead-free fibers. (rGO/PEA)-CS was considered to have the best fiber morphology, with its Gaussian diameter distribution and uniform, non-beaded fibers. Blend electrospinning also produced uniform, non-beaded fibers with a Gaussian diameter distribution.

Once the desired bead-free fiber morphology was obtained, the scaffolds were evaluated for their electrical conductivity using the two-probe set-up. The only coaxial scaffold sample that showed slight improvement in conductivity was the (rGO/PEA)-CS scaffold (Figure 4-5). It is possible that rGO was better dispersed within PEA than CS, as seen with the film preparation, and when trapped within the core. For scaffolds fabricated using the rGO/PEA blend, the difference in rGO addition affected overall scaffold conductivity, where rGO/PEA P showed an increase in conductivity while rGO/PEA B1 and B2 did not. rGO was incorporated through

*in situ* polymerization in the rGO/PEA P scaffold, and incorporated through the solvent mixing method in the rGO/PEA B1 and rGO/PEA B2 scaffolds, as well as the coaxial scaffolds. It is possible that the solvent mixing method resulted in some aggregation and insufficient dispersion and that rGO may have separated from the polymer matrix during electrospinning. In one experiment where the rGO concentration was doubled to 0.2 wt.%, there was a noticeable black agglomeration at the needle tip. So, even at 0.1 wt.%, it is possible that the rGO was not dispersed well enough to form a stable composite with the polymer, and thus it is possible that only some of the rGO in the polymer solution was incorporated into the fibers. *In situ* polymerization often has the potential to improve dispersion and therefore conductivity by improving the interactions between filler and polymer,<sup>35</sup> and this is consistent with the results in this study. Others found success with the solvent mixing methods,<sup>14–16,61–63</sup> but solvent mixing was not effective in this study with these materials and conditions. While other studies stirred the rGO with the polymer blend for at least 12 h,<sup>15,16</sup> this study added the polymer through quick vortexing, or stirring up to 3 h until dissolved. Additional stirring did not appear to be necessary given the complete dissolution of the polymer. While some improvement in conductivity is demonstrated particularly with rGO/PEA P, it is in the order of  $10^{-10}$  S/cm, which is lower than a CNF/CS hydrogel with a reported conductivity in the order of  $10^{-3}$  S/cm.<sup>11</sup> This rGO/PEA P conductivity corresponded to a resistance around  $10^6$   $\Omega$ , where graphene/PVA/alginate fibers achieved a resistance around 20  $\Omega$ .<sup>16</sup> The scaffolds in this study are not as conductive as scaffolds reported in literature, but the objective for the conductive scaffolds is to support electrical stimulation. Future studies exposing the conductive scaffolds to electrical stimulation will clarify if greater scaffold conductivity is required.

All the samples were fairly resistive, so low currents (in the  $\mu$ A to nA range) were required to produce a voltage measurable by the source measure unit. For three representative samples – PEA, (rGO/PEA)-CS and rGO/PEA P – current was varied within the relevant range and voltage was measured, creating a section of current-voltage (IV) curve. For the given range, all three scaffolds showed linear behavior (Figure 4-5B and Figure 4-8B), and acted as pure resistors by following Ohm's Law. Therefore, in this range, the slope of each line (dV/dI) represented resistance. It was interesting to see that rGO/PEA P gave a resistance of approximately  $3 \times 10^4$   $\Omega$ , while PEA gave a resistance of approximately  $5 \times 10^9$   $\Omega$ . This decrease

in scaffold resistance with the addition of rGO confirmed the increase of scaffold resistance shown in Figure 4-8A. (rGO/PEA)-CS gave a resistance of approximately  $2 \times 10^8 \Omega$ , which was only a slight decrease in resistance.

Based on fiber morphology and conductivity improvement, (rGO/PEA)-CS and rGO/PEA P were chosen along with the PEA and 2D controls for cell proliferation and differentiation experiments. In the cell proliferation experiment, 10T1/2 cells were seeded on these three scaffolds (Figure 4-9A). All three fibrous scaffolds had comparable cell growth to the 2D control confirming the scaffolds were not cytotoxic, which was expected as PEA has already been shown to support cells<sup>70</sup> and so have rGO composites.<sup>10</sup> It appears that the scaffolds did not provide additional room for cells to grow compared to the 2D control. This is likely because the cells were not able to properly infiltrate the scaffold; this is common with electrospun scaffolds as the nanofibers pack densely. When iPSC-derived MSCs were treated with L-AA or 5-aza and cultured on the fibrous scaffolds, both scaffold type and culture time significantly affected Nkx2.5 expression (Figure 4-9B-E). Both scaffold type and culture time significantly affected GATA-4 expression with L-AA, while scaffold type alone significantly affected GATA-4 expression with 5-aza. Generally, gene expression upregulation declined after 14 days, demonstrating that 7 day culture was sufficient. GATA-4 and Nkx2.5 are both early markers of cardiac differentiation,<sup>80</sup> and they were upregulated on both rGO-containing fibrous scaffolds. The rGO/PEA P scaffolds showed a two-fold increase in gene expression compared to the PEA control after 7 days, demonstrating that rGO may have some effect in the cardiac differentiation of these cells. This could be due to the increase in conductivity or the presence of rGO and its nanotopography. However, it was interesting to see that the slightly less conductive (rGO/PEA)-CS scaffold upregulated gene expression with over 10x fold expression at all time points with both differentiation factors. CS appears to have a large effect on this overexpression, therefore promoting cardiac differentiation of MSCs. CS is thought to increase calcium transportation into MSCs for enhanced differentiation.<sup>56</sup> While the presence of CS appears to have a greater effect than the presence of rGO and increased conductivity, the conductivity may have to be further increased to see further change.

Cell infiltration is likely a challenge in these scaffolds, due to their electrospun nature and small fiber diameter. There have been numerous attempts to improve cell infiltration by

increasing scaffold porosity with varying rates of success and some include ultrasonication and leaching of a sacrificial polymer.<sup>3,4</sup> When PEA scaffolds were exposed to ultrasonic vibrations, the pore area increased significantly (Figure 4-10B) showing that the vibrations did loosen and mechanically separate the fibers.<sup>4</sup> While the pore areas achieved in this study via ultrasonication were not as large as those reported,<sup>4</sup> this is likely due to smaller fiber diameters, which can lead to more dense fiber packing.<sup>3</sup>

PVP has not been used as a sacrificial polymer before but it has been leached out in an aqueous solution in a previous study.<sup>68</sup> It does not appear to be an effective sacrificial polymer (Figure 4-10); PVP had no significant effect on scaffold pore area and SPE. This means it is possible that the PVP was not entirely leached out of the scaffold and may be because the PVP fibers had larger diameters and therefore a lower surface area per volume that is exposed to water, especially in the inner section of the scaffold.

PEO has been used as a sacrificial polymer previously,<sup>66</sup> but has not been combined with ultrasonication. Ultrasonication has been used to enhance the leaching of a sacrificial polymer but the concept has not been applied for increasing scaffold porosity.<sup>68</sup> Leaching of PEO was sufficient to increase pore area at the 25/75 PEO/PEA ratio but not at the 50/50 ratio as seen in Figure 4-11B. At the 50/50 ratio, there were greater amounts of PEO fibers and the leaching time was potentially insufficient or multiple rinses would be required to remove the innermost PEO. However, the addition of ultrasonication compensated for this and further increased the pore area at both ratios. The combination of leaching and ultrasonication was increasingly important at increasing ratios of PEO. The potential mechanism for this is that ultrasonication loosens the fibers and makes it easier for more PEO to be leached out, even from the innermost areas of the scaffold. As well, at higher ratios of PEO, if all the fibers can be removed, there are a greater number of fibers that are removed from the composite scaffold, leaving behind larger pore areas. Overall, ultrasonication of PEA showed positive improvements in pore area as compared to PEA as spun, and the combination of ultrasonication and leaching of PEO as a sacrificial polymer showed even better results. This study shows the potential of a combination of methods for improving scaffold porosity, particularly with PEO as a sacrificial polymer.

Pore area, as previously discussed, was increased with ultrasonication, leaching of PEO and combination of methods. However, no significance was found with SPE. This means that while the superficial pore areas were increased, there was no significant increase in pore interconnectivity. This might be a result of insufficient loosening and leaching in the inner layers of the composite scaffold. Regardless, pore area is likely a more useful parameter; SPE has the potential to provide useful interconnectivity information using only 2D images but does have limitations given it is a simulated parameter.

These improvements are promising but require further optimization. A typical cell size is 10-15  $\mu\text{m}$ ,<sup>3</sup> and require a pore size of at least 10-15  $\mu\text{m}$  which is equivalent to a approximately 80  $\mu\text{m}^2$ ; this is much higher than the pore areas achieved by scaffold modifications in this study. Achieving these pore sizes is challenging with electrospun scaffolds, particularly with fibers of sub-micrometer diameters.

2D image analysis was useful in its ability to analyze nanofibrous scaffolds that other methods are not able to analyze. Other porosity measurement techniques like mercury porosimetry and micro-CT are not possible with such small fiber diameters; the high pressure from the mercury porosimetry compromised the scaffold and the micro-CT could not resolve individual fibers. As well, 2D image analysis allowed multiple parameters to be obtained, including pore area and SPE. While there was some subjectivity in the manual selection of the top layer of the scaffold, blinded observers were used to select top layer and the bias was determined negligible.



## Chapter 5

### 5 Conclusions and Future Directions

This chapter summarizes and highlights the relevance of the thesis and guides the future work.

#### 5.1 Conclusions

This study modifies both scaffold conductivity and porosity. rGO was incorporated to increase conductivity, and a combination of ultrasonication and leaching of a sacrificial polymer was applied to increase porosity.

GO and rGO syntheses were successful. FTIR confirmed the addition and then removal of oxygen-containing functional groups through the oxidation-reduction method of producing rGO. The rGO produced through different methods resulted in different conductivities.

rGO was incorporated with PEA (and CS where appropriate) in films and fibrous scaffolds. The preparation of composite polymer films confirmed the optimum rGO loading concentration of 0.1 wt.%, because higher concentrations resulted in non-uniform dispersions and rGO aggregation. At this concentration, the PEA film did show a decrease in resistance due to the influence of rGO. rGO had a large effect on electrospinning parameters, and greatly reduced the voltage required for electrospinning. rGO is not as commonly electrospun as GO, and rGO has never been electrospun with PEA before. rGO assisted in fabricating bead-free, uniform fibers, despite the lack of core-shell morphology. Even without core-shell morphology, the coaxial spinneret enabled PEA and CS to combine into a single fiber for the first time despite their differing solvent systems. Without rGO, PEA-CS included electrospayed droplets, and the incorporation of rGO into the core, shell or both resulted in different fiber diameter and morphology.

The conductivity of the fibrous scaffolds was moderately improved with the incorporation of rGO in the (rGO/PEA)-CS and rGO/PEA P samples. (rGO/PEA)-CS had

the greatest conductivity of the coaxial scaffolds, likely because the rGO was trapped in the core during the electrospinning process, so was more likely to be fully incorporated within the fibers. rGO/PEA P showed the largest improvement in conductivity through *in situ* polymerization, which supports the ongoing potential of this composite preparation method. rGO/PEA P likely had the best dispersion and had the strongest interactions between rGO and PEA, resulting in greater rGO quantities within the electrospun fibers and greater rGO percolation. This resulted in greater overall conductivity, and was the first step in extending PEA scaffolds towards cardiac or neural tissue engineering applications.

All three scaffolds (PEA, (rGO/PEA)-CS and rGO/PEA P) showed no cytotoxic effects, and the rGO-containing scaffolds upregulated expression of GATA-4 and Nkx2.5 in iPSC-derived MSCs, known markers of cardiomyogenic differentiation. The incorporation of CS further upregulated GATA-4 and Nkx2.5 expression in (rGO/PEA)-CS. This demonstrates the potential for these scaffolds to support cardiac tissue engineering.

While the scaffolds were not cytotoxic, electrospun scaffolds typically do not promote cell infiltration due to their low porosity, pore area and pore interconnectivity. Ultrasonication of PEA scaffolds, leaching of PEO as a sacrificial polymer and combination of ultrasonication and leaching significantly improved the pore area of PEA scaffolds and showed a general trend of improvement in terms of SPE and scaffold interconnectivity. This novel combination of methods for increasing scaffold porosity did improve pore area but further optimization is required to sufficiently improve porosity of nanofibrous scaffolds.

## **5.2 Future Directions**

To further advance this study, scaffolds should be exposed to electrical stimulation to properly evaluate their ability to propagate electrical signals and support tissue maturation. To improve upon the scaffolds themselves, there could be further optimization with the *in situ* polymerization process, and it could be extended to the coaxial scaffolds as well. In terms of the coaxial scaffolds' core-shell morphology, a

second syringe pump should be assembled to allow for a higher shell flow rate. The ability to create a flow rate differential between the core and shell, along with further optimization of other parameters, has potential to produce a core-shell morphology. The scale-up of rGO synthesis could also be improved.

## References

- (1) Hasan, M. M.; Alam, A. K. M. M.; Nayem, K. A. Application of Electrospinning Techniques for the Production of Tissue Engineering Scaffolds: A Review. *Eur. Sci. J.* **2014**, *10* (15), 265–278.
- (2) Ingavle, G. C.; Leach, J. K. Advancements in Electrospinning of Polymeric Nanofibrous Scaffolds for Tissue Engineering. *Tissue Eng. Part B Rev.* **2014**, *20* (4), 277–293.
- (3) Zhong, S.; Zhang, Y.; Lim, C. T. Fabrication of Large Pores in Electrospun Nanofibrous Scaffolds for Cellular Infiltration: A Review. *Tissue Eng. Part B Rev.* **2012**, *18* (2), 77–87.
- (4) Lee, J. B.; Jeong, S. I.; Bae, M. S.; Yang, D. H.; Heo, D. N.; Kim, C. H.; Alsberg, E.; Kwon, I. K. Highly Porous Electrospun Nanofibers Enhanced by Ultrasonication for Improved Cellular Infiltration. *Tissue Eng. Part A* **2011**, *17* (21–22), 2695–2702.
- (5) Karimi, P.; Rizkalla, A. S.; Mequanint, K. Versatile Biodegradable Poly(ester Amide)s Derived from  $\alpha$ -Amino Acids for Vascular Tissue Engineering. *Materials (Basel)*. **2010**, *3* (4), 2346–2368.
- (6) Balint, R.; Cassidy, N. J.; Cartmell, S. H. Electrical Stimulation: A Novel Tool for Tissue Engineering. *Tissue Eng. Part B Rev.* **2013**, *19* (1), 48–57.
- (7) Shin, S. R.; Li, Y. C.; Jang, H. L.; Khoshakhlagh, P.; Akbari, M.; Nasajpour, A.; Zhang, Y. S.; Tamayol, A.; Khademhosseini, A. Graphene-Based Materials for Tissue Engineering. *Adv. Drug Deliv. Rev.* **2016**, *105*, 255–274.
- (8) Pei, S.; Cheng, H. M. The Reduction of Graphene Oxide. *Carbon N. Y.* **2012**, *50* (9), 3210–3228.
- (9) Ding, X.; Liu, H.; Fan, Y. Graphene-Based Materials in Regenerative Medicine. *Adv. Healthc. Mater.* **2015**, *4* (10), 1451–1468.
- (10) Shin, S. R.; Zihlmann, C.; Akbari, M.; Assawes, P.; Cheung, L.; Zhang, K.; Manoharan, V.; Zhang, Y. S.; Yükksekaya, M.; Wan, K. T.; et al. Reduced Graphene Oxide-GelMA Hybrid Hydrogels as Scaffolds for Cardiac Tissue Engineering. *Small* **2016**, *12* (27), 3677–3689.
- (11) Martins, A. M.; Eng, G.; Caridade, S. G.; Mano, J. F.; Reis, R. L.; Vunjak-Novakovic, G. Electrically Conductive Chitosan/carbon Scaffolds for Cardiac Tissue Engineering. *Biomacromolecules* **2014**, *15* (2), 635–643.
- (12) Kanayama, I.; Miyaji, H.; Takita, H.; Nishida, E.; Tsuji, M.; Fugetsu, B.; Sun, L.; Inoue, K.; Ibara, A.; Akasaka, T.; et al. Comparative Study of Bioactivity of

Collagen Scaffolds Coated with Graphene Oxide and Reduced Graphene Oxide. *Int. J. Nanomedicine* **2014**, *9*, 3363–3373.

- (13) Jin, L.; Wu, D.; Kuddannaya, S.; Zhang, Y.; Wang, Z. Fabrication, Characterization, and Biocompatibility of Polymer Cored Reduced Graphene Oxide Nanofibers. *ACS Appl. Mater. Interfaces* **2016**, *8* (8), 5170–5177.
- (14) Zhang, Y.; Liu, S.; Li, Y.; Deng, D.; Si, X.; Ding, Y.; He, H.; Luo, L.; Wang, Z. Electrospun Graphene Decorated MnCo<sub>2</sub>O<sub>4</sub> composite Nanofibers for Glucose Biosensing. *Biosens. Bioelectron.* **2015**, *66*, 308–315.
- (15) Ramazani, S.; Karimi, M. Aligned Poly( $\epsilon$ -Caprolactone)/graphene Oxide and Reduced Graphene Oxide Nanocomposite Nanofibers: Morphological, Mechanical and Structural Properties. *Mater. Sci. Eng. C* **2015**, *56*, 325–334.
- (16) Golafshan, N.; Kharaziha, M.; Fathi, M. Tough and Conductive Hybrid Graphene-PVA: Alginate Fibrous Scaffolds for Engineering Neural Construct. *Carbon N. Y.* **2017**, *111*, 752–763.
- (17) Muerza-Cascante, M. L.; Haylock, D.; Hutmacher, D. W.; Dalton, P. D. Melt Electrospinning and Its Technologization in Tissue Engineering. *Tissue Eng. Part B Rev.* **2015**, *21* (2), 187–202.
- (18) Golafshan, N.; Kharaziha, M.; Fathi, M.; Larson, B. L.; Giatsidis, G.; Masoumi, N. Anisotropic Architecture and Electrical Stimulation Enhance Neuron Cell Behaviour on a Tough Graphene Embedded PVA: Alginate Fibrous Scaffold. *RSC Adv.* **2018**, *8* (12), 6381–6389.
- (19) Vunjak-Novakovic, G., Tandon, N., Godier, A., Maidhof, R., Marsano, A., Martens, T. P., & Radisic, M. Challenges in Cardiac Tissue Engineering. *Tissue Eng. Part B Rev.* **2010**, *16* (2), 169–187.
- (20) Subia, B.; Kundu, J.; C., S. Biomaterial Scaffold Fabrication Techniques for Potential Tissue Engineering Applications. In *Tissue Engineering*; Eberli, D., Ed.; 2010; pp 141–159.
- (21) Orza, A.; Soritau, O.; Olenic, L.; Diudea, M.; Florea, A.; Rus Ciuca, D.; Miha, C.; Casciano, D.; Biris, A. S. Electrically Conductive Gold-Coated Collagen Nanofibers for Placental-Derived Mesenchymal Stem Cells Enhanced Differentiation and Proliferation. *ACS Nano* **2011**, *5* (6), 4490–4503.
- (22) Shin, S. R.; Jung, S. M.; Zalabany, M.; Kim, K.; Zorlutuna, P.; Kim, S. bok; Nikkhah, M.; Khabiry, M.; Azize, M.; Kong, J.; et al. Carbon-Nanotube-Embedded Hydrogel Sheets for Engineering Cardiac Constructs and Bioactuators. *ACS Nano* **2013**, *7* (3), 2369–2380.
- (23) Dvir, T.; Timko, B. P.; Brigham, M. D.; Naik, S. R.; Karajanagi, S. S.; Levy, O.; Jin, H.; Parker, K. K.; Langer, R.; Kohane, D. S. Nanowired Three Dimensional

Cardiac Patches. *Nat Nanotechnol* **2012**, *6* (11), 720–725.

- (24) Ganji, Y.; Li, Q.; Quabius, E. S.; Böttner, M.; Selhuber-Unkel, C.; Kasra, M. Cardiomyocyte Behavior on Biodegradable Polyurethane/gold Nanocomposite Scaffolds under Electrical Stimulation. *Mater. Sci. Eng. C* **2016**, *59*, 10–18.
- (25) Rodriguez-Galan, A.; Franco, L.; Puiggali, J. Degradable Poly(ester Amide)s for Biomedical Applications. *Polymers*. **2011**, *3*, 65–99.
- (26) Knight, D. K.; Gillies, E. R.; Mequanint, K. Biomimetic L-Aspartic Acid-Derived Functional Poly(ester Amide)s for Vascular Tissue Engineering. *Acta Biomater.* **2014**, *10* (8), 3484–3496.
- (27) Horwitz, J. A.; Shum, K. M.; Bodle, J. C.; Deng, M.; Chu, C. C.; Reinhart-King, C. A. Biological Performance of Biodegradable Amino Acid-Based Poly(ester Amide)s: Endothelial Cell Adhesion and Inflammation in Vitro. *J. Biomed. Mater. Res. - Part A* **2010**, *95 A* (2), 371–380.
- (28) Liu, Y.; Park, M.; Shin, H. K.; Pant, B.; Choi, J.; Park, Y. W.; Lee, J. Y.; Park, S. J.; Kim, H. Y. Facile Preparation and Characterization of Poly(vinyl Alcohol)/chitosan/graphene Oxide Biocomposite Nanofibers. *J. Ind. Eng. Chem.* **2014**, *20* (6), 4415–4420.
- (29) Zhu, Y.; Murali, S.; Cai, W.; Li, X.; Suk, J. W.; Potts, J. R.; Ruoff, R. S. Graphene and Graphene Oxide: Synthesis, Properties, and Applications. *Adv. Mater.* **2010**, *22* (35), 3906–3924.
- (30) Xu, C.; Shi, X.; Ji, A.; Shi, L.; Zhou, C.; Cui, Y. Fabrication and Characteristics of Reduced Graphene Oxide Produced with Different Green Reductants. *PLoS One* **2015**, *10* (12), e0144842.
- (31) Qian, Q.; Qian, H.; Zhang, X.; Zhu, W.; Yan, Y.; Ye, S.; Peng, X.; Li, W.; Xu, Z.; Sun, L.; et al. 5-Azacytidine Induces Cardiac Differentiation of Human Umbilical Cord-Derived Mesenchymal Stem Cells by Activating Extracellular Regulated Kinase. *Stem Cells Dev.* **2012**, *21* (1), 67–75.
- (32) Lee, T.-J.; Park, S.; Bhang, S. H.; Yoon, J.-K.; Jo, I.; Jeong, G.-J.; Hong, B. H.; Kim, B.-S. Graphene Enhances the Cardiomyogenic Differentiation of Human Embryonic Stem Cells. *Biochem. Biophys. Res. Commun.* **2014**, *452* (1), 174–180.
- (33) Cao, N.; Liu, Z.; Chen, Z.; Wang, J.; Chen, T.; Zhao, X.; Ma, Y.; Qin, L.; Kang, J.; Wei, B.; et al. Ascorbic Acid Enhances the Cardiac Differentiation of Induced Pluripotent Stem Cells through Promoting the Proliferation of Cardiac Progenitor Cells. *Cell Res.* **2012**, *22* (1), 219–236.
- (34) Park, J.; Park, S.; Ryu, S.; Bhang, S. H.; Kim, J.; Yoon, J. K.; Park, Y. H.; Cho, S. P.; Lee, S.; Hong, B. H.; et al. Graphene-Regulated Cardiomyogenic Differentiation Process of Mesenchymal Stem Cells by Enhancing the Expression

- of Extracellular Matrix Proteins and Cell Signaling Molecules. *Adv. Healthc. Mater.* **2014**, *3* (2), 176–181.
- (35) Ji, X.; Xu, Y.; Zhang, W.; Cui, L.; Liu, J. Review of Functionalization, Structure and Properties of Graphene/polymer Composite Fibers. *Compos. Part A Appl. Sci. Manuf.* **2016**, *87*, 29–45.
- (36) Bressan, E.; Ferroni, L.; Gardin, C.; Sbricoli, L.; Gobatto, L.; Ludovichetti, F. S.; Tocco, I.; Carraro, A.; Piattelli, A.; Zavan, B. Graphene Based Scaffolds Effects on Stem Cells Commitment. *J. Transl. Med.* **2014**, *12* (1), 296.
- (37) Chowdhury, D. R.; Singh, C.; Paul, A. Role of Graphite Precursor and Sodium Nitrate in Graphite Oxide Synthesis. *RSC Adv.* **2014**, *4* (29), 15138–15145.
- (38) Dreyer, D. R.; Park, S.; Bielawski, C. W.; Ruoff, R. S. The Chemistry of Graphene Oxide. *Chem. Soc. Rev.* **2010**, *39*, 228–240.
- (39) Hummers, W. S.; Offeman, R. E. Preparation of Graphitic Oxide. *J. Am. Chem. Soc.* **1958**, *80* (6), 1339.
- (40) Chen, J.; Yao, B.; Li, C.; Shi, G. An Improved Hummers Method for Eco-Friendly Synthesis of Graphene Oxide. *Carbon N. Y.* **2013**, *64* (1), 225–229.
- (41) Marcano, D. C.; Kosynkin, D. V.; Berlin, J. M.; Sinitskii, A.; Sun, Z.; Slesarev, A.; Alemany, L. B.; Lu, W.; Tour, J. M. Improved Synthesis of Graphene Oxide. *ACS Nano* **2010**, *4* (8), 4806–4814.
- (42) Kovtyukhova, N. I.; Ollivier, P. J.; Martin, B. R.; Mallouk, T. E.; Chizhik, S. A.; Buzaneva, E. V.; Gorchinskiy, A. D. Layer-by-Layer Assembly of Ultrathin Composite Films from Micron-Sized Graphite Oxide Sheets and Polycations. *Chem. Mater.* **1999**, *11* (3), 771–778.
- (43) Dimiev, A. M.; Tour, J. M. Mechanism of Graphene Oxide Formation. *ACS Nano* **2014**, *8* (3), 3060–3068.
- (44) Hu, C.; Zhou, R.; Fan, C.; Zhou, X. Influence of Reducing Reagent Combination in Graphene Oxide Reduction. *Micro Nano Lett.* **2016**, *11* (4), 215–220.
- (45) Zhang, J.; Yang, H.; Shen, G.; Cheng, P.; Zhang, J.; Guo, S. Reduction of Graphene Oxide via L-Ascorbic Acid. *Chem. Commun.* **2010**, *46*, 1112–1114.
- (46) Dua, V.; Surwade, S. P.; Ammu, S.; Agnihotra, S. R.; Jain, S.; Roberts, K. E.; Park, S.; Ruoff, R. S.; Manohar, S. K. All-Organic Vapor Sensor Using Inkjet-Printed Reduced Graphene Oxide. *Angew. Chem. Int. Ed.* **2010**, *49* (12), 2154–2157.
- (47) Abulizi, A.; Okitsu, K.; Zhu, J. J. Ultrasound Assisted Reduction of Graphene Oxide to Graphene in L-Ascorbic Acid Aqueous Solutions: Kinetics and Effects of

- Various Factors on the Rate of Graphene Formation. *Ultrason. Sonochem.* **2014**, *21* (3), 1174–1181.
- (48) Smits, F. M. Measurement of Sheet Resistivities with the Four-Point Probe. *Bell Syst. Tech. J.* **1958**, *37* (3), 711–718.
- (49) Miccoli, I.; Edler, F.; Pfnür, H.; Tegenkamp, C. The 100th Anniversary of the Four-Point Probe Technique: The Role of Probe Geometries in Isotropic and Anisotropic Systems. *J. Phys. Condens. Matter* **2015**, *27* (22).
- (50) Tiusanen, J.; Vlasveld, D.; Vuorinen, J. Review on the Effects of Injection Moulding Parameters on the Electrical Resistivity of Carbon Nanotube Filled Polymer Parts. *Compos. Sci. Technol.* **2012**, *72* (14), 1741–1752.
- (51) Boudriot, U.; Dersch, R.; Greiner, A.; Wendorff, J. H. Electrospinning Approaches toward Scaffold Engineering--a Brief Overview. *Artif. Organs* **2006**, *30* (10), 785–792.
- (52) Murugan, R.; Ramakrishna, S. Design Strategies of Tissue Engineering Scaffolds with Controlled Fiber Orientation. *Tissue Eng.* **2007**, *13* (8), 1845–1866.
- (53) Moghe, a. K.; Gupta, B. S. Co-Axial Electrospinning for Nanofiber Structures: Preparation and Applications. *Polym. Rev.* **2008**, *48* (2), 353–377.
- (54) Reneker, D. H.; Yarin, A. L. Electrospinning Jets and Polymer Nanofibers. *Polymer (Guildf).* **2008**, *49* (10), 2387–2425.
- (55) Kim, I.; Seo, S.; Moon, H.; Yoo, M.; Park, I.; Kim, B.; Cho, C. Chitosan and Its Derivatives for Tissue Engineering Applications. **2008**, *26*, 1–21.
- (56) Yeh, H. Y.; Liu, B. H.; Hsu, S. H. The Calcium-Dependent Regulation of Spheroid Formation and Cardiomyogenic Differentiation for MSCs on Chitosan Membranes. *Biomaterials* **2012**, *33* (35), 8943–8954.
- (57) Cho, Y. W.; Cho, Y. N.; Chung, S. H.; Yoo, G.; Ko, S. W. Water-Soluble Chitin as a Wound Healing Accelerator. *Biomaterials* **1999**, *20* (22), 2139–2145.
- (58) Chakraborty, S.; Liao, I.-C.; Adler, A.; Leong, K. W. Electrohydrodynamics: A Facile Technique to Fabricate Drug Delivery Systems. *Adv. Drug Deliv. Rev.* **2010**, *61* (12), 1043–1054.
- (59) Gebeyehu, M. B.; Chang, Y.-H.; Abay, A. K.; Chang, S.-Y.; Lee, J.-Y.; Wu, C.-M.; Chiang, T.-C.; Murakami, R.-I. Fabrication and Characterization of Continuous Silver Nanofiber/polyvinylpyrrolidone (AgNF/PVP) Core-shell Nanofibers Using the Coaxial Electrospinning Process. *RSC Adv.* **2016**, *6* (59), 54162–54168.
- (60) Hwang, J.; Muth, J.; Ghosh, T. Electrical and Mechanical Properties of Carbon-

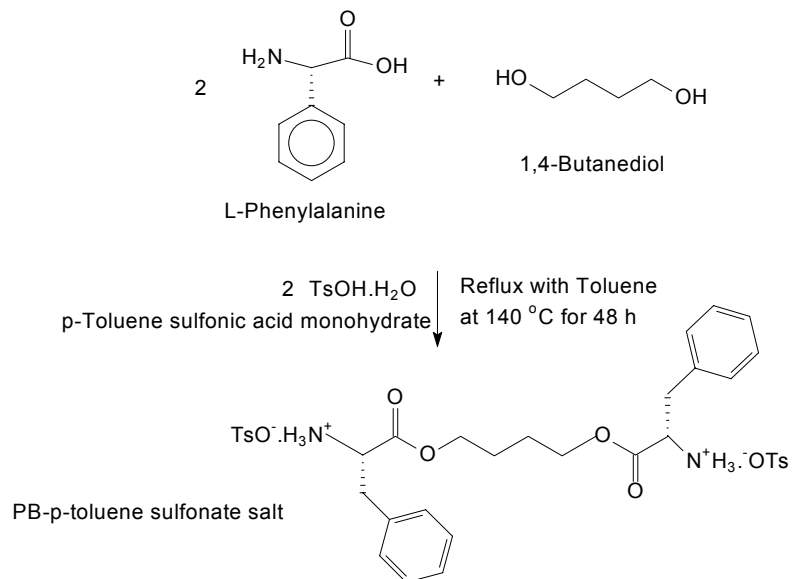


- Black-Filled, Electrospun Nanocomposite Fiber Webs. *J. Appl. Polym. Sci.* **2007**, *104*, 2410–2417.
- (61) Ramazani, S.; Karimi, M. Electrospinning of Poly( $\epsilon$ -Caprolactone) Solutions Containing Graphene Oxide: Effects of Graphene Oxide Content and Oxidation Level. *Polym. Compos.* **2016**, *37* (1), 131–140.
- (62) Yang, Y.; Ding, X.; Zou, T.; Peng, G.; Liu, H.; Fan, Y. Preparation and Characterization of Electrospun Graphene/silk Fibroin Conductive Fibrous Scaffolds. *RSC Adv.* **2017**, *7* (13), 7954–7963.
- (63) Nalvuran, H.; Elçin, A. E.; Elçin, Y. M. Nanofibrous Silk Fibroin/reduced Graphene Oxide Scaffolds for Tissue Engineering and Cell Culture Applications. *Int. J. Biol. Macromol.* **2018**, *114*, 77–84.
- (64) Tan, Y.; Song, Y.; Zheng, Q. Hydrogen Bonding-Driven Rheological Modulation of Chemically Reduced Graphene Oxide/poly(vinyl Alcohol) Suspensions and Its Application in Electrospinning. *Nanoscale* **2012**, *4* (22), 6997.
- (65) Baker, B. M.; Chen, C. S. Deconstructing the Third Dimension – How 3D Culture Microenvironments Alter Cellular Cues. *J. Cell Sci.* **2012**, *125* (13), 3015–3024.
- (66) Baker, B. M.; Gee, A. O.; Metter, R. B.; Nathan, A. S.; Marklein, R. A.; Burdick, J. A.; Mauck, R. L. The Potential to Improve Cell Infiltration in Composite Fiber-Aligned Electrospun Scaffolds by the Selective Removal of Sacrificial Fibers. *Biomaterials* **2008**, *29* (15), 2348–2358.
- (67) Milleret, V.; Simona, B.; Neuenschwander, P.; Hall, H. Tuning Electrospinning Parameters for Production of 3D-Fiberfleeces with Increased Porosity for Soft Tissue Engineering Applications. *Eur. Cells Mater.* **2011**, *21*, 286–303.
- (68) Bogtitzki, M.; Frese, T.; Steinhart, M.; Greiner, A.; Wendorff, J. H.; Schaper, A.; Hellwig, M. Preparation of Fibers with Nanoscaled Morphologies: Electrospinning of Polymer Blends. *Polym. Eng. Sci.* **2001**, *41* (6), 982–989.
- (69) Tehrani, A. H.; Zadhoush, A.; Karbasi, S.; Sadeghi-Aliabadi, H. Scaffold Percolative Efficiency: In Vitro Evaluation of the Structural Criterion for Electrospun Mats. *J. Mater. Sci. Mater. Med.* **2010**, *21* (11), 2989–2998.
- (70) Knight, D. K.; Gillies, E. R.; Mequanint, K. Strategies in Functional Poly(ester Amide) Syntheses to Study Human Coronary Artery Smooth Muscle Cell Interactions. *Biomacromolecules* **2011**, *12*, 2475–2487.
- (71) Shah, S.; Yin, P. T.; Uehara, T. M.; Chueng, S. T. D.; Yang, L.; Lee, K. B. Guiding Stem Cell Differentiation into Oligodendrocytes Using Graphene-Nanofiber Hybrid Scaffolds. *Adv. Mater.* **2014**, *26* (22), 3673–3680.
- (72) Zhang, W.; He, W.; Jing, X. Preparation of a Stable Graphene Dispersion with

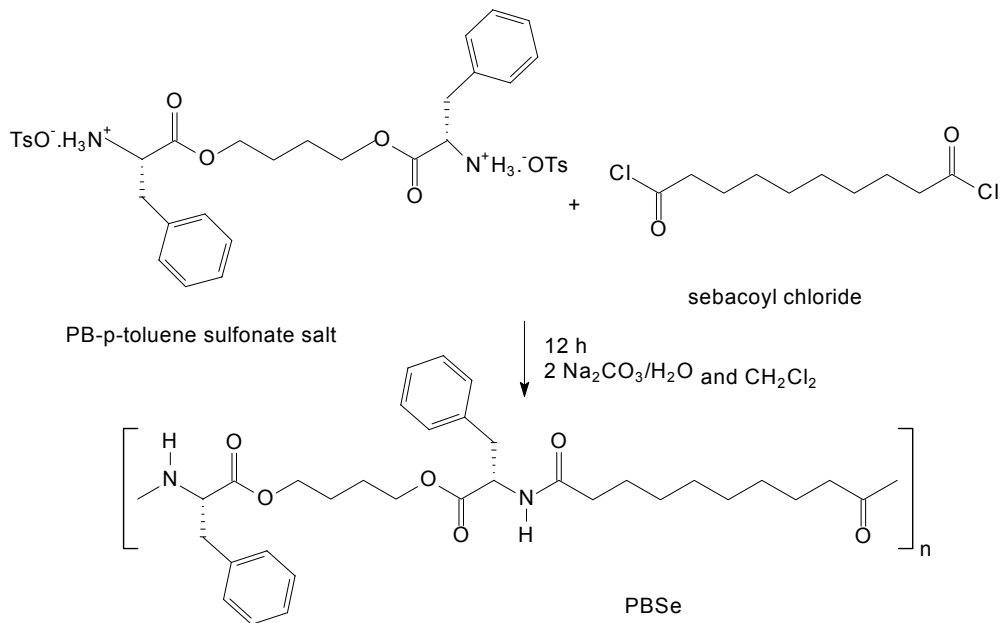
- High Concentration by Ultrasound. *J. Phys. Chem. B* **2010**, *114* (32), 10368–10373.
- (73) Zhang, X.; Xing, M. Personal Communication. University of Manitoba, Winnipeg, Manitoba 2017.
- (74) Saraf, A.; Lozier, G.; Haesslein, A.; Kasper, F. K.; Raphael, R. M.; Baggett, L. S.; Mikos, A. G. Fabrication of Nonwoven Coaxial Fiber Meshes by Electrospinning. *Tissue Eng. Part C Methods* **2009**, *15* (3), 333–344.
- (75) Wang, X.; Bai, H.; Yao, Z.; Liu, A.; Shi, G. Electrically Conductive and Mechanically Strong Biomimetic Chitosan/reduced Graphene Oxide Composite Films. *J. Mater. Chem.* **2010**, *20* (41), 9032.
- (76) Liu, Y.; He, J.-H.; Yu, J.; Zeng, H. Controlling Numbers and Sizes of Beads in Electrospun Nanofibers. *Polym. Int.* **2008**, *57*, 632–636.
- (77) Kishan, A. P.; Cosgriff-hernandez, E. M. Recent Advancements in Electrospinning Design for Tissue Engineering Applications : A Review. *J. Biomed. Mater. Res. Part A* **2017**, *105* (10), 2892–2905.
- (78) Luo, C. J.; Stride, E.; Edirisinghe, M. Mapping the Influence of Solubility and Dielectric Constant on Electrospinning Polycaprolactone Solutions. *Macromolecules* **2012**, *45* (11), 4669–4680.
- (79) Dror, Y.; Salalha, W.; Avrahami, R.; Zussman, E.; Yarin, A. L.; Dersch, R.; Greiner, A.; Wendorff, J. H. One-Step Production of Polymeric Microtubes by Co-Electrospinning. *Small* **2007**, *3* (6), 1064–1073.
- (80) Forough, R.; Scarcello, C.; Perkins, M. Cardiac Biomarkers: A Focus on Cardiac Regeneration. *J. Tehran Univ. Hear. Cent.* **2011**, *6* (4), 179–186.

## Appendices

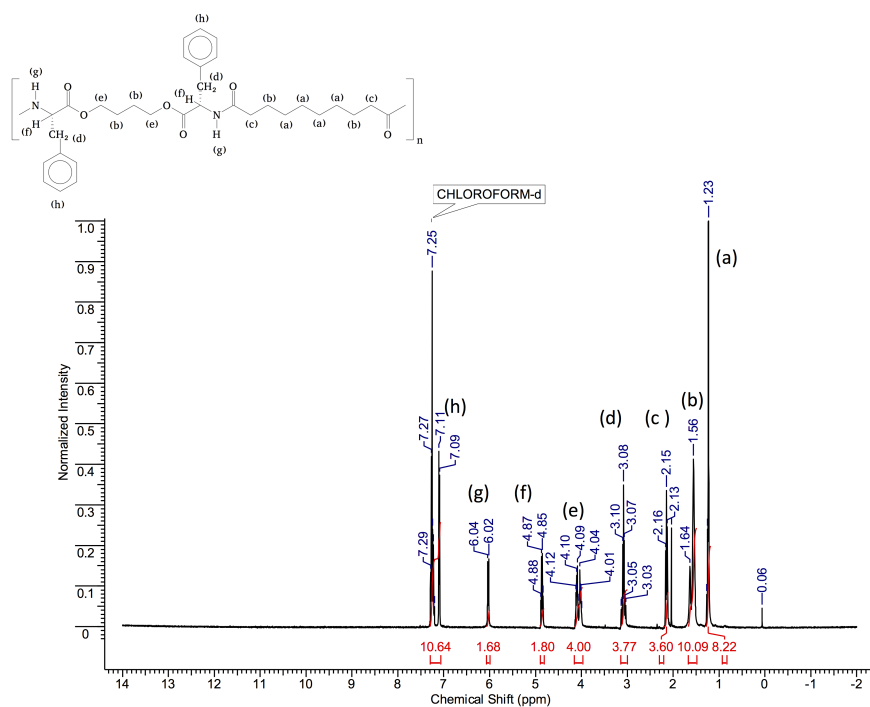
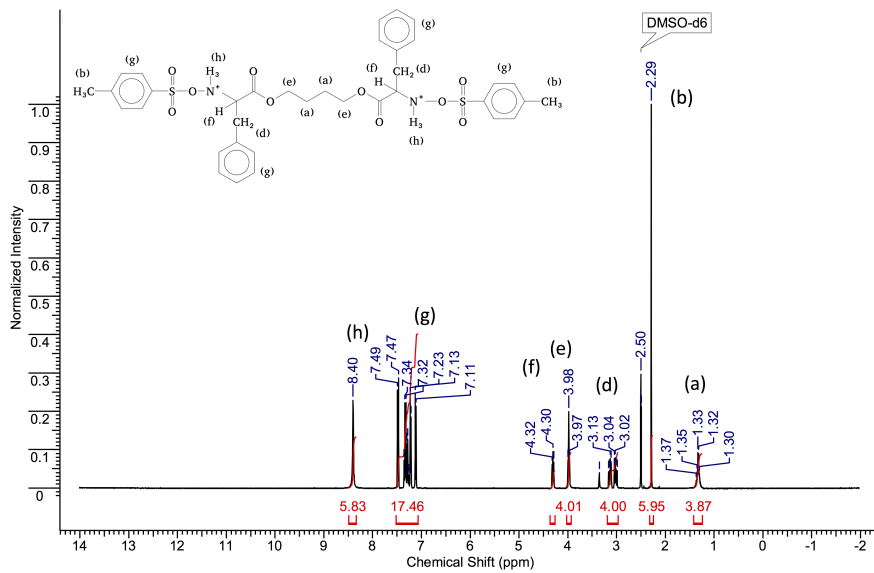
### PB Monomer Synthesis - Acid-Catalyzed Condensation



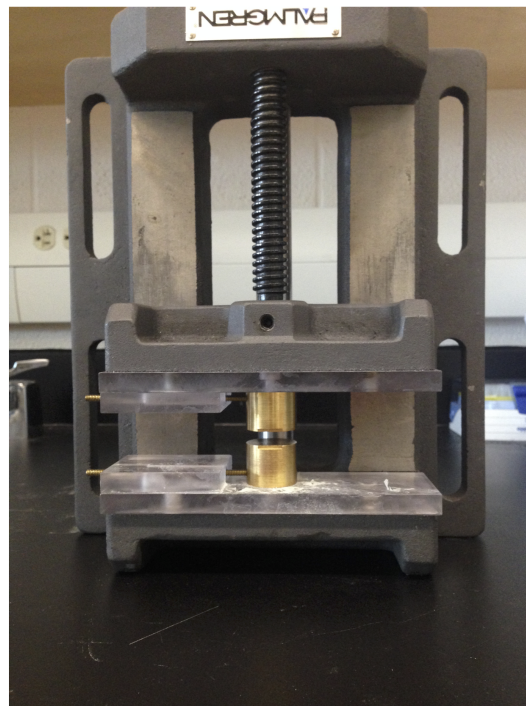
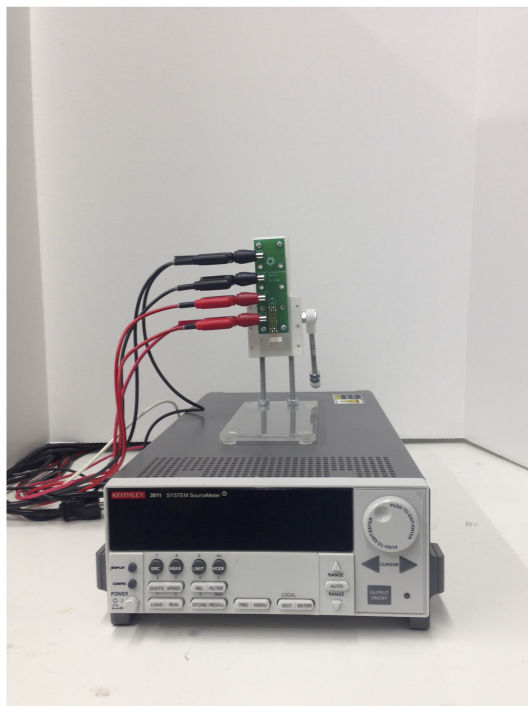
### PBSe Synthesis - Interfacial Polymerization



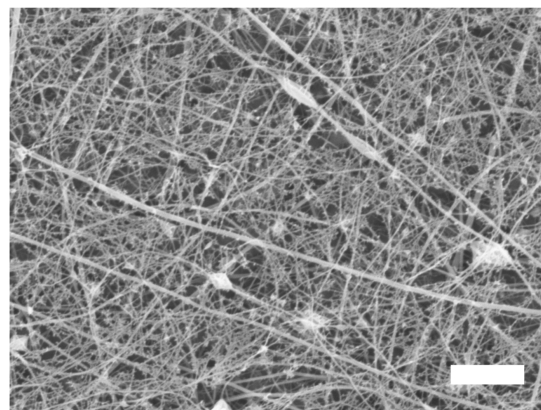
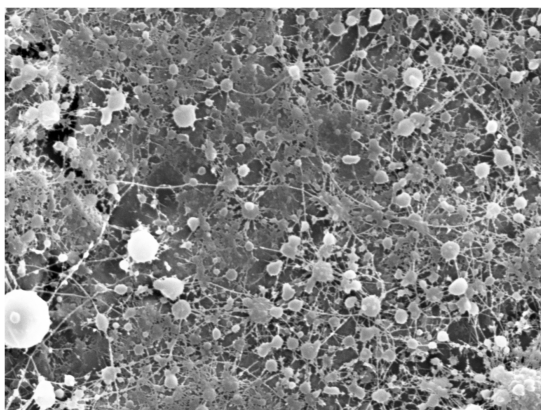
### Appendix 1: Reaction schemes for PEA synthesis



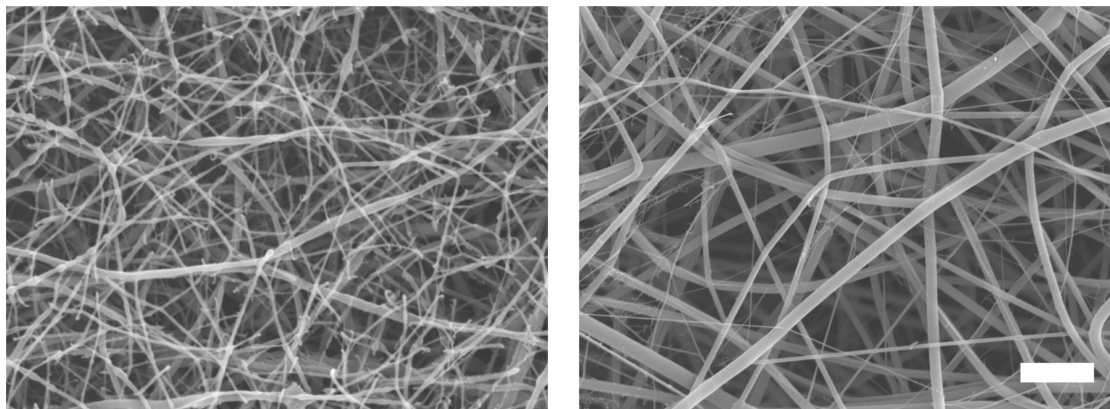
**Appendix 2:**  $^1\text{H}$  NMR results for monomer (top) and polymer (bottom)



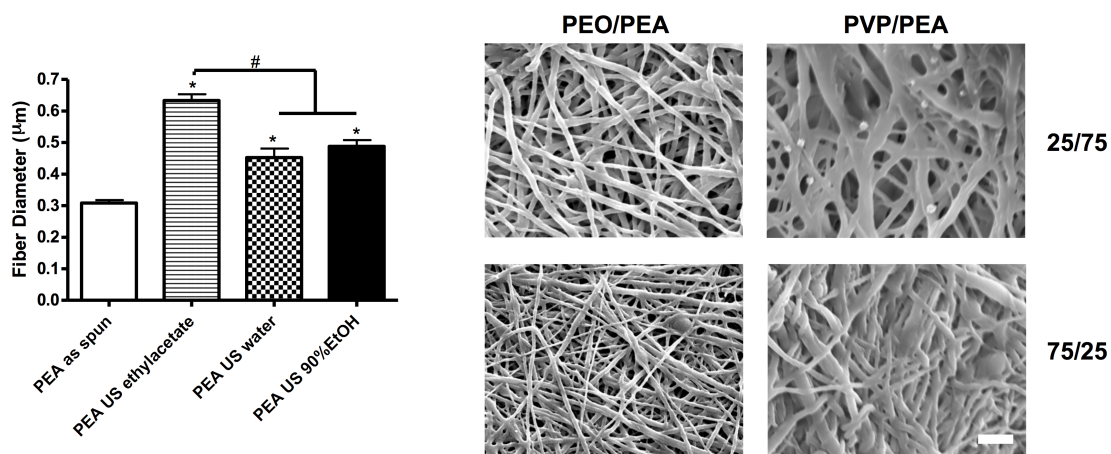
**Appendix 3:** Electrical conductivity measurement set-ups. Four-probe with source measure unit (left) and two-probe (right).



**Appendix 4:** The effect of rGO on CS electrospinning with CS (left) and rGO/CS (right). Scale bar is 3  $\mu\text{m}$ .



**Appendix 5:** Electrospinning optimization for sacrificial polymers PEO (left) and PVP (right). Scale bar is 3  $\mu\text{m}$ .



**Appendix 6:** Scaffold modification optimization. (Left): Different ultrasonication media result in different amounts of fiber swelling. 50 fibers were measured, \* represents significance against the PEA as spun control, and # represents significance between groups where  $p < 0.05$ . (Right): Effect of different ratios of sacrificial polymer where scale bar is 3  $\mu\text{m}$ .

## Appendix 7: Copyright Permissions

Mary Ann Liebert, Inc.  publishers

---

06/14/2018

Dear Hilary Elizabeth Stone,

Permission is granted to use:

Fig 1 from

Jung Bok Lee, Sung In Jeong, Min Soo Bae, Dae Hyeok Yang, Dong Nyoung Heo, Chun Ho Kim, Eben Alsberg, and Il Keun Kwon. *Tissue Engineering Part A*. Nov 2011.

<http://doi.org/10.1089/ten.tea.2010.0709>

Fig 4 and Table 1 (adapted) from

Ingavle Ganesh C. and Leach J. Kent. *Tissue Engineering Part B: Reviews*. Aug 2014.

<http://doi.org/10.1089/ten.teb.2013.0276>

in your thesis, titled "Preparation and Characterization of Electrospun rGO-Poly(ester amide) Tissue Engineering Scaffolds"

Best regards,

6/14/2018

RightsLink Printable License

**ELSEVIER LICENSE  
TERMS AND CONDITIONS**

Jun 14, 2018

---

This Agreement between Hilary Stone ("You") and Elsevier ("Elsevier") consists of your license details and the terms and conditions provided by Elsevier and Copyright Clearance Center.

License Number	4367721304715
License date	Jun 14, 2018
Licensed Content Publisher	Elsevier
Licensed Content Publication	Biomaterials
Licensed Content Title	Water-soluble chitin as a wound healing accelerator
Licensed Content Author	Yong-Woo Cho,Yong-Nam Cho,Sang-Hun Chung,Gyeol Yoo,Sohk-Won Ko
Licensed Content Date	Nov 1, 1999
Licensed Content Volume	20
Licensed Content Issue	22
Licensed Content Pages	7
Start Page	2139
End Page	2145
Type of Use	reuse in a thesis/dissertation
Portion	figures/tables/illustrations
Number of figures/tables/illustrations	1
Format	electronic
Are you the author of this Elsevier article?	No
Will you be translating?	No
Original figure numbers	figure 1b
Title of your thesis/dissertation	Preparation and Characterization of Electrospun rGO-Poly(ester amide) Tissue Engineering Scaffolds
Expected completion date	Jun 2018
Estimated size (number of pages)	93
Requestor Location	Hilary Stone



6/14/2018

RightsLink Printable License

**ELSEVIER LICENSE  
TERMS AND CONDITIONS**

Jun 14, 2018

---

This Agreement between Hilary Stone ("You") and Elsevier ("Elsevier") consists of your license details and the terms and conditions provided by Elsevier and Copyright Clearance Center.

License Number	4367730346473
License date	Jun 14, 2018
Licensed Content Publisher	Elsevier
Licensed Content Publication	Advanced Drug Delivery Reviews
Licensed Content Title	Electrohydrodynamics: A facile technique to fabricate drug delivery systems
Licensed Content Author	Syandan Chakraborty,I-Chien Liao,Andrew Adler,Kam W. Leong
Licensed Content Date	Oct 5, 2009
Licensed Content Volume	61
Licensed Content Issue	12
Licensed Content Pages	12
Start Page	1043
End Page	1054
Type of Use	reuse in a thesis/dissertation
Intended publisher of new work	other
Portion	figures/tables/illustrations
Number of figures/tables/illustrations	1
Format	electronic
Are you the author of this Elsevier article?	No
Will you be translating?	No
Original figure numbers	figure 3b
Title of your thesis/dissertation	Preparation and Characterization of Electrospun rGO-Poly(ester amide) Tissue Engineering Scaffolds
Expected completion date	Jun 2018
Estimated size (number of pages)	93
Requestor Location	Hilary Stone

6/14/2018

RightsLink Printable License

**ROYAL SOCIETY OF CHEMISTRY LICENSE  
TERMS AND CONDITIONS**

Jun 14, 2018

---

This Agreement between Hilary Stone ("You") and Royal Society of Chemistry ("Royal Society of Chemistry") consists of your license details and the terms and conditions provided by Royal Society of Chemistry and Copyright Clearance Center.

License Number	4367730926689
License date	Jun 14, 2018
Licensed Content Publisher	Royal Society of Chemistry
Licensed Content Publication	RSC Advances
Licensed Content Title	Fabrication and characterization of continuous silver nanofiber/polyvinylpyrrolidone (AgNF/PVP) core-shell nanofibers using the coaxial electrospinning process
Licensed Content Author	Molla Bahiru Gebeyehu, Yu-Hao Chang, Angaw Kelemework Abay, Shao-Yen Chang, Jiunn-Yih Lee, Chang-Mou Wu, Tai-Chin Chiang, Ri-Ichi Murakami
Licensed Content Date	May 19, 2016
Licensed Content Volume	6
Licensed Content Issue	59
Type of Use	Thesis/Dissertation
Requestor type	academic/educational
Portion	figures/tables/images
Number of figures/tables/images	1
Format	electronic
Distribution quantity	100000
Will you be translating?	no
Order reference number	
Title of the thesis/dissertation	Preparation and Characterization of Electrospun rGO-Poly(ester amide) Tissue Engineering Scaffolds
Expected completion date	Jun 2018
Estimated size	93
Requestor Location	Hilary Stone

All other reproduced figures were open access and did not require specific permission.

## Curriculum Vitae

**Name:** Hilary Stone

**Post-secondary Education and Degrees:** Masters of Engineering Science  
Major in Biomedical Engineering, Biomaterials  
The University of Western Ontario  
London, Ontario, Canada  
2017-2018

Bachelor of Engineering Science  
Major in Chemical and Biochemical Engineering  
WE Go Global Certificate  
The University of Western Ontario  
London, Ontario, Canada  
2012-2016

**Honours and Awards:** Ontario Graduate Scholarship, \$15,000  
The University of Western Ontario  
2017

NSERC Undergraduate Summer Research Award, \$9,000  
The University of Western Ontario  
2014, 2016

James M. Hay Gold Medal: Chemical/Biochemical Engineering  
The University of Western Ontario  
2016

Society of Chemical Industry Merit Award  
The University of Western Ontario  
2016

Leaders for the Future Scholarship, \$2,000  
Ontario Professional Engineers Foundation for Education  
2016

Dean's Honour List  
The University of Western Ontario  
2013-2016

National Scholarship Winner, \$50,000  
The University of Western Ontario  
2012-2016

Parsons Corporation Scholarship, \$2,000  
Parsons Corporation  
2015

Global Opportunities Award, \$2,000  
The University of Western Ontario  
2015

Union Gas Award  
The University of Western Ontario, \$1,000  
2014

**Related Work  
Experience**

Teaching Assistant, 2<sup>nd</sup> Year Chemical/Biochemical  
Engineering course  
The University of Western Ontario  
2018

Summer Research Student, NSERC USRA  
The University of Western Ontario  
2014, 2016

Operational Researcher  
VOTO Mobile, Ghana  
2015, 2016

**Presentations**

Three-Minute Thesis Finalist (Top 20 at UWO)  
The University of Western Ontario  
2018

Poster Presentation, Inspiring Women in STEM Conference  
The University of Western Ontario  
2016

Third Place Oral Presentation Undergraduate Thesis Competition,  
Chemical/Biochemical Engineering  
The University of Western Ontario  
2016